Aspects of gauge-string duality in SUSY and non-SUSY systems.

Bennett, Stephen Thomas

Aspects of Gauge-String Duality in SUSY and non-SUSY systems

Stephen Bennett

Department of Physics,
Swansea University,
Swansea, SA2 8PP, UK

Submitted to Swansea University in fulfilment of the requirements for the Degree of Doctor of Philosophy.

Swansea University, 2014.

Summary

We study various aspects of type IIB supergravity backgrounds related to those of Klebanov-Strassler and Chamseddine-Volkov/Maldacena-Núñez, in the context of gauge-gravity duality. We first examine the structure which can be found in the family of supersymmetric solutions, and in particular the effect of adding flavour.

We then turn to the problem of finding non-supersymmetric generalisations of the well-understood supersymmetric solutions. Using a combination of analytic and numerical techniques we find a two-dimensional space of such solutions, corresponding to the baryonic branch of Klebanov-Strassler deformed by a SUSY-breaking irrelevant operator. We explore the parameter space in some detail, and find several interesting special cases and limits, including one in which supersymmetry is completely broken and unusual periodic behavior is present in the warp factors.

Finally, we look in detail at some of the methods which can be used to probe the field theory corresponding to these kinds of backgrounds.

This thesis is based in part on the papers arXiv:1102.5731 [1] (chapter 2), and arXiv:1111.1727 [2] and arXiv:1204.2799 [3] (chapter 3).

DECLARATION

This work has not previously been accepted in substance for any degree and is not being concurrently submitted in candidature for any degree.

Signed ... . (candidate)

Date ..... 10/4/14 .....

STATEMENT 1

This thesis is the result of my own investigations, except where otherwise stated. Where correction services have been used, the extent and nature of the correction is clearly marked in a footnote. Other sources are acknowledged by footnotes giving explicit references. A bibliography is appended.

Signed ..... (candidate)

Date ..... 10/4/14 .....

STATEMENT 2

I hereby give consent for my thesis, if accepted, to be available for photocopying and for inter-library loan, and for the title and summary to be made available to outside organisations.

Signed .... (candidate)

Date ..... 10/4/14 .....

Contents

Acknowledgements

Firstly, I would like to thank my supervisor Carlos Núñez and Tim Hollowood for their support and assistance throughout. Carlos Núñez collaborated with me together with Elena Caceres, Daniel Schofield and Steve Young on the project presented in chapter 3. I would like to further thank Daniel Schofield for valuable discussions on many subjects, and particular the work that became chapter 4.

Chapter 1

Introduction

1.1 Background

Much of the recent focus of research in many areas of physics has been on strongly-interacting theories, in which the methods of perturbation theory are not applicable. This is of course true of the ongoing attempt to understand QCD at low energies, and in particular the mechanism of confinement. There have also been many attempts to extend these ideas to physics beyond the Standard Model. For example, the idea behind technicolor is essentially to consider an additional strongly-coupled sector more or less analogous to QCD, the dynamics of which is responsible for electroweak symmetry breaking. Further afield, non-perturbative, strongly-coupled physics is important in the study of condensed matter and phenomena such as superfluidity, as well as in string theory as a fundamental theory of quantum gravity.

Without the methods of perturbation theory, progress in these areas can be difficult. As a result, the AdS/CFT correspondence conjectured by Maldacena [4] has become one of the most important tools for studying strongly-coupled gauge theories. The key point is that *strongly* coupled dynamics on one side of the duality correspond to *weakly* coupled dynamics on the other. This opens up the prospect of our gaining an understanding of strongly-coupled gauge theories like QCD in terms of weakly-coupled (classical) gravity, and conversely learning about non-perturbative string theory by studying a weakly-coupled gauge theory. Indeed it may be that some form of the duality will serve as the *definition* (in terms of a perturbative gauge theory) of string or M theory in the strongly-coupled regime.

Although string theory had originally been developed as a model for the strong interaction this interpretation was discarded in favour of QCD, and string theory became primarily a prospect for a theory of quantum gravity. However, in the 90s the deep connection with traditional gauge theories became apparent, culminating in Maldacena's conjecture. In its original and best-established form, the conjecture asserts the equivalence between Type IIB string theory on $AdS_5 \times S^5$ and the $\mathcal{N} = 4$ SYM gauge field theory in 4 dimensions. By using the prescription relating quantities on either side of the duality [4, 5, 6], extensive work has been (and continues to be) done to test the conjecture. As a result, although the duality is not proven, the variety of effects which have been successfully checked between the two sides of the correspondence strongly suggests that we can trust it.

Furthermore, beyond this original formulation progress has been made in applying the principles of gauge-gravity duality to more generic cases, which lack confor-

mal symmetry and possess less supersymmetry. In this line there has also been significant successes, to the extent that here also it is possible to regard gauge/gravity duality as a tool to use, rather than a conjecture to test. These developments are of particular interest because they raise the prospect of finding the dual gravity description of theories which more closely resemble QCD. This would enable us to gain insight into the strongly-coupled dynamics of QCD by studying the behaviour of classical supergravity on appropriate backgrounds. While a gravity dual of QCD itself is clearly out of reach, duals of similar theories would be of considerable use in understanding QCD, and are likely to have similar applicability to beyond the Standard Model and condensed matter physics. It is to this programme of approaching the dual of 'realistic' gauge theories that the work presented here aims to contribute.

The approach taken is to start from a case in which the duality is well understood [7] and in which many of the desired properties (primarily reduced symmetries compared to the original AdS case) are already present to some extent. We will then study modifications to the gravity background which bring us to seemingly even more QCD-like theories. In this case, we will look at some of the consequences of adding flavour, and at how we could break supersymmetry altogether.

The discussion is primarily from the point of view of the gravity side of the duality, and so it will be useful to have looked at the chain of related supergravity solutions linking the systems of interest to the original $AdS_5 \times S^5$ case. We postpone any detailed discussion of the dual gauge theories to later chapters.

We start with the 'near-horizon' (small r) limit of the solution describing a stack of coincident D3 branes in type IIB supergravity. This has the form

$$ds^2 = H(r)^{-1/2} dx_{1,3}^2 + H(r)^{1/2} \mathrm{d}r^2 + L^2 d\Omega_5^2, \tag{1.1.1}$$

where $H(r) = L^4/r^4$ and $d\Omega_5^2$ is the metric on S^5. The first two terms in (1.1.1) constitute the metric on AdS_5.

The first step on the journey towards the duals of more 'realistic' theories is to reduce the number of supersymmetries. A particularly successful approach has been to consider a more general transverse space, resulting in $AdS_5 \times X_5$, where X_5 is some Einstein space. The background is still AdS, and so the dual field theory is still conformal, but if $X_5 \neq S^5$ there will generically be less supersymmetry. Of interest here is the Klebanov-Witten (KW) case [8], which preserves $\mathcal{N} = 1$ supersymmetry. Here the transverse space is chosen to be $X_5 = (SU(2) \times SU(2))/U(1) = T^{1,1}$ in the notation of [9], which is topologically $S^2 \times S^3$. The resulting 6-dimensional transverse space is the conifold, with a metric of the form

$$\begin{aligned} ds_6^2 = \mathrm{d}r^2 + r^2 \Bigg[\frac{1}{6} \Big(\mathrm{d}\theta^2 + \sin^2\theta \mathrm{d}\varphi^2 + \sin^2\tilde{\theta} + \sin^2\tilde{\theta} \mathrm{d}\tilde{\varphi}^2 \Big) \\ + \frac{1}{9} \Big(\mathrm{d}\psi + \cos\theta \mathrm{d}\varphi + \cos\tilde{\theta} \mathrm{d}\tilde{\varphi} \Big)^2 \Bigg], \end{aligned} \tag{1.1.2}$$

while the overall metric on $AdS_5 \times T^{1,1}$ is still simply

$$ds^2 = H(r)^{-1/2} dx_{1,3}^2 + H(r)^{1/2} ds_6^2. \tag{1.1.3}$$

By adding 'fractional' D3 branes (D5 branes wrapped on a two-cycle) to obtain the Klebanov-Tseytlin (KT) solution [10, 11] we move away from AdS, and so break the conformal symmetry; we now have $H(r) \sim \log r/r^4$. Note that despite this the

background is still 'almost AdS' in the UV (large r) in the sense that we have only log-corrections to the original $H \sim 1/r^4$. As a result, in solutions like this we still have a good chance of understanding the dual gauge theory with some of the intuition from the original conformal case.

Unfortunately, the background is now singular in the IR. In fact the KW background already has a conical singularity at $r = 0$, and the situation is made worse by the modified from of the warp factor $H(r)$. We can fix this by going to the Klebanov-Strassler (KS) background [12], which replaces the conifold with the *deformed* conifold. This is warped such that $X_5 \sim S^3$ in the IR with the S^2 collapsing smoothly. The UV asymptotic behaviour is unchanged from KT.

The final step which is necessary to reach the starting point for most of the work described is to break some additional symmetry. The conifold metric (1.1.2) possesses a $\mathbb{Z}_2$ symmetry which interchanges $(\theta, \varphi) \leftrightarrow (\tilde{\theta}, \tilde{\varphi})$. Starting from KS, there is a one-dimensional family of solutions [13, 14] which break this symmetry. As we will see in chapter 3 this corresponds in the field theory to turning on a VEV, and the resulting family of solutions is known as the baryonic branch of KS.

1.2 Outline

The KS and baryonic branch solutions, together with the related Chamseddine-Volkov/Maldacena-Núñez (CVMN) [15, 16] backgrounds, provide a substantial amount of rich structure, dual to $\mathcal{N} = 1$ gauge theories. An example of some of this structure, together with a potential application, is discussed in chapter 5.

Starting from the KS-like solutions there are two obvious directions one could take in order to seek more 'realistic' (i.e. QCD-like) systems. The first would be to add flavour. In the case of the baryonic branch this was achieved in the solutions of [17]. Unfortunately, the solutions obtained, in addition to being singular in the IR, exhibit some unwanted UV behaviour. This can be seen, for example, in the behaviour of observables as calculated in chapter 2. The correct way to approach this problem was subsequently described in [18, 19].

In all the cases mentioned so far, the presence of some remaining supersymmetry played a critical role, both in simplifying the search for solutions and in guaranteeing their stability. Despite this, considerable progress has been made with respect to the problem of finding dual descriptions which completely lack supersymmetry. One natural way in which this can be achieved is by finding solutions in which a black hole is present, corresponding to a gauge theory at finite temperature [20]. See for example [21, 22, 23, 24].

Alternatively, one can consider field theories in which supersymmetry is softly broken by the insertion of relevant operators into the Lagrangian. By using as a starting point theories for which the duality is well understood, it is then possible to find dual gravity theories which are deformations of the SUSY case, as was achieved, for example, in [24, 25, 26, 27, 28, 29, 30, 31, 32].

In chapter 3 this approach is used to obtain a non-SUSY generalisation of the baryonic branch, yielding a two-dimensional parameter space. This is explored further in chapter 4.

In summary, chapter 2 demonstrates calculations of Wilson loops in a simple flavoured extension of the baryonic branch.

In chapter 3 we change focus to SUSY-breaking, and find a natural extension of the baryonic branch to a two-parameter family. After exploring the parameter space in more detail we turn in chapter 4 to an particular limit and note some interesting effects that occur when the SUSY-breaking is made large.

In chapter 5 we return to the SUSY baryonic-branch type backgrounds and consider a possible application to five-dimensional models. This serves as an example in order for us to demonstrate the numerical methods which are necessary for the study of these systems.

Chapter 2

Wilson Loops in Warped Resolved Deformed Conifolds

2.1 Introduction

We first present the work of [1], in which we consider the effect of adding flavour to some of the baryonic-branch-like solutions. One of the most important observables in a field theory is the Wilson loop [33], given by

$$W(\mathcal{C}) = \frac{1}{N_c} \operatorname{tr} P e^{i \oint_{\mathcal{C}} A}, \tag{2.1.1}$$

for a closed curve $\mathcal{C}$. In particular, the potential E of a quark-antiquark pair is given by the VEV of a Wilson loop. For a separation L, take the loop $\mathcal{C}$ to be a rectangle of sides L, $\mathcal{T}$, with $\mathcal{T} \to \infty$. Then the expectation value is simply given by the normal time-evolution operator, so that

$$\langle W(\mathcal{C}) \rangle \sim e^{-E\mathcal{T}}. \tag{2.1.2}$$

The Wilson loop is particularly significant in the context of gauge-string duality and the Maldacena conjecture [4], because it is accessible from the string side of the correspondence. For a review see [34]. As proposed in [35, 36], the associated quantity in the dual string theory is the action of a string world-sheet which ends on $\mathcal{C}$ at the boundary of the AdS space (Figure 2.1). That is

$$W(\mathcal{C}) = \int_{\partial F(\mathcal{C})} \mathcal{D}F e^{-S[F]}, \tag{2.1.3}$$

where F describes the fields of the string theory, with boundary values $\partial F(\mathcal{C})$. In the limit of strong coupling the result is that the Wilson loop corresponds to the area of a surface bounded by $\mathcal{C}$, extending into the bulk and forming the world-sheet of a classical string. This means that

$$\langle W(\mathcal{C}) \rangle \sim e^{-S_{\mathrm{NG}}}, \tag{2.1.4}$$

and referring to Equation 2.1.2, the energy of the quark-antiquark pair corresponds to the Nambu-Goto action of the string [34, 37]

$$E = \frac{S_{\mathrm{NG}}}{\mathcal{T}}. \tag{2.1.5}$$

This is divergent, and is renormalised by subtracting the (infinite) quark masses, given by the action of two rods from the ends of the string to the end of the space, as descibed in [36, 34, 37].

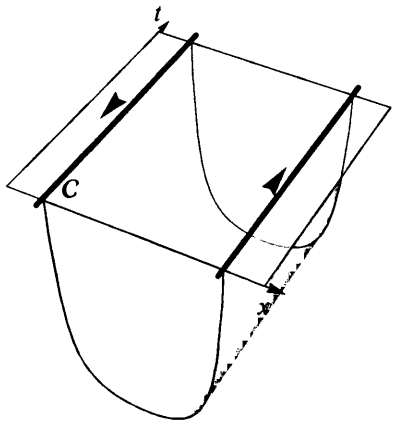

Figure 2.1: Schematic diagram of how the Wilson loop $\mathcal{C}$ (blue) relates to the world-sheet of a string extending into the bulk. The loop should be taken to extend an infinite distance in the t direction.

The aim is therefore to solve the equations of motion resulting from the action and so determine the shape of the string formed for a given L in a given background.

We first review the necessary methods, which have been discussed extensively in the literature (for example [35, 36]), and bring together some results which will be useful. In section 2.2 we discuss the equations of motion for a string, following the derivation in [37], and describe a generalisation to Dp-branes.

We discuss the possible behaviour of the function $E(L)$, and of the string shape in sections 2.3-2.4.

We then demonstrate the results of the preceding sections with respect to some well-understood backgrounds (section 2.5), before applying them to the flavoured resolved deformed conifold [17] in section 2.6.

2.2 The action and equations of motion

2.2.1 Action

We will consider backgrounds of the form

$$ds^2 = g_{\mu\nu}\mathrm{d}x^\mu \mathrm{d}x^\nu = -g_{tt}\mathrm{d}t^2 + g_{xx}\mathrm{d}\vec{x}^2 + g_{\rho\rho}\mathrm{d}\rho^2 + g_{ij}\mathrm{d}\theta^i \mathrm{d}\theta^j, \tag{2.2.1}$$

where g_{tt}, g_{xx} and $g_{\rho\rho}$ are functions only of ρ. Here and throughout this chapter we use the string frame. We will restrict our attention to p-dimensional objects which extend on time and one spatial Minkowski direction x, and probe the radial direction according to

$$x = x(X^1), \qquad \rho = \rho(X^1), \tag{2.2.2}$$

where we use world-volume coordinates X^α, $0 \leq \alpha \leq p$. For $p > 1$, the object also extends in the internal space described by the coordinates θ^i. We are interested only

in the static case, so we can identify $X^0 = t$. We follow the method of [37], with some slight generalisations. A more extensive discussion can be found in [34].

The action for such an object, with tension T_0, is

$$S = T_0 \int \mathrm{d}^{p+1} X e^{-\alpha\Phi} \sqrt{-\det G_{\alpha\beta}}, \tag{2.2.3}$$

where

$$G_{\alpha\beta} = g_{\mu\nu} \frac{\partial x^\mu}{\partial X^\alpha} \frac{\partial x^\nu}{\partial X^\beta} \tag{2.2.4}$$

is the induced metric on the world volume, and $\alpha = 1$ for a Dp brane, with $\alpha = 0$ otherwise. For the configuration described, the induced metric is

$$ds^2_{\text{induced}} = -g_{tt}(\mathrm{d}X^0)^2 + \left(g_{xx}x'^2 + g_{\rho\rho}\rho'^2\right)(\mathrm{d}X^1)^2 + G^{(p-1)}_{ab}\mathrm{d}X^a\mathrm{d}X^b, \tag{2.2.5}$$

$$G^{(p-1)}_{ab} = g_{ij} \frac{\partial\theta^i}{\partial X^a} \frac{\partial\theta^j}{\partial X^b}, \tag{2.2.6}$$

where $x' = \mathrm{d}x/\mathrm{d}X^1$. Writing the time interval as $\mathcal{T}$, the action (2.2.3) is then

$$S = T_0 \mathcal{T} \int \mathrm{d}^p X \; e^{-\alpha\Phi} \sqrt{g_{tt}\left(g_{xx}x'^2 + g_{\rho\rho}\rho'^2\right) \det G^{(p-1)}_{ab}}. \tag{2.2.7}$$

This can be written in a form corresponding to a 1-dimensional 'effective string' with tension $T_{\text{str}}(\rho)$. Defining $f(\rho)^2 = g_{tt}g_{xx}$ and $g(\rho)^2 = g_{tt}g_{\rho\rho}$,

$$S = \mathcal{T} \int \mathrm{d}X^1 \left(f\sqrt{x'^2 + \frac{g^2}{f^2}\rho'^2}\right) T_{\text{str}}, \tag{2.2.8}$$

where

$$T_{\text{str}}(\rho) = T_0 e^{-\alpha\Phi} \int \mathrm{d}^{p-1} X \sqrt{\det G^{(p-1)}_{ab}}. \tag{2.2.9}$$

This has a simple interpretation: The tension T_{str} is as expected the energy density on the effective string, while the factor

$$\mathrm{d}X^1 \, f\sqrt{x'^2 + \frac{g^2}{f^2}\rho'^2} \tag{2.2.10}$$

is the length element on a string embedded according to (2.2.2) in the geometry (2.2.1). The action (2.2.8) is therefore an obvious generalisation of the case considered in [34, 37] to a string with ρ-dependent tension. In fact (2.2.8) can also be obtained from the action used in [37, section II.A] by the replacements

$$f \to T_{\text{str}} f, \qquad g \to T_{\text{str}} g. \tag{2.2.11}$$

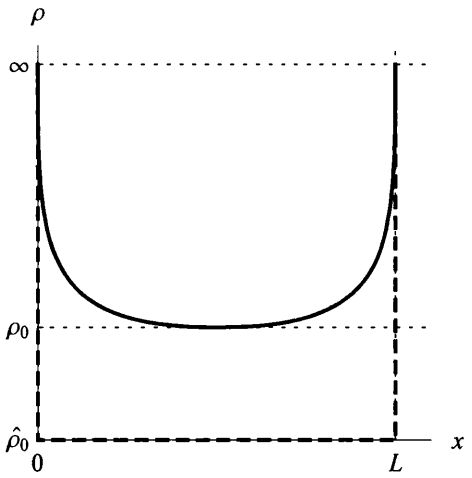

Figure 2.2: The generic shape of the effective string (solid line). The dashed line shows the 'free' solution (2.2.20), discussed in subsection 2.2.3.

2.2.2 Rescaled radial coordinate

The following discussion will be considerably simplified by the introduction of a rescaled coordinate R defined by

$$\frac{\mathrm{d}R}{\mathrm{d}\rho} = \frac{g}{f}. \tag{2.2.12}$$

Then the metric (2.2.1) becomes

$$ds^2 = -g_{tt}\mathrm{d}t^2 + \frac{f^2}{g_{tt}}\left(\mathrm{d}\vec{x}^2 + \mathrm{d}R^2\right) + g_{ij}\mathrm{d}\theta^i\mathrm{d}\theta^j, \tag{2.2.13}$$

and the action (2.2.8) is

$$S = \mathcal{T}\int \mathrm{d}X^1\,\sqrt{x'^2 + R'^2}\,T_{\text{eff}}, \tag{2.2.14}$$

where $T_{\text{eff}} = fT_{\text{str}}$. Notice we can interpret this action as being that of a string in any metric of the form

$$\mathrm{d}s^2_{\text{eff}} = -\gamma_{tt}\mathrm{d}t^2 + \gamma_{xx}(\mathrm{d}x^2 + \mathrm{d}R^2), \tag{2.2.15}$$

provided we give the string a tension equal to $T_{\text{eff}}/\sqrt{\gamma_{tt}\gamma_{xx}}$. In particular, interpreting T_{eff} itself as the string tension results in Minkowski space. The behaviour of the effective string is then described completely by the function T_{eff}. This is in contrast to the description in terms of the original metric in equations (2.2.1) and (2.2.13), for which the natural interpretation involved a geometric factor (2.2.10) as well as an R-dependent tension T_{str}.

Although useful in the general discussion, the integration involved in obtaining $R(\rho)$ means that this coordinate system will be difficult to apply to any specific case except for extremely simple backgrounds.

2.2.3 Equations of motion and separation

The derivation of the equation of motion from (2.2.14) is essentially the same as the calculation in [34, 37]. Imposing time independence, we get the single equation

$$C\frac{\mathrm{d}R}{\mathrm{d}X^1} = \pm\frac{\mathrm{d}x}{\mathrm{d}X^1}\sqrt{T_{\text{eff}}^2 - C^2}. \tag{2.2.16}$$

Parametrising the effective string as

$$X^1 = x, \qquad R = R(x), \tag{2.2.17}$$

we can integrate to obtain the shape of a string with a minimum radial coordinate at $R = R_0$. We impose $C = T_{\text{eff}}(R_0)$, and obtain

$$x(R) = \begin{cases} \displaystyle\int_R^{R_\infty} \mathrm{d}R' \frac{T_{\text{eff}}(R_0)}{\sqrt{T_{\text{eff}}(R')^2 - T_{\text{eff}}(R_0)^2}}, & 0 \le x \le \frac{L}{2}, \\ \displaystyle L - \int_R^{R_\infty} \mathrm{d}R' \frac{T_{\text{eff}}(R_0)}{\sqrt{T_{\text{eff}}(R')^2 - T_{\text{eff}}(R_0)^2}}, & \frac{L}{2} \le x \le L, \end{cases} \tag{2.2.18}$$

where

$$L(R_0) = 2\int_{R_0}^{R_\infty} \mathrm{d}R \frac{T_{\text{eff}}(R_0)}{\sqrt{T_{\text{eff}}(R)^2 - T_{\text{eff}}(R_0)^2}} \tag{2.2.19}$$

is the separation of the endpoints of the effective string and $R_\infty = R(\rho \to \infty)$. This is the same as is obtained by modifying the result of [37] according to the prescription (2.2.11).

In some cases we will find that $T(\hat{R}_0) = 0$, where $\hat{R}_0$ is the minimum radial coordinate contained in the space. Then there is an additional solution to (2.2.16) (with $C = 0$) which is not compatible with the parametrisation (2.2.17). This corresponds to a string which drops vertically from the endpoints and stretches horizontally along the 'bottom of the space', $R = \hat{R}_0$, as shown in Figure 2.2. A suitable parametrisation is

$$(x, R) = \begin{cases} (0,\ \hat{R}_0 - X^1), & X^1 \le 0, \\ (X^1,\ \hat{R}_0), & 0 \le X^1 \le L, \\ (L,\ \hat{R}_0 - L + X^1), & X^1 \ge L. \end{cases} \tag{2.2.20}$$

As we shall see, generically $L(R_0)$ has inversion points, and together with the possibility of the extra solution (2.2.20) this means that $R_0(L)$ can be multivalued. The different branches can be interpreted as corresponding to stable, metastable and unstable configurations for the effective string (see section 2.3).

2.2.4 Boundary conditions in the UV

When we consider a fundamental string we must enforce Dirichlet boundary conditions at $R \to R_\infty$, as described in [37]. This corresponds to the string ending on a D-brane at large R. Specifically, we require that

$$\frac{\mathrm{d}x}{\mathrm{d}X^1} \to 0 \tag{2.2.21}$$

for $R \to R_\infty$. Referring to (2.2.16) this means that we need

$$\lim_{R\to R_\infty} \frac{T_{\text{eff}}(R)^2 - C^2}{C^2} = \infty. \tag{2.2.22}$$

Recalling that we have imposed $C = T_{\text{eff}}(R_0)$ and that for a fundamental string $T_{\text{eff}} = f$, this becomes

$$\lim_{R\to R_\infty} \frac{f(R)^2 - f(R_0)^2}{f(R_0)^2} = \infty. \tag{2.2.23}$$

As this must hold for all R_0, we can simply require that

$$\lim_{R\to R_\infty} f(R) = \infty. \tag{2.2.24}$$

Although this condition is not required when the string is replaced by a D-brane, we will restrict our attention to those backgrounds in which (2.2.24) holds.

2.3 Energy and stability

As noted in section 2.1, energy of the quark-antiquark pair is simply given by $S/\mathcal{T}$, which as would be expected corresponds to the tension integrated along the string. This is in general infinite, and so we renormalise by subtracting the action of two vertical rods extending from $\hat{R}_0$ to infinity [36, 34, 38, 37]. For the smooth solution (2.2.18), which we can parametrise as $R(x)$, this gives

$$E(R_0) = 2\int_{R_0}^{R_\infty} \mathrm{d}R \sqrt{1 + \left(\frac{\mathrm{d}x}{\mathrm{d}R}\right)^2}\, T_{\text{eff}} - 2\int_{\hat{R}_0}^{R_\infty} \mathrm{d}R\, T_{\text{eff}}. \tag{2.3.1}$$

A rigourous discussion of this renormalisation procedure can be found in [38].

Using the equation of motion (2.2.16), this can be written

$$E(R_0) = 2\int_{R_0}^{R_\infty} \mathrm{d}R\, T_{\text{eff}}(R) \left[\frac{T_{\text{eff}}(R)}{\sqrt{T_{\text{eff}}(R)^2 - T_{\text{eff}}(R_0)^2}} - 1\right] - 2\int_{\hat{R}_0}^{R_0} \mathrm{d}R\, T_{\text{eff}}(R). \tag{2.3.2}$$

Given a form for the function $L(R_0)$ it is simple to obtain the qualitative behaviour of $E(L)$ without evaluating (2.3.2). Generalising the result obtained in [37, 39] using (2.2.11) we have that the force is

$$\frac{\mathrm{d}E}{\mathrm{d}L} = T_{\text{eff}}(R_0). \tag{2.3.3}$$

Given the reasonable assumption $T_{\text{eff}}(R_0)$ is continuous and positive this implies that the extrema of $E(R_0)$ correspond to those of $L(R_0)$, and to cusps in $E(L)$.

The possible presence of extrema in the function $L(R_0)$ raises the question of which branches of the solution represent stable classical configurations of the string for a given L. This is significant because the dominant contribution to the Wilson loop comes from the stable configuration with the minimal value of the action.

It was shown in [40] that the extrema also correspond to the boundaries between stable and unstable configurations (although additional regions of instability may exist due to fluctuations in the angular directions θ^i). Although this implies that only one side of the extremum describes a stable classical solution (as opposed to two stable configurations with different values of the action), it is not clear how to identify the physical branch. However, we can make progress if we assume that $T_{\text{eff}}(R_0)$ is always increasing with R_0. Referring to (2.3.3), this is equivalent to the statement that

$$\frac{\mathrm{d}}{\mathrm{d}R_0}\left[E'\big(L(R_0)\big)\right] > 0. \tag{2.3.4}$$

In terms of the function $E(L)$, we see that $E''(L)$ changes sign at each cusp (Figure 2.3), with $E''(L) > 0$ for the upper (higher E) branch and $E''(L) < 0$ for the lower. We can relate this to the concavity condition discussed in [41], namely that for a physical interaction between quarks we must have $E''(L) \leq 0$. We therefore expect that the upper branch at each cusp is unstable.

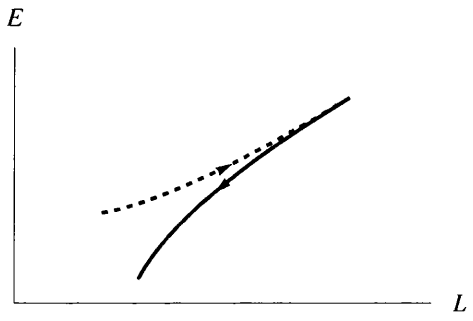

Figure 2.3: A generic cusp in $E(L)$. The concavity condition [41] leads us to expect that the upper (dotted) branch is unstable. The arrows show the direction of increasing R_0.

Probably the simplest form of behaviour occurs when $T_{\text{eff}}(\hat{R}_0) \neq 0$. By the argument of [42, 34] this means that $E(L)$ becomes linear at large L, corresponding to confinement. If $L(R_0)$ is decreasing for all R_0, we obtain the qualitatively simple behaviour exhibited, for example, by the Klebanov-Strassler [12] and Maldacena-Nunez [15] models. This is depicted schematically in Figure 2.4.

A useful example which illustrates more complicated behaviour is that of a string in the walking D5 background discussed in detail in [37]. There $L(R_0)$ has two local extrema, leading to two cusps in $E(L)$, as shown in Figure 2.5. We still have $T(\hat{R}_0) \neq 0$, and confinement is again seen for large L. In [37] an analogy with a van der Waals gas was proposed. This again suggests that the upper branch at the cusps, corresponding to $L'(R_0) > 0$, should be identified as unstable.

When $T_{\text{eff}}(\hat{R}_0) = 0$ we also obtain the second solution (2.2.20). As we renormalise by subtracting the action of two vertical rods, and there is no contribution to the energy from the part of the string with $R = \hat{R}_0$, this solution has $E = 0$ independent of L. This is the stable solution for sufficiently large L, so at large separations the endpoints of the string behave like free particles.

As pointed out in [40], this is analogous to the case of a soap film stretched between two circular rings. In fact, if $T_{\text{eff}}(R) \propto R$, corresponding to a string in

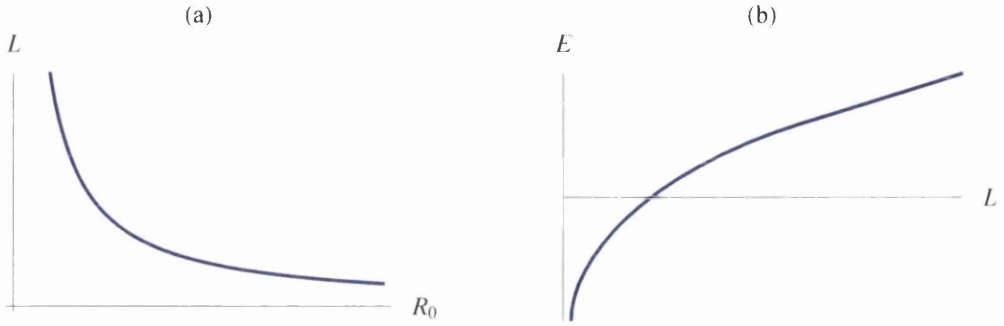

Figure 2.4: The qualitative behaviour of (a) $L(R_0)$ and (b) $E(L)$ in a simple confining case, such as Klebanov-Strassler.

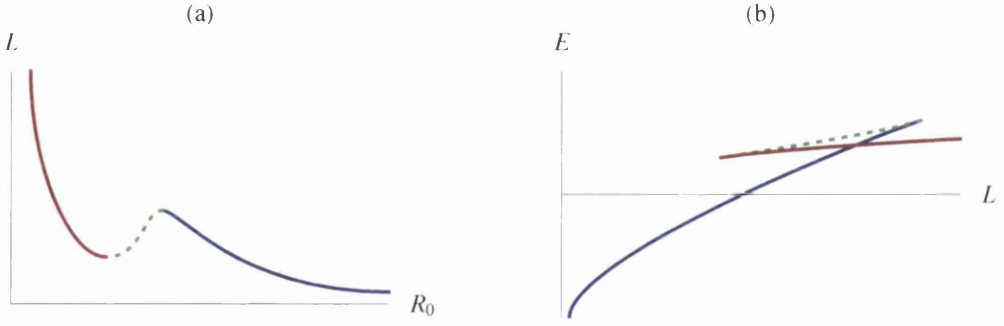

Figure 2.5: The qualitative behaviour of (a) $L(R_0)$ and (b) $E(L)$ in the 'van der Waals' case. The dotted region is unphysical and is expected to correspond to an unstable string configuration.

Rindler space, the analogy becomes exact [43], as the action (2.2.14) is then identical to that of the soap film. The 'free' solution (2.2.20) corresponds in the case of the soap film to a disconnected configuration, with the film forming a disc over each of the rings.

Additionally, when $R_0 = \hat{R}_0$ the integrand in (2.2.19) vanishes for all $R \neq R_0$. This means that unless the lower limit of the integral gives a non-zero contribution the separation given by the smooth solution (2.2.18) will go to zero as the string approaches the end of the space: $L(\hat{R}_0) = 0$. As can be seen from Figure 2.6, this can be considered a special case of the 'van der Waals' behaviour (Figure 2.5), in which the minimum in $L(R_0)$ moves to the origin.

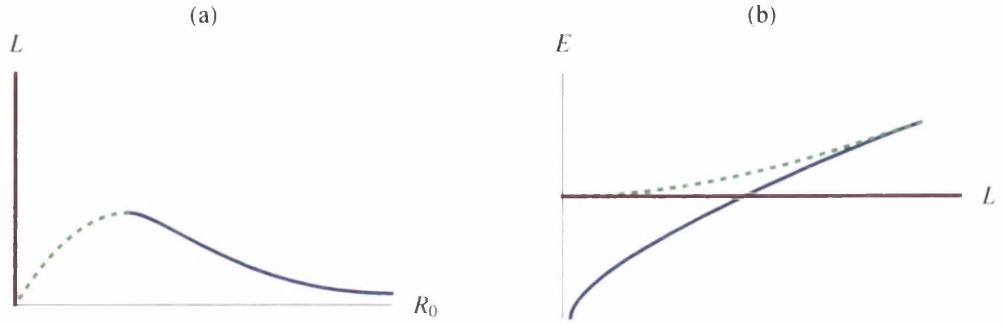

Figure 2.6: The qualitative behaviour of (a) $L(R_0)$ and (b) $E(L)$ in the 'soap film' case. The red region now corresponds to the solution (2.2.20).

If the lower limit of the integral in (2.2.19) diverges, the separation will diverge for $R_0 \to \hat{R}_0$ despite having $T_{\text{eff}}(\hat{R}_0) = 0$. This is the case for a string in $AdS_5 \times S^5$ [44, 45]. As before, we can consider this a special case of the 'soap film' case, with the maximum in $L(R_0)$ moving to $(R_0 = \hat{R}_0, L = \infty)$, as shown in Figure 2.7. This results in a qualitatively Coulombic potential (exact in the case of AdS.). The 'free' solution is now presumably metastable for all L.

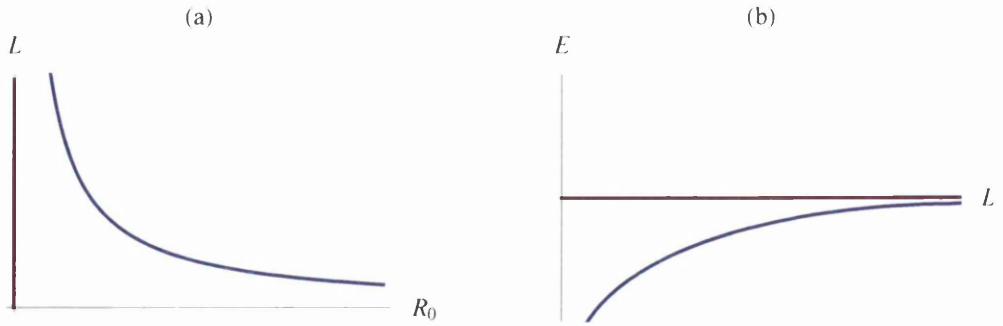

Figure 2.7: The qualitative behaviour of (a) $L(R_0)$ and (b) $E(L)$ in the 'Coulomb' case.

Finally, it is possible for any of these forms of behaviour to be further modified by the development of an additional local maximum and minimum, as in the 'van der Waals' case, Figure 2.5. This will again result in a pair of cusps.

2.4 General results on the behaviour of L and E for large R_0

2.4.1 Non-zero L for large R_0

In the discussion of section 2.3 it was implicitly assumed that $L \to 0$ for $R_0 \to R_\infty$. This is not always the case. We will find cases where we instead have $L \to L_\infty \neq 0$. Here we derive a condition which determines whether this occurs, and find the value of L_∞.

Assuming that $T(R_0) \to \infty$ for $R_0 \to R_\infty$, we can write the separation (2.2.19) as

$$L(R_0) = 2\int_{T_0}^{\infty} \mathrm{d}T \, \frac{T}{T'(R)} \frac{1}{T\sqrt{T^2/T_0^2 - 1}}, \tag{2.4.1}$$

where in this section we write $T \equiv T_{\text{eff}}(R)$ and $T_0 \equiv T_{\text{eff}}(R_0)$. Defining $t = T/T_0$, this is simply

$$L(R_0) = 2\int_{1}^{\infty} \mathrm{d}t \, \frac{t}{t'(R)} \frac{1}{t\sqrt{t^2 - 1}}, \tag{2.4.2}$$

in which the R_0 dependence is entirely contained in the factor

$$\frac{t}{t'(R)} = \frac{T(R(t, R_0))}{T'(R(t, R_0))}, \tag{2.4.3}$$

where the factors of T_0 from the definition of t cancel.

We are interested in the case when the separation is constant for large R_0. The integrand in (2.4.2) must therefore be a function only of t, which is equivalent to requiring that (2.4.3) is a function only of t for large R. That is

$$\frac{T}{T'(R)} = \mathcal{F}\left(\frac{T}{T_0}\right) \qquad \text{for } R \to R_\infty. \tag{2.4.4}$$

However, the left hand side is explicitly independent of R_0 so this can only be satisfied if $\mathcal{F}(t)$ is a constant. This gives the required condition: $L(R_0 \to R_\infty) =$ constant if and only if

$$\frac{T}{T'(R)} = \text{constant} \qquad \text{for } R \to R_\infty. \tag{2.4.5}$$

In this case we can take the factor T/T' out of the integral (2.4.2), and obtain the an expression for L_∞:

$$L_\infty \equiv \lim_{R_0 \to R_\infty} L(R_0) = \pi \lim_{R \to R_\infty} \left(\frac{T}{T'(R)}\right). \tag{2.4.6}$$

2.4.2 Energy for $L \to L_\infty$

The above calculation of L_∞ relied on the fact that the integral for $L(R_0)$ covers only the range $R_0 \leq R < R_\infty$. The integral (2.3.2) for $E(R_0)$ covers the whole range $\hat{R}_0 < R < R_\infty$, and so an analogous calculation is not possible. When

$L(R_0 \to R_\infty) \to$ constant, it is however possible to find a condition which determines whether $E(R_0 \to R_\infty) \to$ constant.

Referring to (2.4.6), for large R we can write

$$\frac{T}{T'(R)} = \frac{L_\infty}{\pi} + \Delta'(T(R)), \tag{2.4.7}$$

where $\Delta'(T(R)) \to 0$ for $R \to R_\infty$, so that by (2.4.2)

$$L(R_0) = L_\infty + 2\int_1^\infty \mathrm{d}t\ \Delta'(T(t, R_0))\frac{1}{t\sqrt{t^2-1}}. \tag{2.4.8}$$

The energy is given by (2.3.2), which becomes

$$E(R_0) = 2\int_{T_0}^\infty \mathrm{d}T\ \left[\frac{L_\infty}{\pi} + \Delta'(T)\right]\left(\frac{T}{\sqrt{T^2-T_0^2}} - 1\right) - 2\int_{\hat{T}_0}^\infty \mathrm{d}T\ \left[\frac{L_\infty}{\pi} + \Delta'(T)\right], \tag{2.4.9}$$

where $\hat{T}_0 \equiv T_{\text{eff}}(\hat{R}_0)$. After evaluating some integrals this can be written as

$$E(R_0) = \frac{2L_\infty \hat{T}_0}{\pi} + 2\Delta(\hat{T}_0) - 2\Delta(T_0) + 2\int_{T_0}^\infty \mathrm{d}T\ \Delta'(T)\left(\frac{T}{\sqrt{T^2-T_0^2}} - 1\right). \tag{2.4.10}$$

The first two terms are constants, and the last two, which contain the R_0 dependence, involve only the region $R_0 \le R < R_\infty$. Whether the energy approaches a constant is therefore determined by the large R behaviour of $\Delta'(T(R))$. The condition is that $E(R_0) \to$ constant for $R_0 \to R_\infty$ if and only if $\Delta'(T)$ vanishes at least as fast as

$$\Delta'(T) \sim \frac{1}{T^{1+\epsilon}}, \qquad \epsilon > 0 \tag{2.4.11}$$

for $T \to \infty$.

The generalisation of the discussion of section 2.3 to account for non-zero L_∞ is simple. In general there is a region with $L < L_\infty$ in which the 'free' solution (2.2.20) is the stable one, as in Figure 2.8. If there is a minimum, so that $L(R)$ approaches the asymptote from below, then there is an additional (presumably unstable) branch as in Figure 2.8 (c,d).

However, in some cases $L(R)$ is always increasing, as in Figure 2.8 (e,f). In this case the considerations discussed in section 2.3 suggest that the 'free' solution is the only stable one for all L.

2.5 Application to specific cases

The results obtained above are not immediately useful when we are interested in a specific background, as opposed to general considerations. This is because, as was noted in subsection 2.2.2, the integral

$$R(\rho) = \int^\rho \mathrm{d}\rho' \frac{g(\rho')}{f(\rho')} \tag{2.5.1}$$

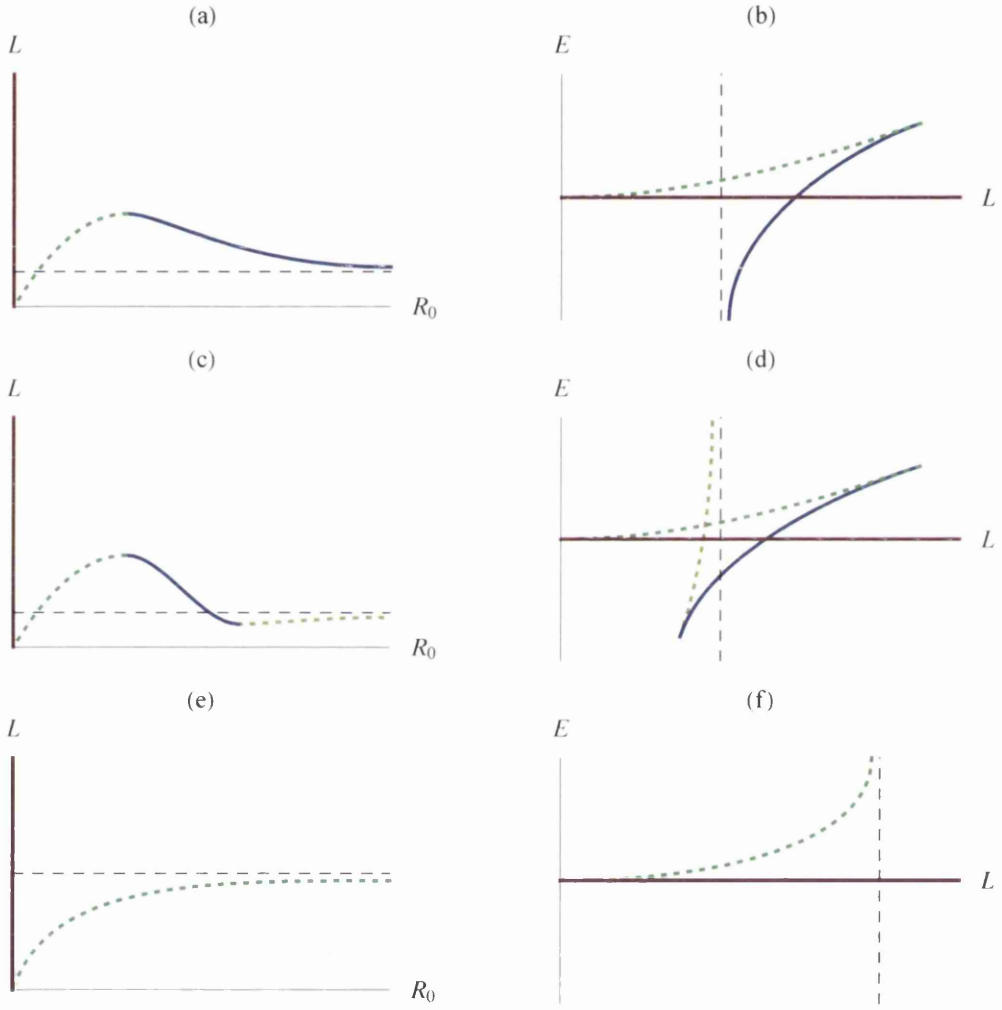

Figure 2.8: The qualitative behaviour of $L(R_0)$ and $E(L)$ in the 'soap film' case when $L(R_\infty) \neq 0$.

is either difficult or impossible to evaluate analytically in all but the simplest cases. The results of sections 2.2-2.4 are easily generalised to allow the more general coordinate ρ, by the insertion of factors of

$$\frac{\mathrm{d}R}{\mathrm{d}\rho} = \frac{g}{f}. \tag{2.5.2}$$

In particular,

$$L(\rho_0) = 2\int_{\rho_0}^{\infty} \mathrm{d}\rho\, \frac{g(\rho)}{f(\rho)} \frac{T_{\mathrm{eff}}(\rho_0)}{\sqrt{T_{\mathrm{eff}}(\rho)^2 - T_{\mathrm{eff}}(\rho_0)^2}}, \tag{2.5.3}$$

$$E(\rho_0) = 2\int_{\rho_0}^{\infty} \mathrm{d}\rho\, \frac{g(\rho)T_{\mathrm{eff}}(\rho)}{f(\rho)} \left[\frac{T_{\mathrm{eff}}(\rho_0)}{\sqrt{T_{\mathrm{eff}}(\rho)^2 - T_{\mathrm{eff}}(\rho_0)^2}} - 1\right] - 2\int_{\hat{\rho}_0}^{\rho_0} \mathrm{d}\rho\, \frac{g(\rho)T_{\mathrm{eff}}(R)}{f(\rho)}. \tag{2.5.4}$$

Similarly, (2.4.6) is more conveniently written

$$L_\infty = \pi \lim_{\rho\to\infty} \frac{T_{\mathrm{eff}}(\rho)}{T'_{\mathrm{eff}}(\rho)} \frac{g(\rho)}{f(\rho)}. \tag{2.5.5}$$

2.5.1 The Klebanov-Strassler model

To demonstrate these ideas, we will look at the case of a string in the Klebanov-Strassler background [12], for which the behaviour is well-understood [46]. This is a convenient, relatively simple, example of a theory which results in confining behaviour for large L.

If we restrict our attention to 1-dimensional objects, we need only the non-compact part of the metric,

$$ds^2 = h^{-1/2}\mathrm{d}x_{1,3}^2 + \frac{1}{6}\epsilon^{4/3}\frac{h^{1/2}}{K^2}\mathrm{d}\rho^2 + \mathrm{d}s_{\mathrm{int}}^2, \tag{2.5.6}$$

where

$$h(\rho) = \alpha\frac{2^{2/3}}{4}\int_{\rho}^{\infty} \mathrm{d}x\, \frac{x\coth x - 1}{\sinh^2 x}(\sinh 2x - 2x)^{1/3}, \tag{2.5.7}$$

$$K(\rho)^3 = \frac{\sinh 2\rho - 2\rho}{2\sinh^3\rho}. \tag{2.5.8}$$

The functions appearing in the action (2.2.8) are

$$\begin{aligned} f(\rho)^2 &= h^{-1}, \\ g(\rho)^2 &= \frac{\epsilon^{4/3}}{6K^2}, \end{aligned} \tag{2.5.9}$$

while for a string $T_{\mathrm{eff}} = f$.

For small ρ, we have

$$h = h_0 - h_2\rho^2 + \cdots, \qquad g \sim \frac{1}{K} = g_0 + g_2\rho^2 + \cdots. \tag{2.5.10}$$

Then the contribution from the lower limit of the integral (2.5.3) is

$$L(\rho_0) = \int_{\rho_0} \frac{g_0 h_0}{\sqrt{h_2}} \frac{1}{\sqrt{\rho^2 - \rho_0^2 + \cdots}}, \tag{2.5.11}$$

so that L diverges logarithmically for $\rho_0 \to 0$. Using (2.3.3), we find that for small ρ_0

$$E'(L) \to T_{\text{eff}}(0) = \text{constant}, \tag{2.5.12}$$

as expected for a confining theory.

The results described in section 2.4 have limited application to this case, as L simply approaches zero for large ρ_0. The relevant function (2.5.5) is for large ρ

$$\frac{T_{\text{eff}}(\rho)}{T'_{\text{eff}}(\rho)} \frac{g(\rho)}{f(\rho)} = \frac{g(\rho)}{f'(\rho)} \sim \sqrt{\rho} e^{-\rho/3}. \tag{2.5.13}$$

To obtain the behaviour over the full range of ρ it is necessary to integrate (2.5.3-2.5.4) numerically. The result is shown in Figure 2.9. The expected confining behaviour is seen for large L, and the form is qualitatively that of Figure 2.4.

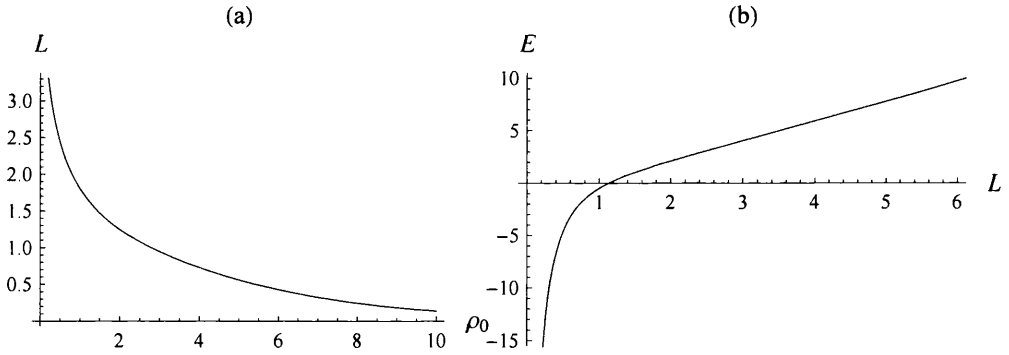

Figure 2.9: Plots of (a) $L(\rho_0)$ and (b) $E(L)$ for a string in the Klebanov-Strassler background (2.5.6-2.5.8), obtained numerically.

2.5.2 AdS_5-Schwarzschild $\times$ S^5

An example which produces the 'soap film' behaviour (Figure 2.6) is the large mass limit of the AdS_5-Schwarzschild black hole, expected to describe finite-temperature $\mathcal{N} = 4$ SYM [20]. This was discussed in [45, 44, 46].

The metric is

$$ds^2 = \frac{r^2}{\mathcal{R}^2}\left[-\left(1 - \frac{\mu^4}{r^4}\right) \mathrm{d}t^2 + \mathrm{d}\vec{x}^2\right] + \frac{\mathcal{R}^2}{r^2}\left(1 - \frac{\mu^4}{r^4}\right)^{-1} \mathrm{d}r^2 + \mathcal{R}^2 \mathrm{d}\Omega_5^2, \tag{2.5.14}$$

so that $g(r) = 1$ and

$$f(r) = \frac{1}{\mathcal{R}^2}\sqrt{r^4 - \mu^4}. \tag{2.5.15}$$

The horizon is at $\hat{r}_0 = \mu$, and we will consider strings, for which $T_{\text{eff}} = f$. Then $T_{\text{eff}}(r) \to 0$ for $r \to \hat{r}_0$, as is necessary for the'soap film' behaviour.

This background is in fact simple enough that we can obtain the rescaled coordinate $R(r)$ exactly, although not in a form which is particularly useful. We have

$$\frac{\mathrm{d}R}{\mathrm{d}r} = \frac{g}{f} = \frac{\mathcal{R}^2}{\sqrt{r^4 - \mu^4}}, \tag{2.5.16}$$

and so we can define

$$R(r) \equiv \mathcal{R}^2 \int_\mu^r \frac{\mathrm{d}r'}{\sqrt{r'^4 - \mu^4}} = \frac{\sqrt{\pi}\Gamma\left(\frac{5}{4}\right)}{\Gamma\left(\frac{3}{4}\right)}\frac{\mathcal{R}^2}{\mu} - \frac{\mathcal{R}^2}{r}\,{}_2F_1\left(\frac{1}{4}, \frac{1}{2}; \frac{5}{4}; \frac{\mu^4}{r^4}\right). \tag{2.5.17}$$

This results in $R(\hat{r}_0) = 0$ and

$$R_\infty \equiv R(r \to \infty) = \frac{\sqrt{\pi}\Gamma\left(\frac{5}{4}\right)}{\Gamma\left(\frac{3}{4}\right)}\frac{\mathcal{R}^2}{\mu}. \tag{2.5.18}$$

To find the behaviour for large r we need the function

$$\frac{T(r)}{T'(r)}\frac{g}{f} = \frac{\mathcal{R}^2}{2}\frac{\sqrt{r^4 - \mu^4}}{r^3} \underset{r\to\infty}{\to} \frac{\mathcal{R}^2}{2r}. \tag{2.5.19}$$

Referring to section 2.4 we see that this will result in $L(r_0) \to 0$ for $r_0 \to \infty$.

We can write the separation in the form of (2.4.1), as

$$L(r_0) = \mathcal{R}T_{\text{eff}}(r_0)\int_{T_{\text{eff}}(r_0)}^\infty \mathrm{d}T_{\text{eff}}\left[T_{\text{eff}}^2 + \frac{\mu^4}{\mathcal{R}^4}\right]^{-3/4}\frac{1}{\sqrt{T_{\text{eff}}^2 - T_{\text{eff}}(r_0)^2}} \tag{2.5.20}$$

For small r, $T_{\text{eff}}(r) \to 0$, and so the lower limit of the integral contributes

$$L(r_0) = \mathcal{R}T_{\text{eff}}(r_0)\int_{T_{\text{eff}}(r_0)} \frac{\mathcal{R}^3}{\mu^3}\frac{1}{\sqrt{T_{\text{eff}}^2 - T_{\text{eff}}(r_0)^2}} \sim T_{\text{eff}}(r_0)\log T_{\text{eff}}(r_0) \underset{r_0\to\hat{r}_0}{\to} 0. \tag{2.5.21}$$

It is actually possible to evaluate (2.5.20) exactly, resulting in

$$L(r_0) = \frac{2\sqrt{\pi}\Gamma\left(\frac{3}{4}\right)}{\Gamma\left(\frac{1}{4}\right)}\frac{\mathcal{R}^2}{(r^4 - \mu^4)^{1/4}}\,{}_2F_1\left(\frac{3}{4}, \frac{3}{4}; \frac{5}{4}; -\frac{\mu^4}{r^4 - \mu^4}\right). \tag{2.5.22}$$

Together with the function $E(L)$, obtained numerically, this is shown in Figure 2.10. The relationship to Figure 2.6 is clear.

2.6 The flavoured resolved deformed conifold

Having discussed the necessary techniques and general results, we can turn to the main material presented in this chapter. The analysis of [47] describes a system of solutions related by a chain of dualities, together with a boost in eleven dimensions. More specifically, the 'unrotated' solution, obtained by setting the boost parameter $\beta = 0$, corresponds D5 branes wrapping the S^2 of the resolved conifold [48], and

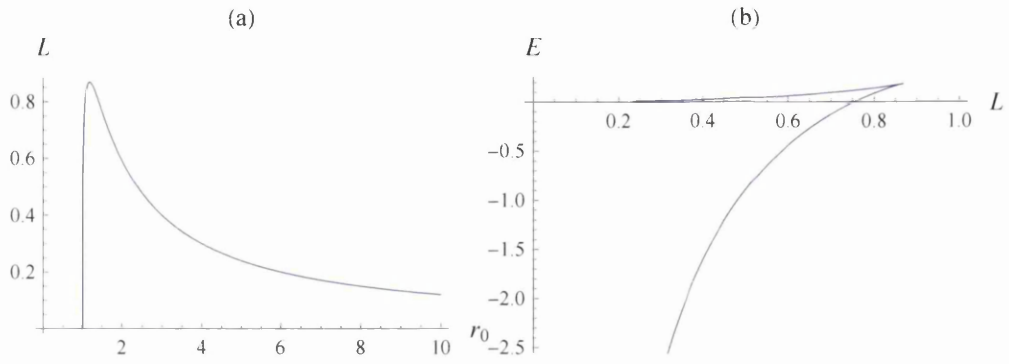

Figure 2.10: Plots of (a) $L(r_0)$ and (b) $E(L)$ for a string in the AdS_5-Schwarzschild$\times$ S^5 background (2.5.14), for $\mu = \mathcal{R} = 1$.

is a simpler limit of the solution with general β as introduced in [13]. This has additional D3 brane charges which are not present in the 'unrotated' case.

Taking the limit $\beta \to \infty$, we obtain the 'rotated' solution, which describes the baryonic branch of the Klebanov-Strassler theory.

The metric is of the form

$$ds^2 = h^{-1/2}\mathrm{d}x_{1,3}^2 + e^{2\Phi}h^{1/2}ds_6^2. \tag{2.6.1}$$

The warp factor is related to the dilaton by

$$h = e^{-2\Phi} - e^{-2\Phi_\infty}\tanh\beta, \tag{2.6.2}$$

where Φ_∞ is the asymptotic value of Φ for large ρ.

These expressions also apply in the flavoured generalisation, described in [17]. However, the ρ-dependence of the functions is different. Most significantly, the solutions are now singular in the IR: $\Phi \to -\infty$ for $\rho \to 0$.

Turning to the UV, we find that to leading order $\Phi(\rho)$ is unchanged by the addition of flavours. However, the form of (2.6.2) is such that in the 'rotated' case ($\beta \to \infty$), $h(\rho)$ is sensitive to the sub-leading behaviour of Φ. The 'rotated' solution therefore has different UV asymptotics in the flavoured case. This is interpreted in [17] as resulting from smeared source D3 branes, uniformly distributed in ρ. These result from the action of the 'rotation' on the source D5 branes, in the same way as in the unflavoured case the 'rotated' solution has bulk D3 branes resulting from the colour D5 branes in the 'unrotated' solution.

The aim here is to use the methods discussed in the previous sections to assess the physical significance of these changes with respect to the unflavoured solutions. The changes in the UV asymptotics can be isolated by considering strings which do not descend close to $\rho = 0$. The results derived in section 2.4 will therefore apply.

It appears more difficult to isolate the effects of the IR singularity, as the string always probes the large ρ region as well. However, in most cases we will find that the effective tension T_{eff} vanishes for small ρ. As discussed in section 2.3, this means that only the lower limit of the integral (2.2.19) contributes to $L(\rho)$. The limiting behaviour of $L(\rho_0)$ for small ρ_0 is therefore presumably insensitive to changes to the UV.

2.6.1 The solutions

We will now define the solutions of interest more concretely. The metric is of the form

$$\begin{aligned} ds^2 &= h^{-1/2}\mathrm{d}x_{1,3}^2 + e^{2\Phi}h^{1/2}ds_6^2, \\ ds_6^2 &= e^{2k}\mathrm{d}\rho^2 + e^{2q}(\omega_1^2+\omega_2^2) + \frac{1}{4}e^{2g}\left[(\tilde{\omega}_1 + a\omega_1)^2 + (\tilde{\omega}_2 - a\omega_2)^2\right] + \frac{1}{4}e^{2k}(\tilde{\omega}_3+\omega_3)^2, \end{aligned} \tag{2.6.3}$$

where

$$\begin{aligned} \omega_1 &= \mathrm{d}\theta, & \tilde{\omega}_1 &= \cos\psi\,\mathrm{d}\tilde{\theta} + \sin\psi\,\sin\tilde{\theta}\,\mathrm{d}\tilde{\varphi}, \\ \omega_2 &= \sin\theta\,\mathrm{d}\varphi, & \tilde{\omega}_2 &= -\sin\psi\,\mathrm{d}\tilde{\theta} + \cos\psi\,\sin\tilde{\theta}\,\mathrm{d}\tilde{\varphi}, \\ \omega_3 &= \cos\theta\,\mathrm{d}\varphi, & \tilde{\omega}_3 &= \mathrm{d}\psi + \cos\tilde{\theta}\,\mathrm{d}\tilde{\varphi}. \end{aligned}$$

The coefficient functions $\{\Phi, g, k, q, a\}$ depend only on ρ, and as above

$$h = e^{-2\Phi} - e^{-2\Phi_\infty}\tanh\beta. \tag{2.6.4}$$

The coefficient functions were shown in [49, 50] to be given by

$$e^{2q} = \frac{1}{4}\frac{P^2-Q^2}{P\cosh\tau - Q}, \qquad e^{2g} = P\cosh\tau - Q, \qquad a = \frac{P\sinh\tau}{P\cosh\tau - Q}, \tag{2.6.5}$$

and the BPS equations reduce (after some choices for constants of integration) to

$$\begin{aligned} \sinh\tau &= \frac{1}{\sinh 2\rho}, \\ Q &= \frac{2N_\mathrm{c} - N_\mathrm{f}}{2}(2\rho\cosh\tau - 1), \\ e^{4(\Phi-\Phi_0)} &= \frac{4}{(P^2-Q^2)e^{2k}\sinh^2\tau}, \\ e^{2k} &= \frac{1}{2}(P' + N_\mathrm{f}), \end{aligned} \tag{2.6.6}$$

together with

$$P'' + (P'+N_\mathrm{f})\left(\frac{P'+Q'+2N_\mathrm{f}}{P-Q} + \frac{P'+Q'+2N_\mathrm{f}}{P+Q} - 4\cosh\tau\right) = 0. \tag{2.6.7}$$

The solution discussed in [17] is given by the asymptotic behaviour of $P(\rho)$,

$$P = \begin{cases} h_1\rho + \frac{4N_\mathrm{f}}{3}\left[-\rho\log\rho - \frac{1}{12}\rho\log(-\log\rho) + \mathcal{O}\left(\frac{\rho\log(-\log\rho)}{\log\rho}\right)\right] + \mathcal{O}(\rho^3\log\rho), & \rho\to 0 \\ ce^{4\rho/3} + \frac{9N_\mathrm{f}}{8} + \frac{1}{c}\left[(2N_\mathrm{c}-N_\mathrm{f})^2\left(\rho^2 - \rho + \frac{13}{16}\right) - \frac{81N_\mathrm{f}^2}{64}\right]e^{-4\rho/3} + \mathcal{O}(\rho e^{-8\rho/3}), & \rho\to\infty, \end{cases} \tag{2.6.8}$$

where the two arbitrary constants h_1 and c are related in a non-trivial way.

The full solution to (2.6.7) can then be found numerically, interpolating between the two regimes in (2.6.8).

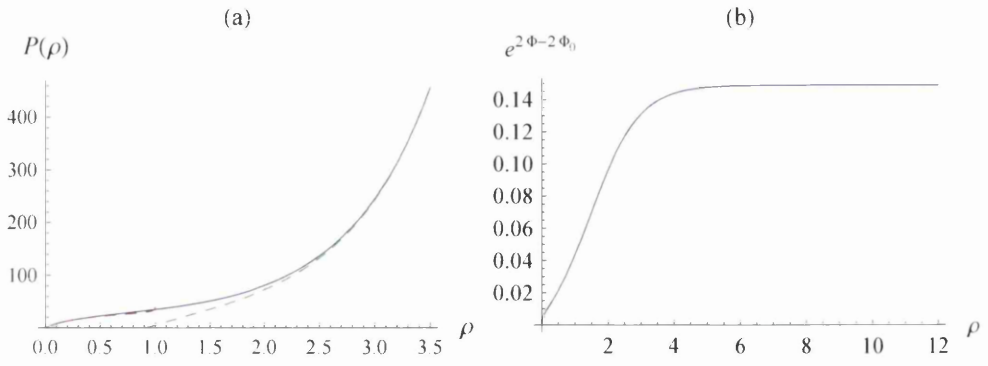

Figure 2.11: The generic behaviour of (a) $P(\rho)$ and (b) $\Phi(\rho)$, obtained numerically. The red and green dashed curves show the first few terms of the expansions (2.6.8) for small and large ρ respectively.

2.6.2 The 'rotated' case

The functions appearing in the action (2.2.8) are

$$\begin{aligned} f(\rho)^2 = h^{-1} &= \frac{1}{e^{-2\Phi} - e^{-2\Phi_\infty}\tanh\beta}, \\ g(\rho)^2 &= e^{2\Phi+2k}. \end{aligned} \tag{2.6.9}$$

To obtain $f(\rho \to \infty) \to \infty$, as required by the boundary conditions for a string (subsection 2.2.4) we therefore require the limit $\beta \to \infty$. This is the 'rotated' solution, described in [17] as the field theory limit.

Fundamental string

In the case of a fundamental string we simply have $T_{\text{eff}} = f/2\pi\alpha'$. We first consider strings which descend deep into the space. For small ρ, the functions we need have the asymptotic behaviour [17, Appendix B]

$$e^{4(\Phi-\Phi_0)} = \frac{27}{2N_{\text{f}}^3}(-\log\rho)^{-3}\left[1 + \mathcal{O}\left(\frac{\log(-\log\rho)}{-\log\rho}\right)\right], \tag{2.6.10}$$

$$e^{2k} = \frac{2N_{\text{f}}}{3}(-\log\rho)\left[1 + \mathcal{O}\left(\frac{\log(-\log\rho)}{-\log\rho}\right)\right]. \tag{2.6.11}$$

Writing $2\pi\alpha' = 1$ this results in

$$T_{\text{eff}}(\rho) = f(\rho) = \left(\frac{27}{2N_{\text{f}}^3}\right)^{1/4} e^{\Phi_0}(-\log\rho)^{-3/4}\left[1 + \mathcal{O}\left(\frac{\log(-\log\rho)}{-\log\rho}\right)\right]. \tag{2.6.12}$$

In particular, $T_{\text{eff}}(0) = 0$, so we generically expect qualitatively 'soap film' behavior as in Figure 2.6, or one of the modifications discussed subsequently. The 'free' solution (2.2.20), with $\rho_0 = 0$, exists for all L. In the case of the the smooth solution (2.2.18) the separation is given, as in section 2.4, by

$$L(\rho_0) = 2\int_1^\infty \mathrm{d}t\ \frac{t}{t'(R)}\frac{1}{t\sqrt{t^2-1}}. \tag{2.6.13}$$

Generalising this to allow us to continue working with ρ rather than R, we can write

$$L(\rho_0) = 2\int_1^{t(\rho_*)} \mathrm{d}t\, \frac{t}{t'(\rho)}\frac{g(\rho)}{f(\rho)}\frac{1}{t\sqrt{t^2-1}} + 2\int_{t(\rho_*)}^{\infty} \mathrm{d}t\, \frac{t}{t'(\rho)}\frac{g(\rho)}{f(\rho)}\frac{1}{t\sqrt{t^2-1}}, \tag{2.6.14}$$

where we have split the integral at an arbitrary point $\rho = \rho_*$ As $T_{\text{eff}}(0) = 0$, the limit $\rho_0 \to 0$ results in

$$t(\rho_*) \equiv \frac{T_{\text{eff}}(\rho_*)}{T_{\text{eff}}(\rho_0)} \to \infty. \tag{2.6.15}$$

The separation is then

$$L(\rho_0 \to 0) = 2\int_1^{\infty} \mathrm{d}t\, \frac{t}{t'(\rho)}\frac{g(\rho)}{f(\rho)}\frac{1}{t\sqrt{t^2-1}}. \tag{2.6.16}$$

This integral covers only the range $0 < \rho < \rho_*$. As ρ_* was arbitrary, we can take the limit $\rho_* \to 0$ and evaluate (2.6.16) exactly using the small-ρ asymptotic expression for $tg/t'f$. Then, using (2.6.10-2.6.11),

$$\frac{t(\rho)}{t'(\rho)}\frac{g(\rho)}{f(\rho)} = \frac{g(\rho)}{f'(\rho)} = \frac{4}{3}\sqrt{\frac{2N_{\text{f}}}{3}}\rho(-\log\rho)^{3/2}\left[1 + \mathcal{O}\left(\frac{\log(-\log\rho)}{-\log\rho}\right)\right]. \tag{2.6.17}$$

We also have

$$t = \frac{f(\rho)}{f(\rho_0)} = \left(\frac{\log\rho_0}{\log\rho}\right)^{3/4} + \cdots, \tag{2.6.18}$$

so

$$\frac{tg}{t'f} = \frac{4}{3}\sqrt{\frac{2N_{\text{f}}}{3}}\rho_0(-\log\rho_0)^{3/2}e^{t^{-4/3}}t^{-2} + \cdots, \tag{2.6.19}$$

and

$$L(0) = \frac{4}{3}\sqrt{\frac{2N_{\text{f}}}{3}}\left[\lim_{\rho_0\to 0}\rho_0(-\log\rho_0)^{3/2}\int_1^{\infty}\mathrm{d}t\, \frac{e^{t^{-4/3}}}{t^3\sqrt{t^2-1}}\right]. \tag{2.6.20}$$

The integral is finite, so $L(0) = 0$, as in Figure 2.6 and Figure 2.8.

We now turn to the behaviour of strings with large ρ_0. For large ρ, the metric functions are

$$e^{4(\Phi-\Phi_\infty)} = 1 - \frac{3N_{\text{f}}}{c}e^{-4\rho/3} + \frac{3}{16c^2}\left[(2N_{\text{c}} - N_{\text{f}})^2(1-8\rho) + 297N_{\text{f}}^2\right]e^{-8\rho/3} + \mathcal{O}\left(e^{-4\rho}\right), \tag{2.6.21}$$

$$e^{2k} = \frac{2c}{3}e^{4\rho/3}\left[1 + \frac{3N_{\text{f}}}{4c}e^{-4\rho/3} + \mathcal{O}\left(\rho^2 e^{-8\rho/3}\right)\right], \tag{2.6.22}$$

where

$$e^{2\Phi_\infty} = \sqrt{\frac{3}{2}}\frac{e^{2\Phi_0}}{c^{3/2}}. \tag{2.6.23}$$

This results in

$$f = \sqrt{\frac{2c}{3N_{\rm f}}} e^{\Phi_\infty} e^{2\rho/3} \left\{ 1 + \frac{1}{32cN_{\rm f}} \left[(2N_{\rm c} - N_{\rm f})^2 (1 - 8\rho) + 216 N_{\rm f}^2 \right] e^{-4\rho/3} + \mathcal{O}\left(e^{-8\rho/3}\right) \right\}, \tag{2.6.24}$$

$$g = \sqrt{\frac{2c}{3}} e^{\Phi_\infty} e^{2\rho/3} \left[1 - \frac{3N_{\rm f}}{8c} e^{-4\rho/3} + \mathcal{O}\left(\rho^2 e^{-8\rho/3}\right) \right]. \tag{2.6.25}$$

We again need the function $tg/t'f$, which for large ρ is

$$\frac{tg}{t'f} = \frac{3}{2}\sqrt{N_{\rm f}} - \frac{3}{64c\sqrt{N_{\rm f}}} \left[(2N_{\rm c} - N_{\rm f})^2 (8\rho + 11) - 249 N_{\rm f}^2 \right] e^{-4\rho/3} + \mathcal{O}\left(\rho^2 e^{-8\rho/3}\right). \tag{2.6.26}$$

Using (2.5.5), for large ρ the separation therefore approaches

$$L_\infty = \frac{3\pi}{2}\sqrt{N_{\rm f}}. \tag{2.6.27}$$

Notice that setting $N_{\rm f} = 0$ recovers the more usual behaviour, with $L \to 0$ for $\rho \to \infty$.

If we include the next term of the expansion (2.6.26) in the integral (2.4.2), we get

$$L(\rho_0) = L_\infty - 2\int_1^\infty {\rm d}t \, \frac{\epsilon(\rho(t,\rho_0))}{t\sqrt{t^2-1}} + \cdots, \tag{2.6.28}$$

where

$$\epsilon(\rho) = \frac{3(2N_{\rm c} - N_{\rm f})^2}{8c\sqrt{N_{\rm f}}} \rho e^{-4\rho/3} > 0. \tag{2.6.29}$$

This means that L approaches L_∞ from below. Together with the fact that the smooth solution has $L(0) = 0$, the result is behaviour which is qualitatively that of Figure 2.8 (c-f). In the case $N_{\rm f} = 0$, we obtain the more normal situation, with $L \to 0$.

For the behaviour of E, we need the function $\Delta'(T_{\rm eff})$, defined in (2.4.7). In this case, for large ρ we simply have

$$\begin{aligned} \Delta'(T_{\rm eff}) &= -\epsilon(\rho(T_{\rm eff})) + \mathcal{O}(e^{-4\rho/3}) \\ &= -\frac{3(2N_{\rm c} - N_{\rm f})^2}{8N_{\rm f}} \sqrt{\frac{3}{2c}} \frac{\log T_{\rm eff}}{T_{\rm eff}^2} + \mathcal{O}\left(\frac{1}{T_{\rm eff}^2}\right). \end{aligned} \tag{2.6.30}$$

This satisfies the condition (2.4.11), so the energy approaches a constant for large ρ. More precisely, (2.4.10) results in

$$E(\rho_0) = E_\infty - \frac{3(2N_{\rm c} - N_{\rm f})^2}{4N_{\rm f}} \sqrt{\frac{3}{2c}} (2\pi - 3) \frac{\log(T_{\rm eff}(\rho_0))}{T_{\rm eff}(\rho_0)} + \mathcal{O}\left(\frac{1}{T_{\rm eff}(\rho_0)}\right), \tag{2.6.31}$$

where

$$E_\infty \equiv 2\Delta(0) = 2\int_0^\infty {\rm d}T_{\rm eff} \left[\frac{L_\infty}{\pi} - \frac{T_{\rm eff}}{T'_{\rm eff}(R)} \right] \tag{2.6.32}$$

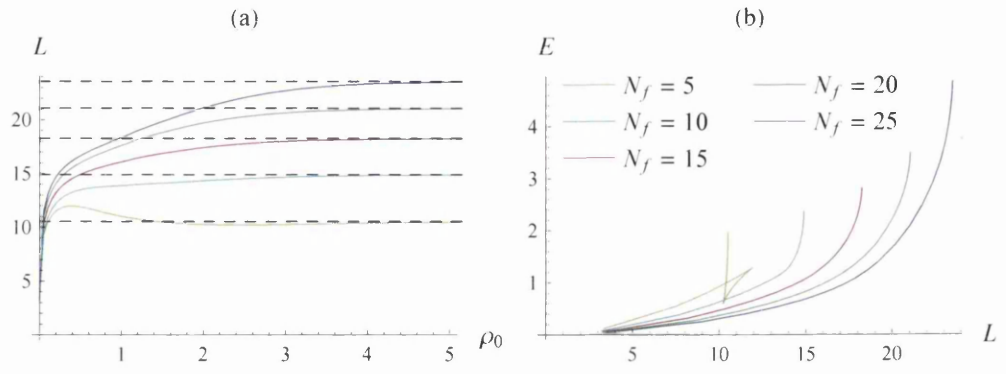

Figure 2.12: The results of the numerical calculation of (a) $L(\rho_0)$ and (b) $E(L)$ for a string in the 'rotated' background, for various values of N_f. Here $N_\mathrm{c} = 10$ and $h_1 = 25$, resulting in values of c in the range $2.8 \lesssim c \lesssim 5.5$, depending on N_f.

is a constant.

The numerical calculation (Figure 2.12) confirms this, and reveals that a local maximum and minimum occur in $L(\rho)$ for small N_f, while for large N_f we find that $L(\rho)$ is always increasing, so that $E(L)$ is smooth. In all the cases calculated $E > 0$ for all L, and so the stable configuration is presumably the 'free' solution (2.2.20).

Note that because a finite upper limit (in this case $\rho_1 = 20$) is needed for the integrals, the numerical calculations cannot be trusted for large ρ. In particular, the numerical integration of (2.5.3) will always yield $L(\rho_1) = 0$. The plots in Figure 2.12 have been terminated before L decreases significantly away from L_∞.

By evaluating (2.2.18) numerically, we can determine the shape of the string. This is shown in Figure 2.13. Of the strings shown all are unstable, except that with $N_\mathrm{f} = 5$, $\rho_0 = 1$, which falls within the region between the cusps in $E(L)$ (Figure 2.12) and so is metastable.

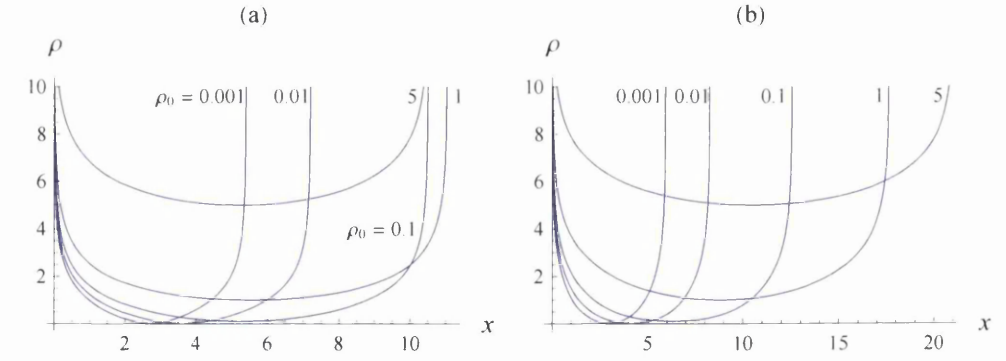

Figure 2.13: The shapes of strings with varying ρ_0. Here the parameters are as in Figure 2.12, with (a) $N_\mathrm{f} = 5$ and (b) $N_\mathrm{f} = 20$.

D3 brane

The 't Hooft loop can be obtained by replacing the string in the above discussion with a D3 brane [50], with

$$\theta = \tilde{\theta}, \qquad \varphi = 2\pi - \tilde{\varphi}, \qquad \psi = \pi. \tag{2.6.33}$$

As described in section 2.2, we therefore need to calculate

$$T_{\text{eff}}(\rho) = T_{\text{D3}} e^{-\Phi} f \int \mathrm{d}^2 X \, \sqrt{\det G^{(2)}_{ab}}, \tag{2.6.34}$$

where

$$G^{(2)}_{ab} = g_{ij} \frac{\partial \theta^i}{\partial X^a} \frac{\partial \theta^j}{\partial X^b} \tag{2.6.35}$$

is the internal part of the induced metric on the D3 brane. If we choose the parametrisation $\{X^2 = \theta, X^3 = \varphi\}$, we obtain from (2.6.3)

$$G^{(2)}_{ab} \mathrm{d}X^a \mathrm{d}X^b = h^{1/2} e^{2\Phi} \left[e^{2q} + \frac{1}{4} e^{2g} (a-1)^2 \right] \left(\mathrm{d}\theta^2 + \sin^2\theta \, \mathrm{d}\varphi^2 \right). \tag{2.6.36}$$

Setting $T_{\text{D3}} = 1$ for convenience, this results in

$$T_{\text{eff}} = 4\pi e^{\Phi} \left[e^{2q} + \frac{1}{4} e^{2g} (a-1)^2 \right]. \tag{2.6.37}$$

Again using the asymptotic expansions in [17], this is

$$T_{\text{eff}} = \begin{cases} 8\pi e^{\Phi_0} \rho^2 \left(-\dfrac{2N_{\text{f}}}{3} \log\rho \right)^{1/4} \left[1 + \mathcal{O}\left(\dfrac{\log(-\log\rho)}{\log\rho} \right) \right], & \rho \to 0, \\ 2\pi c e^{\Phi_\infty} e^{4\rho/3} \left\{ 1 + \dfrac{1}{4c} \left[(2N_{\text{c}} - N_{\text{f}})\rho + \dfrac{3N_{\text{f}}}{4} \right] e^{-4\rho/3} + \mathcal{O}(e^{-2\rho}) \right\}, & \rho \to \infty. \end{cases} \tag{2.6.38}$$

As $T_{\text{eff}}(0) = 0$ we generically expect the smooth solution to have $L(0) = 0$, as in the case of the string, but to be sure it would again be necessary to evaluate the integral (2.6.16).

To obtain the large ρ_0 behaviour, we again need the ρ-dependence of $T_{\text{eff}} g / T'_{\text{eff}} f$, and in this case we get an asymptotically constant separation

$$L_\infty = \frac{3\pi}{4} \sqrt{N_{\text{f}}}, \tag{2.6.39}$$

which is equal to half that obtained for the string.

The results of the numerical calculations are shown in Figure 2.14. The behaviour is qualitatively similar to that of the string (Figure 2.12), with the exception of the fact that in this case L approaches L_∞ from above. Although this appears to be an insignificant difference when viewed in terms of $L(\rho_0)$, the effect is that E decreases for large ρ_0. This means that there is a (small) range of L for which the smooth configuration is stable.

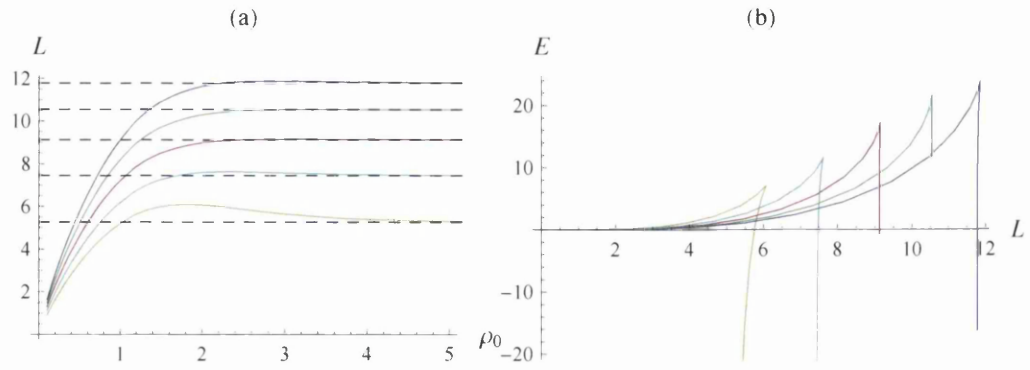

Figure 2.14: The results of the numerical calculation of (a) $L(\rho_0)$ and (b) $E(L)$ for a D3 brane in the 'rotated' background. The parameters have the same values as in Figure 2.12. Note that the endpoints of the curves were determined by the limitations of the numerical calculation.

D1 brane

For a D1 brane the effective tension is

$$T_{\text{eff}} = e^{-\Phi} f, \tag{2.6.40}$$

where we set $T_{\text{D1}} = 1$. By (2.6.21), we see that for large ρ the tension approaches a constant multiple of that of the fundamental string,

$$T_{\text{eff}}^{\text{D1}} \to e^{-\Phi_\infty} T_{\text{eff}}^{\text{string}}. \tag{2.6.41}$$

The asymptotic value of L depends on the ratio $T_{\text{eff}}/T'_{\text{eff}}$ and is therefore the same as in the case of the string,

$$L_\infty = \frac{3\pi}{2}\sqrt{N_{\text{f}}}. \tag{2.6.42}$$

For $\rho \to 0$, we can write

$$f = e^{\Phi}\left[1 + \frac{1}{2}e^{2(\Phi-\Phi_\infty)} + \mathcal{O}\left(e^{4(\Phi-\Phi_\infty)}\right)\right], \tag{2.6.43}$$

which results in

$$T_{\text{eff}} = 1 + \frac{3}{2}\left(-\frac{N_{\text{f}}}{c}\log\rho\right)^{-3/2} + \mathcal{O}\left(\frac{\log(-\log\rho)}{(-\log\rho)^{5/2}}\right). \tag{2.6.44}$$

As $T_{\text{eff}}(0) \neq 0$, the integrand in (2.5.3) is non-zero for $\rho \neq 0$, meaning that $L(0) \neq 0$. The contribution from the lower limit is of the form

$$\int_0 \mathrm{d}\rho\ (-\log\rho)^{-3/2}, \tag{2.6.45}$$

which is finite. The separation is therefore finite and non-zero for $\rho_0 = 0$, and the 'free' solution (2.2.20) does not exist. It is unfortunately not possible to determine $L(0)$ analytically, because it would be necessary to evaluate the integral (2.5.3) over the whole range $0 \leq \rho < \infty$.

The results of the numerical calculations are shown in Figure 2.15. The behaviour for large ρ_0 is confining, as expected when $T_{\text{eff}} \neq 0$.

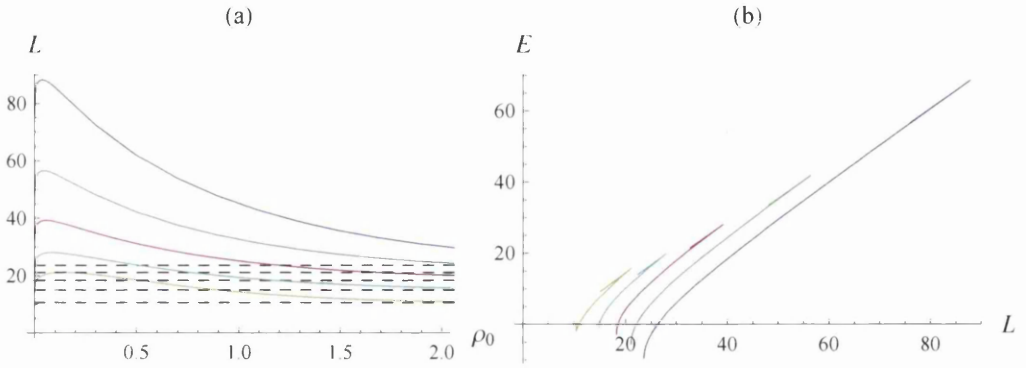

Figure 2.15: The results of the numerical calculation of (a) $L(\rho_0)$ and (b) $E(L)$ for a D1 brane in the 'rotated' background. The parameters have the same values as in Figure 2.12. As before, the endpoints of the curves were determined by the limitations of the numerical calculation; the behaviour corresponds to that shown in Figure 2.8 (a-b).

2.6.3 The 'unrotated' case

In the case with $\beta \to 0$, the metric is simply

$$ds^2 = e^{\Phi}\left(\mathrm{d}x_{1,3}^2 + ds_6^2\right), \tag{2.6.46}$$

and $f = e^{\Phi}$. However, generically $\Phi \to$ constant for large ρ, and so the boundary condition (2.2.24) is not satisfied without $\beta \to \infty$. This problem can be overcome by taking the limit $c \to 0$, which can be considered the flavoured generalisation of the solutions discussed in [15]. This case was discussed in [50], from which we obtain the asymptotic expansion for large ρ,

$$P = |2N_c - N_f|\,\rho\left[1 + \frac{N_f}{2\,|2N_c - N_f|}\frac{1}{\rho} + \mathcal{O}\left(\frac{1}{\rho^2}\right)\right]. \tag{2.6.47}$$

For small ρ the solution is unchanged from (2.6.8). Using (2.6.6) this results in

$$\begin{aligned} f = e^{\Phi} &= A e^{\Phi_0}\rho^{-1/4}e^{\rho}\left[1 + \mathcal{O}(\rho^{-1})\right], \\ g = e^{\Phi+k} &= \frac{A}{\sqrt{2}}\sqrt{|2N_c - N_f| + N_f}\,\rho^{-1/4}e^{\rho}\left[1 + \mathcal{O}(\rho^{-1})\right], \end{aligned} \tag{2.6.48}$$

where

$$\frac{1}{A^4} = \frac{1}{2}(|2N_c - N_f| + N_f)^2\,|2N_c - N_f|\,. \tag{2.6.49}$$

In this limit we still have $f \to \infty$ for $\rho \to \infty$, so (2.2.24) is satisfied.

For the purposes of our discussion, the only difference between the 'rotated' and 'unrotated' backgrounds is

$$f^{-2}_{\text{unrotated}} = e^{-2\Phi}, \qquad f^{-2}_{\text{rotated}} = e^{-2\Phi} - e^{-2\Phi_\infty}. \tag{2.6.50}$$

For small ρ we have $\Phi \to -\infty$, and so f is unchanged by the 'rotation'. The discussion of the previous section resulting in $L(0) = 0$ for the string and D3 brane therefore also applies in the 'unrotated' case.

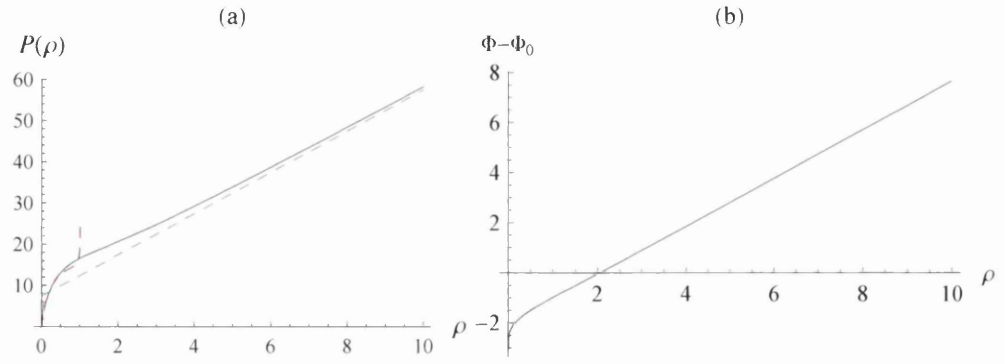

Figure 2.16: The behaviour of (a) $P(\rho)$ and (b) $\Phi(\rho)$ with $c \to 0$, showing the linear behaviour (2.6.47-2.6.48) for large ρ.

Fundamental string

Using (2.6.48), and the fact that for a fundamental string $T_{\text{eff}} = f$, we find that for large ρ,

$$\frac{tg}{t'f} = \frac{g(\rho)}{f'(\rho)} = \frac{1}{\sqrt{2}}\sqrt{|2N_c - N_f| + N_f}\left[1 + \mathcal{O}(\rho^{-1})\right], \tag{2.6.51}$$

so that the separation is asymptotically

$$L_\infty = \frac{\pi}{\sqrt{2}}\sqrt{|2N_c - N_f| + N_f}. \tag{2.6.52}$$

The calculations here apply also in the case $N_f = 0$. However, unlike in the 'rotated' case, here $L_\infty \neq 0$ even with zero flavour.

The numerical calculation again results in the expected modified 'soap film' behaviour (as in Figure 2.8), as shown in Figure 2.17.

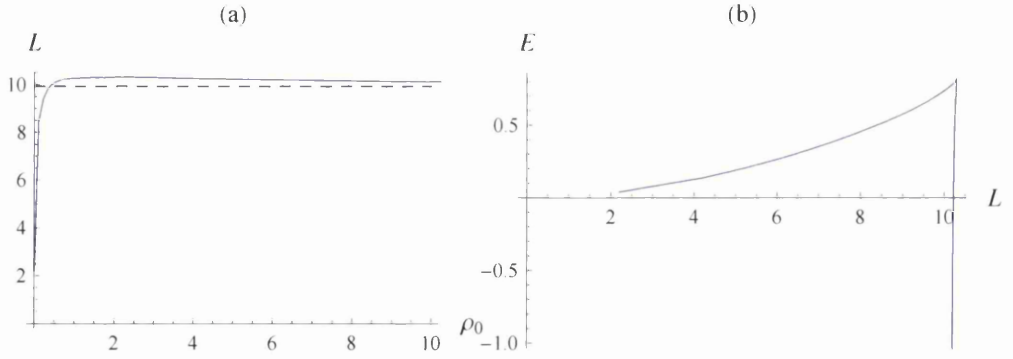

Figure 2.17: The results of the numerical calculation of (a) $L(\rho_0)$ and (b) $E(L)$ for a string in the 'unrotated' background, with $N_c = 10$ and $N_f = 15$. To obtain the linear behaviour (2.6.47), $h_1 \approx 11.198$, so as to give $c = 0$.

D3 brane

The internal space is unaffected by the 'rotation', so the D3 brane effective tension is still given by (2.6.37). However, we now have the limit $c \to 0$, so the large-ρ asymptotic expression (2.6.38) is no longer valid. Instead, using the asymptotic solutions in [50],

$$T_{\text{eff}} = 2\pi A e^{\Phi_0} |2N_c - N_f| \rho^{3/4} e^{\rho} \left[1 + \mathcal{O}\left(\frac{1}{\rho}\right)\right]. \tag{2.6.53}$$

Together with (2.6.48), this results in

$$L_\infty = \frac{\pi}{\sqrt{2}} \sqrt{|2N_c - N_f| + N_f}, \tag{2.6.54}$$

as for the fundamental string.

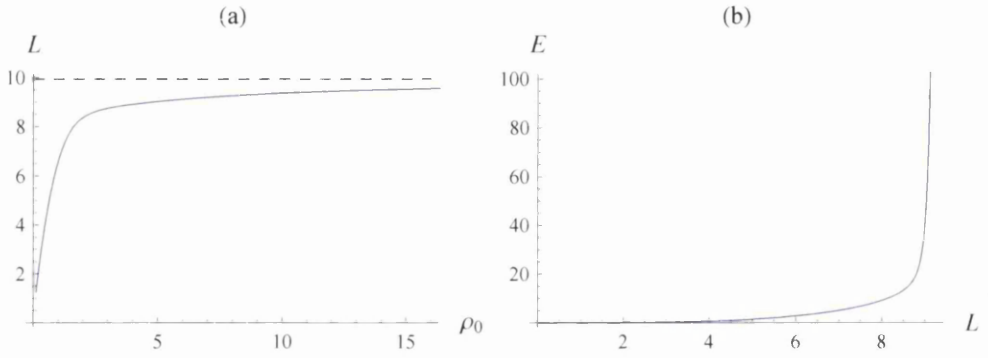

Figure 2.18: The results of the numerical calculation of (a) $L(\rho_0)$ and (b) $E(L)$ for a D3 brane in the 'unrotated' background. The parameters have the same values as in Figure 2.17.

D1 brane

In the 'unrotated' background a D1 brane has constant tension

$$T_{\text{eff}} = T_{\text{D1}} e^{-\Phi} f = T_{\text{D1}}. \tag{2.6.55}$$

The minimum-energy solution to (2.2.16) is then simply a string which does not descend into the bulk, resulting in confining behaviour $E = T_{\text{D1}} L$.

2.6.4 Discussion

Qualitatively, the clearest result of the preceding analysis is the unusual behaviour seen in the flavoured solutions for small ρ_0. For both strings and D3 branes we find the 'soap film' behaviour shown in Figure 2.6, the primary result of which is that at large separations the only solution to the equation of motion (2.2.16) is the 'free' solution (2.2.20). This not particularly unusual; it is also seen, for example, in the case of the AdS_5-Schwarzschild $\times S^5$ background discussed in subsection 2.5.2.

In section 2.3 we related this behaviour to the fact that the effective tension vanishes for $R_0 = \hat{R}_0$. It seems reasonable to suppose that this change relative to the unflavoured case is related to the introduction of the IR singularity. For example, in the case of the fundamental string we have $T_{\text{eff}}(\rho_0) \sim e^{\Phi}(\rho_0)$ for small ρ_0, and we see that this effect follows immediately from the fact that the dilaton diverges, $\Phi(\rho) \to -\infty$, for small ρ.

The modified behaviour for large ρ_0 manifests itself in the fact that the separation goes to a non-zero constant for large $\rho_0 \to \infty$. This is also simplest when considered in the context of the fundamental string, so that $T_{\text{eff}} \propto f$. In that case the condition (2.4.5) for constant separation in the UV becomes

$$\frac{g(r)}{f'(r)} = \text{constant} \qquad \text{for } r \to r_\infty, \tag{2.6.56}$$

for a generic radial coordinate r. In terms of the specific radial coordinate ρ used above the condition becomes even simpler. From equations (2.6.24) and (2.6.48), we see that in the UV f is an exponential function of ρ, so that $f'(\rho) \sim f(\rho)$, and the relevant condition is

$$\frac{g(\rho)}{f(\rho)} = \text{constant} \qquad \text{for } \rho \to \infty. \tag{2.6.57}$$

It is clear that the constant-separation behaviour results from a precise cancellation between the functions f and g. This can be viewed as the fact that the 'exponential' coordinate ρ becomes identical (up to a constant) to the rescaled coordinate R introduced in subsection 2.2.2.

As taking $\rho_0 \to \infty$ does not result in $L(\rho_0) \to 0$, we find that the UV of the field theory (small separations) is no longer described by the large-ρ region of the bulk theory. This is in contrast to the normal behaviour, and in particular that in the unflavoured case, where increasing ρ_0 corresponds to decreasing L.

Instead, for separations less than some critical value the 'free' solution is stable, as is the case for large separations. In particular $L = 0$ corresponds to a string reaching straight down to $\rho = 0$, which can be considered a degenerate case of both the 'free' and smooth solutions. Aside from this, the smooth solution describes at most only a small range of separations, and in many cases is unstable for all L. This describes non-interacting particles.

Given that in the 'unrotated' solutions the unusual large-ρ_0 behavior persists in the limit $N_{\text{f}} = 0$, it is difficult to argue that in the 'rotated' case it is a result of the introduction of the IR singularity by adding flavours.

However, it is not clear how much of this behaviour is physical. In particular, we might expect that resolving the IR singularity would result in $L(\hat{R}_0) \neq 0$, presumably giving a confining IR as in the unflavoured case (see the 'van der Waals' case, Figure 2.5). Unless we also then have $L \to 0$ for $R \to R_\infty$ we would generically expect a minimum separation, which would be difficult to understand physically.

2.6.5 The resolution

Subsequent work [19, 18] clarifies the interpretation of the strange UV behaviour. In [19] the IR singularity was cured by adding flavour sources according to a density profile $S(\rho)$ which varies radially, vanishing in the IR. The method used to generate

the solutions discussed above essentially corresponds to instead having a constant profile. However, in [18] it was shown that the effective density of D3 charge goes like $e^{4\rho/3}S$ for large ρ, and so the naive 'constant' profile used above results in an exponentially enhanced density in the UV. When a more natural profile which decays correctly in the UV is used, the expected behaviour is seen in the Wilson loops [51].

Chapter 3

Breaking SUSY on the Baryonic Branch

3.1 Introduction and Summary

We now turn the second line of inquiry discussed in chapter 1: breaking supersymmetry.

The various successes of the gauge-gravity duality, while more numerous and spectacular in highly (super)symmetric theories, are not restricted to examples of this sort. As a matter of fact, there are many applications where black holes (and hence dual field theories at finite temperature) play a fundamental role. In these cases the dynamics is neither driven by SUSY nor by conformal symmetry.

As a result, an interesting problem is to construct backgrounds duals to field theories where supersymmetry has been broken in a soft way. These systems should conserve some of the dynamics of the SUSY case with the addition of the deformations by relevant operators that break the supersymmetry. The low energy dynamics should then be determined by a combination of SUSY and non-SUSY effects. This is an interesting problem, on which it seems feasible to make progress.

In this chapter [2, 3], we will construct duals to field theories in four dimensions where SUSY has been explicitly and softly broken by the addition of relevant operators to the Lagrangian. The original field theories will be those obtained by a twisted compactification of five branes wrapping a calibrated two cycle in the resolved conifold and those obtained by studying the dynamics of D3 and fractional D5 branes on the tip of a conifold. Both are non-conformal theories with interesting low energy dynamics (confinement, R-symmetry breaking, formation of domain walls, k-strings, etc.)

We will construct our non-SUSY backgrounds by finding an explicit solution of the Einstein, dilaton and RR-form equations of motion. We also impose that irrelevant operators are absent from the dynamics and that the string backgrounds are regular all along the space.

These will then be examples of backgrounds dual to the strongly coupled dynamics of well understood SUSY field theories in which SUSY has been softly and controllably broken. Some examples of this sort have appeared in the past for deformations of well-known SUSY backgrounds, see for example [26].

We will find that the non-SUSY solutions share much of the structure of the SUSY baryonic branch. This enables us to investigate in detail the solution space to

which these backgrounds belong. By consideration of the asymptotic expansions we find a two-dimensional parameter space which includes several previously studied solutions. In addition to the SUSY baryonic branch (and its limits, CVMN and KS itself), we also find the non-SUSY solutions of [24] and [32] as limiting cases. By combining the structure described in [24] with that of the SUSY baryonic branch, it is possible to describe a generic non-SUSY solution in terms of transitions between regions in which SUSY and non-SUSY effects dominate.

Additionally, we find some interesting special cases, one corresponding to a natural non-SUSY generalisation of KS itself, and the other to solutions in which SUSY is no longer *softly* broken and the UV does not match the SUSY case asymptotically.

We begin in section 3.2 by reviewing relevant aspects of the SUSY baryonic branch and CVMN solutions. In section 3.3 we turn to the non-SUSY solutions. First we review the solutions of [24], obtained as a deformation of the CVMN background, before moving on to the main solutions of interest — the generalisation of the baryonic branch obtained in [2]. The details of the numerical work necessary to find the solutions can be found in appendices A.4 and A.5. In section 3.4 we discuss the structure of the solution space. We first discuss the behaviour of generic solutions, and then concentrate on various special cases and limits.

We then discuss in more detail various properties of the generic non-SUSY solutions (at least for small values of the SUSY-breaking parameters). First, in section 3.5 we calculate the ADM Energy of the new solutions (with the SUSY solutions as reference backgrounds). Then in section 3.6 we perform a detailed study of various field theory quantities, whose strong-coupling result points us to an interpretation of the dual field theory being deformed by the insertion of relevant operators, like gaugino masses that break SUSY and may also influence VEVs.

3.2 The SUSY system

3.2.1 Overview

Here we present two field theories, which although on the face of it appear different, are in fact connected via 'higgsing' (as discussed in [47, 7]). The two theories are firstly that found when N_c D5-branes are wrapped on the 2-cycle of the resolved conifold ('theory A'), and secondly the baryonic branch of the Klebanov-Strassler quantum field theory ('theory B').

Theory A is given by performing a special twisted compactification (to four dimensions), of six dimensional $SU(N_c)$ supersymmetric Yang-Mills with 16 supercharges, preserving only 4 of them. It was studied in [15, 52, 53] and has a field content (in the four dimensional language) consisting of a massless vector multiplet alongside a 'Kaluza-Klein' tower of massive chiral and vector multiplets. The form of the Lagrangian, the weakly coupled mass spectrum and degeneracies of the theory are written in [52, 53]. The local and global symmetries are

$$SU(N_c) \times SU(2)_L \times SU(2)_R \times U(1)_R, \tag{3.2.1}$$

where the R-symmetry is anomalous, breaking $U(1)_R \to \mathbb{Z}_{2N_c}$.

Theory B is a quiver with gauge group $SU(n+N_c) \times SU(n)$ and bifundamental matter multiplets A_i, B_α with $i, \alpha = 1, 2$. The global symmetries are (where again,

the R-symmetry is anomalous)

$$SU(2)_L \times SU(2)_R \times U(1)_B \times U(1)_R. \tag{3.2.2}$$

These bifundamentals transform under the local and global symmetries as

$$A_i = \left(n + N_c,\ \bar{n},\ 2,\ 1,\ 1,\ \tfrac{1}{2}\right), \qquad B_\alpha = \left(\bar{n} + \bar{N}_c,\ n,\ 1,\ 2,\ -1,\ \tfrac{1}{2}\right). \tag{3.2.3}$$

There is a superpotential which can be written as $W = \frac{1}{\mu}\epsilon_{ij}\epsilon_{\alpha\beta}\ \mathrm{tr}[A_i B_\alpha A_j B_\beta]$. The field theory is taken to be close to a strongly coupled fixed point at high energies and it can be shown that the anomalous dimension should be $\gamma_{A,B} \sim -\frac{1}{2}$. This field theory is known to be dual to the Klebanov-Strassler (KS) background [12] and its generalization to the baryonic branch [13].

The connection between theories A and B is via 'higgsing' as mentioned above. If we give a (classical) baryonic vacuum expectation value to the fields (A_i, B_α) and then expand around it, we find that the degeneracies and field content of [52, 53] are recovered.

In terms of the Type IIB string backgrounds dual to each of the field theories, this weakly coupled field theory connection is manifest as a U-duality [47] (and was further studied in [7, 17, 54, 55, 56]). The first background (dual to theory A) can be presented using the vielbeins

$$\begin{aligned}
&E^{x_i} = e^{\frac{\Phi}{4}} dx_i, \qquad E^{\rho} = e^{\frac{\Phi}{4}+k} d\rho, \qquad E^{\theta} = e^{\frac{\Phi}{4}+h} d\theta, \qquad E^{\varphi} = e^{\frac{\Phi}{4}+h} \sin\theta d\varphi, \\
&E^1 = \frac{1}{2} e^{\frac{\Phi}{4}+g}(\tilde{\omega}_1 + a d\theta), \qquad E^2 = \frac{1}{2} e^{\frac{\Phi}{4}+g}(\tilde{\omega}_2 - a \sin\theta d\varphi), \\
&E^3 = \frac{1}{2} e^{\frac{\Phi}{4}+k}(\tilde{\omega}_3 + \cos\theta d\varphi)
\end{aligned} \tag{3.2.4}$$

where we have used the following $SU(2)$ left-invariant 1-forms

$$\begin{aligned}
&\tilde{\omega}_1 = \cos\psi d\tilde{\theta} + \sin\psi \sin\tilde{\theta} d\tilde{\varphi}, \qquad \tilde{\omega}_2 = -\sin\psi d\tilde{\theta} + \cos\psi \sin\tilde{\theta} d\tilde{\varphi} \\
&\tilde{\omega}_3 = d\psi + \cos\tilde{\theta} d\tilde{\varphi}.
\end{aligned} \tag{3.2.5}$$

This means we can write the background and the Ramond-Ramond 3-form compactly as

$$\begin{aligned}
&ds_E^2 = \sum_i (E^i)^2, \\
&F_3 = e^{-\frac{3}{4}\Phi}\Big[f_1 E^{123} + f_2 E^{\theta\varphi 3} + f_3(E^{\theta 23} + E^{\varphi 13}) + f_4(E^{\rho 1\theta} + E^{\rho\varphi 2})\Big],
\end{aligned} \tag{3.2.6}$$

where we have defined

$$\begin{aligned}
&E^{ijk\ldots l} = E^i \wedge E^j \wedge E^k \wedge \cdots \wedge E^l, \\
&f_1 = -2N_c e^{-k-2g}, \qquad f_2 = \frac{N_c}{2} e^{-k-2h}(a^2 - 2ab + 1), \\
&f_3 = N_c e^{-k-h-g}(a-b), \qquad f_4 = \frac{N_c}{2} e^{-k-h-g} b'.
\end{aligned} \tag{3.2.7}$$

In this setup, the dilaton is a function $\Phi(\rho)$ of the radial coordinate only, and we set $\alpha' g_s = 1$. Then the background is written in terms of six functions, $\{g, h, k, \Phi, a, b\}$,

which all depend on the radial coordinate ρ only. It is possible to solve the SUSY system using a set of BPS equations that can be derived for the above ansatz.

The family of solutions we will present in section 3.2.2 correspond to a dual field theory deformed by the insertion of an eight-dimensional operator in the Lagrangian which couples the field theory to gravity. This calls for a completion in the context of the field theory which is achieved on the supergravity side with a U-duality [47]. We will refer to this procedure as the 'rotation'. It amounts to a solution generating technique which yields the 'rotated' background, in which the vielbeins are

$$\begin{aligned}
&e^{x_i} = e^{\frac{\Phi}{4}}\hat{h}^{-\frac{1}{4}}dx_i, \qquad e^{\rho} = e^{\frac{\Phi}{4}+k}\hat{h}^{\frac{1}{4}}d\rho, \quad e^{\theta} = e^{\frac{\Phi}{4}+h}\hat{h}^{\frac{1}{4}}d\theta, \qquad e^{\varphi} = e^{\frac{\Phi}{4}+h}\hat{h}^{\frac{1}{4}}\sin\theta d\varphi,\\
&e^{1} = \frac{1}{2}e^{\frac{\Phi}{4}+g}\hat{h}^{\frac{1}{4}}(\tilde{\omega}_1 + a d\theta), \qquad e^{2} = \frac{1}{2}e^{\frac{\Phi}{4}+g}\hat{h}^{\frac{1}{4}}(\tilde{\omega}_2 - a\sin\theta d\varphi),\\
&e^{3} = \frac{1}{2}e^{\frac{\Phi}{4}+k}\hat{h}^{\frac{1}{4}}(\tilde{\omega}_3 + \cos\theta d\varphi).
\end{aligned} \tag{3.2.8}$$

The 'rotation' leaves the RR 3-form invariant[1] but turns on some new fluxes. The new metric, RR and NS fields are then

$$\begin{aligned}
ds_E^2 &= \sum_i (e^i)^2,\\
F_3 &= \frac{e^{-\frac{3}{4}\Phi}}{\hat{h}^{3/4}}\Big[f_1 e^{123} + f_2 e^{\theta\varphi 3} + f_3(e^{\theta 23} + e^{\varphi 13}) + f_4(e^{\rho 1\theta} + e^{\rho\varphi 2})\Big],\\
H_3 &= -\kappa\frac{e^{\frac{5}{4}\Phi}}{\hat{h}^{3/4}}\Big[-f_1 e^{\theta\varphi\rho} - f_2 e^{\rho 12} - f_3(e^{\theta 2\rho} + e^{\varphi 1\rho}) + f_4(e^{1\theta 3} + e^{\varphi 23})\Big],\\
C_4 &= -\kappa\frac{e^{2\Phi}}{\hat{h}}dt\wedge dx_1\wedge dx_2\wedge dx_3,\\
F_5 &= \kappa e^{-\frac{5}{4}\Phi - k}\hat{h}^{\frac{3}{4}}\partial_\rho\left(\frac{e^{2\Phi}}{\hat{h}}\right)\left[e^{\theta\varphi 123} - e^{tx_1x_2x_3\rho}\right].
\end{aligned} \tag{3.2.9}$$

In the above equations we have a new factor defined as

$$\hat{h} = 1 - \kappa^2 e^{2\Phi}. \tag{3.2.10}$$

We choose the constant κ to be such that the dual QFT will decouple from gravity (corresponding to careful removal of the eight-dimensional operator). The choice that allows this is $\kappa = e^{-\Phi_\infty}$, where Φ_∞ is the asymptotic value of the dilaton for large ρ. This requirement restricts us to those solutions in which the dilaton is bounded at large distances. The rationale behind this choice is discussed in more detail in [7, 56].

3.2.2 The SUSY solutions

The background described in (3.2.4–3.2.7) results in a system of non-linear, coupled, first-order BPS equations (which are derived in the appendix of [48]). These can be repackaged using a certain change of basis functions [49, 50, 57] into a much

[1]The factor of $\hat{h}^{-3/4}$ in (3.2.9) relative to in (3.2.6) simply cancels the factors contained in the new vielbeins (3.2.8).

simpler form where the equations decouple: We rewrite the background functions $\{g, h, k, a, b\}$ in terms of five new functions $\{P, Q, Y, \tau, \sigma\}$ according to

$$\begin{aligned} 4e^{2h} &= \frac{P^2 - Q^2}{P\cosh\tau - Q}, & e^{2g} &= P\cosh\tau - Q, & e^{2k} &= 4Y, \\ a &= \frac{\sinh\tau}{P\cosh\tau - Q}, & N_c b &= \sigma. \end{aligned} \tag{3.2.11}$$

Then most of the BPS equations can be reduced to algebraic relations between the functions, leaving a single decoupled second-order equation for P (referred to in the literature as the 'master equation'):

$$P'' + P'\left[\frac{P'+Q'}{P-Q} + \frac{P'-Q'}{P+Q} - 4\coth(2\rho - 2\rho_o)\right] = 0, \tag{3.2.12}$$

with

$$Q = (Q_o + N_c)\coth(2\rho - 2\rho_o) + N_c\left[2\rho\coth(2\rho - 2\rho_o) - 1\right], \tag{3.2.13}$$

where Q_o and ρ_o are two integration constants. Each solution to the master equation (3.2.12) generically provides us with two backgrounds, related by the U-duality or rotation described in section 3.2.1.[2] We will be most interested in the rotated solutions, which correspond to the baryonic branch. However, much of what follows will be concerned simply with the behaviour of the background functions, and so will apply equally to the unrotated case (corresponding to theory A in section 3.2.1). Additionally, we will at times deal with solutions in which the dilaton grows without bound in the UV. Then, as discussed above, we can see from (3.2.10) that we cannot apply the rotation procedure without the warp factor $\hat{h}$ vanishing.[3]

The master equation (3.2.12) describes all solutions compatible with the ansatz (3.2.4–3.2.7). However, we will restrict our attention to globally regular solutions. In this case we find the solutions have an IR (for $\rho \to 0$) of the form

$$\begin{aligned} e^{2g} &= \frac{h_1}{2} + \frac{4h_1}{15}\left(3 - \frac{5N_c}{h_1} - \frac{2N_c^2}{h_1^2}\right)\rho^2 + O(\rho^4), \\ e^{2h} &= \frac{h_1}{2}\rho^2 - \frac{4h_1}{45}\left(6 - \frac{15N_c}{h_1} + \frac{16N_c^2}{h_1^2}\right)\rho^4 + O(\rho^6), \\ e^{2k} &= \frac{h_1}{2} + \frac{2h_1}{5}\left(1 - \frac{4N_c^2}{h_1^2}\right)\rho^2 + O(\rho^4), \\ e^{\Phi-\phi_0} &= 1 + \frac{16N_c^2}{9h_1^2}\rho^2 + O(\rho^4), \\ a &= 1 - \left(2 - \frac{8N_c}{3h_1}\right)\rho^2 + O(\rho^4), \qquad b = \frac{2\rho}{\sinh 2\rho}, \end{aligned} \tag{3.2.14}$$

where the exact expression for b holds for all ρ. Aside from the ability to shift the dilaton, encoded in ϕ_0, we therefore have a family of solutions parametrised by h_1.

[2] Or, more generally, a family of backgrounds parametrised by κ in (3.2.10).

[3] This does not necessarily mean that we cannot consider these solutions as belonging to the rotated family. The issue is in fact slightly more subtle, and we will return to this point in section 3.2.3.

The second integration constant we expect from the second-order equation (3.2.12) has been fixed to ensure regularity. The same requirement also leads us to fix the values of the integration constants appearing in (3.2.12–3.2.13) as $Q_o = -N_c$ and $\rho_o = 0$.

Turning to the UV, we find that for $\rho \to \infty$

$$
\begin{aligned}
e^{2g} &= c_+ e^{\frac{4}{3}\rho} + N_c(1-2\rho) + \frac{N_c^2}{c_+}\left(\frac{13}{4} - 4\rho + 4\rho^2\right) e^{-\frac{4}{3}\rho} + O\big(e^{-\frac{8}{3}\rho}\big), \\
e^{2h} &= \frac{c_+}{4} e^{\frac{4}{3}\rho} - \frac{N_c}{4}(1-2\rho) + \frac{N_c^2}{c_+}\left(\frac{13}{16} - \rho + \rho^2\right) e^{-\frac{4}{3}\rho} + O\big(e^{-\frac{8}{3}\rho}\big), \\
e^{2g} &= \frac{2c_+}{3} e^{\frac{4}{3}\rho} - \frac{N_c^2}{3c_+}\left(\frac{25}{2} - 20\rho - 8\rho^2\right) e^{-\frac{4}{3}\rho} + O\big(e^{-\frac{8}{3}\rho}\big), \\
e^{4(\Phi-\Phi_\infty)} &= 1 + \frac{3N_c^2}{4c_+^2}(1-8\rho)\, e^{-\frac{8}{3}\rho} + O\big(e^{-\frac{16}{3}\rho}\big), \\
a &= 2e^{-2\rho} - \frac{2N_c}{c_+}(1-8\rho)e^{-\frac{10}{3}\rho} + O\big(e^{-\frac{14}{3}\rho}\big), \qquad b = \frac{2\rho}{\sinh 2\rho}
\end{aligned}
\tag{3.2.15}
$$

with an additional parameter c_- appearing at the next order, giving two non-trivial parameters. Of course, we require a smooth solution joining the two expansions (3.2.14–3.2.15), and this can be seen to be the case numerically. However, there is then only one non-trivial independent parameter; given a value for one of $\{h_1, c_+, c_-\}$, the requirement that the interpolating solution matches both the IR and UV expansions is sufficient to determine the values of the other two. This can be seen numerically; a solution found starting from (3.2.15) with arbitrary values of c_+ and c_- will generically be singular in the IR, with a divergent Kretschmann scalar [7].

3.2.3 Exploring the baryonic branch

We saw in section 3.2.2 that, constrained by the requirement of regularity, and ignoring the possible shift of the dilaton, the SUSY solutions form a one dimensional family. It is convenient to parametrise the solutions either by h_1, which is defined by the IR expansions (3.2.14), or by c_+, which is defined by the UV expansions (3.2.15). The relationship between h_1 and c_+ is known only numerically, but for these SUSY solutions we have

$$
c_+ \sim \frac{3^{1/3} h_1}{4} \tag{3.2.16}
$$

for large values of c_+ and h_1 [17]. As we will see in section 3.6.1, in the rotated solutions h_1 and c_+ correspond to the parameter which explores the baryonic branch; we recover the KS solution [12] itself in the limit $h_1, c_+ \to \infty$. We postpone further discussion of this limit until section 3.4.4, where we consider its non-SUSY generalisation [32].

Taking the opposite limit, $c_+ \to 0$, we find that $h_1 \to 2N_c$. This corresponds to the Chamseddine-Volkov/Maldacena-Núñez (CVMN) solution [15, 16]. This is considerably simpler than the general case, and exact expressions are known for the

functions which describe the solution:

$$\frac{e^{2g}}{N_c} = \frac{e^{2k}}{N_c} = 1, \qquad \frac{e^{2h}}{N_c} = \rho\coth 2\rho - \frac{\rho^2}{\sinh^2 2\rho} - \frac{1}{4},$$
$$a = b = \frac{2\rho}{\sinh 2\rho}, \qquad e^{4\Phi-4\phi_0} = \frac{N_c}{4}e^{-2h}\sinh^2 2\rho. \tag{3.2.17}$$

Note that while the IR can be obtained simply by setting $h_1 = 2N_c$ in (3.2.14),

$$\frac{e^{2h}}{N_c} = \rho^2 - \frac{4}{9}\rho^4 + O(\rho^6), \quad a = 1 - \frac{2}{3}\rho^2 + O(\rho^4), \quad e^{4\Phi-4\phi_0} = 1 + \frac{16}{9}\rho^2 + O(\rho^4), \tag{3.2.18}$$

the UV is qualitatively different from the general case:

$$\frac{e^{2h}}{N_c} = \rho - \frac{1}{4} + O\big(e^{-4\rho}\big), \qquad a = 4\rho e^{-2\rho} + O\big(e^{-6\rho}\big), \qquad \Phi = \rho + O(\log\rho). \tag{3.2.19}$$

Of particular significance here is the fact that the dilaton grows without bound in the UV. As anticipated above, this means that we cannot apply the rotation procedure (3.2.10).

In the general case $h_1 > 2N_c$ the system follows the CVMN solution closely, before switching to the generic UV (3.2.15) for large ρ (figure 3.1). That is, we can identify a scale ρ_{h_1} below which (3.2.17) is almost satisfied, and above which g, h, and k grow exponentially, Φ quickly goes to a constant, and $a \neq b$. Notice that b is completely unaffected by this; the exact result $b = 2\rho/\sinh 2\rho$ holds for all h_1. As h_1 is increased, ρ_{h_1} moves further into the IR (figure 3.2).

We noted above that the rotation procedure could not be applied to the CVMN solution (3.2.17–3.2.19). Specifically, in section 3.2.1 we chose a particular value for the constant appearing in the warp factor $\hat{h} = 1 - \kappa^2 e^{2\Phi}$, namely $\kappa = e^{-\Phi_\infty}$. In the CVMN solution Φ grows without bound and this identification is no longer possible. Nevertheless, it turns out that there is a sense in which we do obtain the (unrotated) CVMN solution by taking the limit $h_1 \to 2N_c$ in the (rotated) baryonic branch. To see this, note that as we take the limit $h_1 \to 2N_c$, we find that $\Phi_\infty \to \infty$, and so $\kappa \to 0$. In this limit we see that $\hat{h} \to 1$ and the additional fields in (3.2.9) vanish, returning us to the unrotated system (3.2.4–3.2.6) at any finite ρ.

More explicitly, in a generic solution on the baryonic branch, the dilaton becomes almost constant approximately at the scale ρ_{h_1} (figure 3.1). Provided ρ_{h_1} is large enough that the UV expansions are valid, we see from (3.2.19) that for $\rho < \rho_{h_1}$ we have $\Phi \sim \rho$. Taken together, these observations mean that we can write $\Phi_\infty \sim \rho_{h_1}$. We then find numerically (figure 3.2) that $\kappa^2 \sim e^{-2\rho_{h_1}} \sim h_1 - 2N_c \to 0$ for $h_1 \to 2N_c$.

In effect, taking the limit $h_1 \to 2N_c$ in the rotated solutions simply pushes the scale ρ_{h_1} to infinity, while in the region $\rho < \rho_{h_1}$ the solution becomes exactly the CVMN one. However, it is important to note that the two cases are qualitatively different, and the limit is not entirely smooth. In particular, we can expect any quantity which depends on the the UV asymptotics of the background to behave discontinuously as we take the limit.

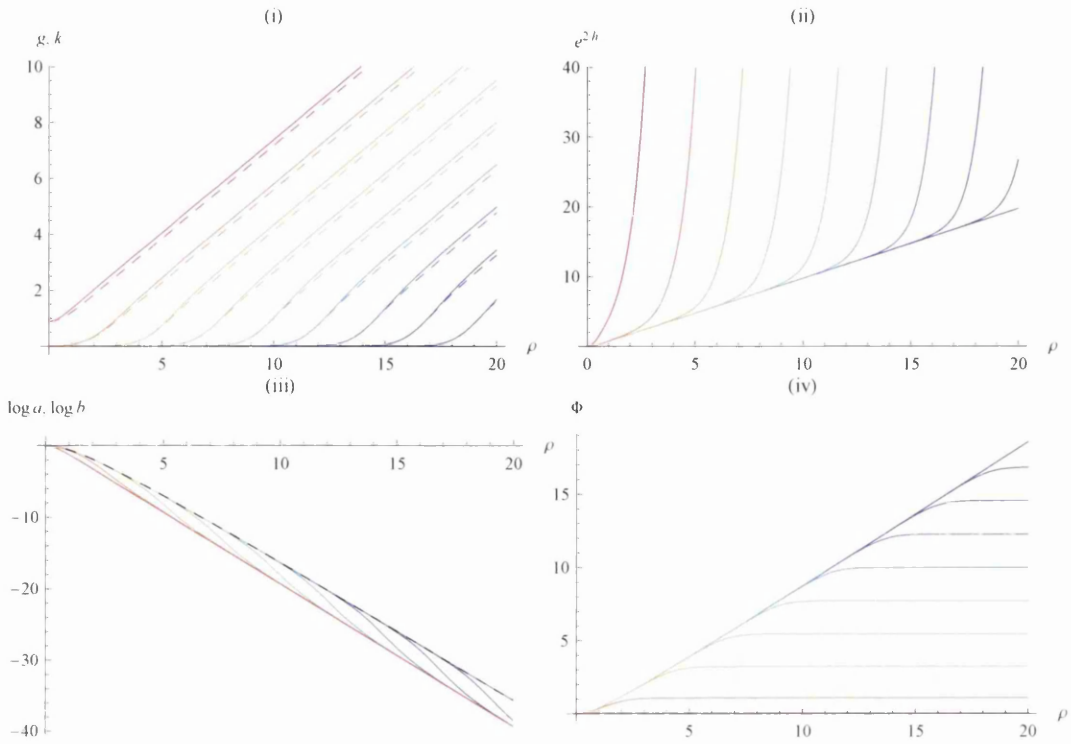

Figure 3.1: Plots of (i) g (solid) and k (dashed), (ii) e^{2h}, (iii) $\log a$ (solid) and $\log b$ (dashed, black), and (iv) Φ, for the SUSY solutions with $2 \leq h_1 \leq 12$, increasing from purple to red. Here we set $N_c = 1$ and $\phi_0 = 0$.

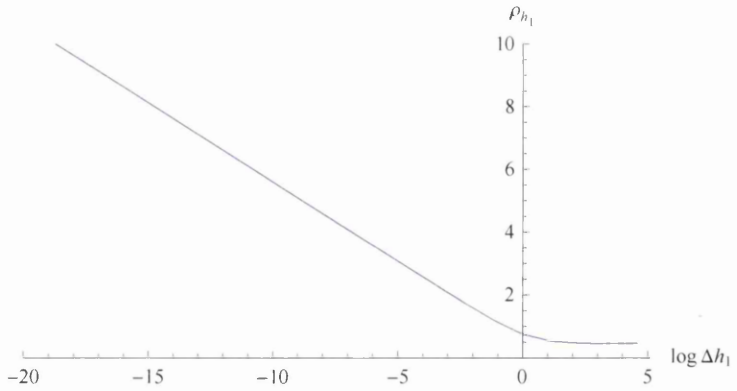

Figure 3.2: Plot showing the dependence of ρ_{h_1} on $\Delta h_1 = h_1 - 2N_c$ in the SUSY solutions. For the purposes of this plot we define ρ_{h_1} by $k'(\rho_{h_1}) = 1/3$, corresponding to the transition between the CVMN UV (k = constant) and the generic UV ($k \sim 2\rho/3$).

3.3 Breaking SUSY

3.3.1 Deformation of $h_1 = 2N_2$ case

The CVMN solution [15, 16] which we obtain in the limit $h_1 = 2N_c$ (section 3.2.3) can be described in terms of $SO(4)$ gauged seven-dimensional supergravity. The $SO(4)$ gauge group corresponds in the full ten-dimensional description to rotations of the 3-sphere $(\tilde{\theta}, \tilde{\varphi}, \psi)$.

In order to get a four-dimensional world-volume theory we wrap 5-branes on the S^2 (θ, φ). There is no covariantly constant spinor on S^2, so to preserve some supersymmetry we have to turn on a gauge field so as to cancel the spin connection of the S^2 in the variation of a fermion:

$$\delta\Psi \sim D_\mu \epsilon = (\partial_\mu + \omega_\mu^{\nu\rho}\gamma^{\nu\rho} - A_\mu^{ij}\Gamma^{ij})\epsilon. \tag{3.3.1}$$

This can be achieved, preserving $\mathcal{N} = 1$ SUSY, with an abelian field $U(1) \subset SU(2)_L$, where $SO(4) \sim SU(2)_R \times SU(2)_L$.[4] In the ten-dimensional description, this corresponds to the 'twist' given by the mixing with the S^2 coordinates θ and φ in (3.2.4),

$$E^3 \sim \tilde{\omega}_3 + \cos\theta d\varphi. \tag{3.3.2}$$

The resulting solution is singular in the IR. However, we can obtain the regular CVMN solution by allowing a non-abelian $SU(2)$ field. In the ten-dimensional description this shows up in the additional mixing parametrised by $a(\rho)$ in (3.2.4). When $a(\rho) = 1$, as occurs for instance at the origin in the SUSY solution, the gauge field is pure gauge; the gauge transformation which removes the field can be written as a coordinate transformation which removes the mixing [60, 61].

This solution was generalised in [27] by solving the full equations of motion rather than the BPS equations, and by allowing a full $SO(4)$ gauge field. We are interested here in the simplest SUSY-breaking deformation of the CVMN solution, where we keep the $SU(2)$ gauge group, and introduce a mass term which breaks SUSY. This corresponds to the globally regular extremal solutions obtained by Gubser, Tseytlin and Volkov (GTV) [24].

For these non-SUSY solutions we no longer have an exact solution as in (3.2.17), although we still have

$$\frac{e^{2g}}{N_c} = \frac{e^{2k}}{N_c} = 1, \qquad a = b \tag{3.3.3}$$

for all ρ. Instead we must rely on expansions in the IR and UV. In the IR, we have qualitatively the same as in (3.2.18):

$$\frac{e^{2h}}{N_c} = \rho^2 - \left(\frac{2}{9} + \frac{v_2^2}{2}\right)\rho^4 + O(\rho^6), \qquad a = 1 + v_2\rho^2 + O(\rho^4),$$
$$e^{4\Phi - 4\phi_0} = 1 + \left(\frac{4}{3} + v_2^2\right)\rho^2 + O(\rho^4), \tag{3.3.4}$$

[4] Alternatively, we could preserve $\mathcal{N} = 2$ SUSY by choosing the $U(1)$ to be in a diagonal $SU(2)_D \subset SU(2)_R \times SU(2)_L$, as in [58, 59, 53].

where we have introduced v_2 to parametrise the SUSY-breaking deformation. Comparing to (3.2.18) we see that setting $v_2 = -2/3$ recovers the SUSY CVMN solution.

As explained in [24], to obtain a regular UV we need $-2 \leq v_2 \leq 0$. We then obtain substantially different behaviour to that in the SUSY case. Adapting the notation of [27],

$$\frac{e^{2h}}{N_c} = \rho + G_\infty + O\left(\frac{1}{\rho}\right), \qquad a = M_a \rho^{-1/2} + O(\rho^{-3/2}), \qquad \Phi = \rho + O(\log \rho), \tag{3.3.5}$$

where the parameters M_a and G_∞ can be considered functions of v_2. The main qualitative difference is the presence of additional terms decaying slower than exponentially in the expansions for e^{2h} and a. This is interpreted in [27] as corresponding to a mass which breaks SUSY.

The effect of the SUSY-breaking deformation is most clearly understood by considering a, which is affected at leading order (figure 3.3 (i)). We see that the non-SUSY solutions are characterised by a scale ρ_{SUSY}. For $\rho < \rho_{\text{SUSY}}$, the qualitative behaviour is that of the SUSY solution, (3.2.17–3.2.19), while for $\rho > \rho_{\text{SUSY}}$ the non-SUSY UV of (3.3.5) takes over. For a generic non-SUSY solution we can define the deformation to a as

$$\Delta a = a - a_{\text{SUSY}}. \tag{3.3.6}$$

Then we can think of ρ_{SUSY} as the scale at which the deformation Δa, which decays slowly in the UV, is of comparable magnitude to a_{SUSY}, which decays much faster. As a result, ρ_{SUSY} moves towards the IR as we move further from the SUSY solution (figure 3.4). Note that this does not relate in a obvious way to the SUSY-breaking scale, which it would be more natural to associate with the scale above which Δa has decayed significantly, and which moves into the UV as we move further from the SUSY solution.

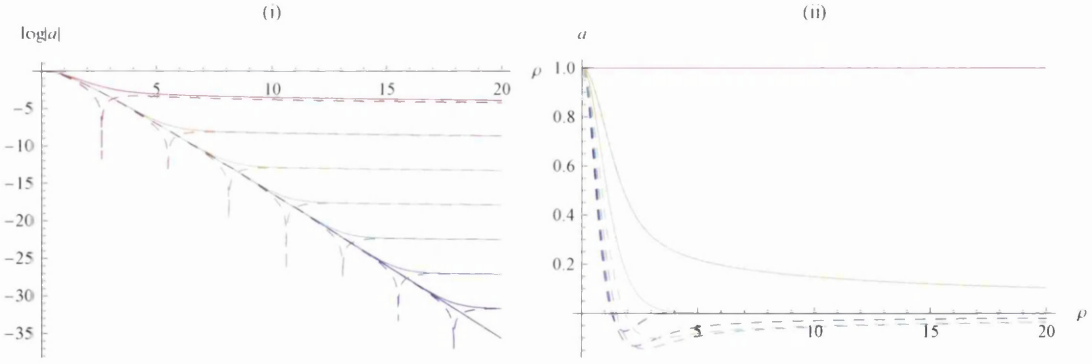

Figure 3.3: (i) Plot of $\log a$ against ρ for $-1/10 \leq \Delta v_2 \leq 1/10$, where $\Delta v_2 = v_2 + 2/3$, showing the transition between $a \sim e^{-2\rho}$ and $a \sim \sqrt{\rho}$ at $\rho \sim \rho_{\text{SUSY}}$. The dashed curves correspond to $v_2 < -2/3$, for which $a = 0$ at ρ_{SUSY}.
(ii) Plot of a against ρ for the full range $-2 \leq v_2 \leq 0$. Again, the dashed curves correspond to $v_2 < -2/3$, for which a has at least one zero. The additional oscillations which are in fact present in the case $v_2 = -2$ (purple) are not visible at this scale.

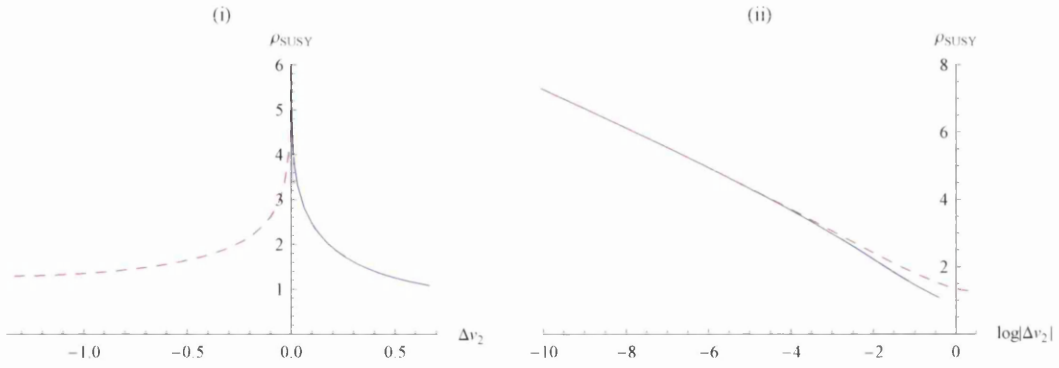

Figure 3.4: Plots showing the dependence of ρ_{SUSY} on $\Delta v_2 = v_2 + 2/3$. For the purposes of this plot we define ρ_{SUSY} by $|\Delta a| = a_{\mathrm{SUSY}}$. The solid blue curve corresponds to $v_2 > -2/3$ and the dashed red curve to $v_2 < -2/3$.

For $v_2 \geq 0$, a is always positive, and for $v_2 = 0$, $a = 1$ for all ρ. As noted above, this means that the gauge field is pure gauge, and we can remove the mixing between the spheres by a change of coordinates. Thus in this case the internal geometry is simply $S^2 \times S^3$. Aside from the behavior of a, the UV is otherwise unchanged — the other functions h and Φ still behave according to (3.3.5).

For $v_2 < -2/3$, a has at least one zero. As v_2 is reduced, a picks up more oscillations, and in the limiting case there are infinitely many zeros. In this limit the UV of the other functions no longer that of (3.3.5) (see figure 3.5). Instead the system approaches the 'special Abelian solution' of [24];

$$\frac{e^{2h}}{N_c} \to \frac{1}{4}, \qquad \Phi \to \sqrt{2}\rho. \tag{3.3.7}$$

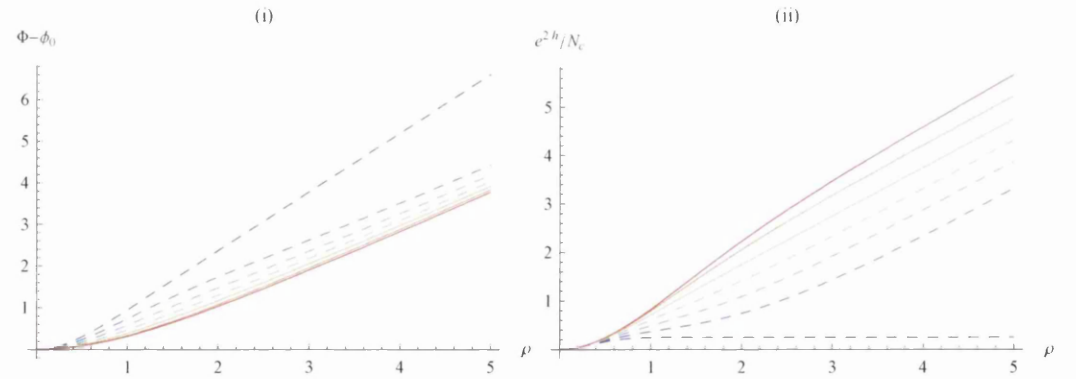

Figure 3.5: Plots of (i) Φ and (ii) e^{2h} against ρ, for $-2 \leq v_2 < -2/3$ (dashed curves) and $-2/3 \leq v_2 \leq 0$ (solid curves), showing the difference between the generic UV (3.3.5) and the limiting case (3.3.7).

3.3.2 Deformation of general case

We now turn to the solution which was originally presented in [2]. The aim there was to find a non-supersymmetric generalisation, preserving the symmetries and

structure of the baryonic branch solutions with $h_1 \neq 2N_c$ discussed in section 3.2. This is analogous to the way in which the GTV solutions (section 3.3.1) generalise the CVMN solution (3.2.17).

In the non-SUSY case we can no longer make use of the master equation (3.2.12), which was derived from the BPS equations. Instead we have to solve the full Einstein, Maxwell, dilaton and Bianchi equations of the system. This amounts to a system of six coupled non-linear second-order equations, together with a first-order Hamiltonian constraint. These are included in appendix A.2. We look for solutions to these equations in the form of IR and UV expansions with similar forms to the SUSY case (3.2.14–3.2.15).

In the IR we simply impose that the solution is regular, and that the 2-sphere shrinks to zero radius at $\rho = 0$, as in (3.2.14). We then have expansions of the form

$$\begin{aligned} e^{2g} &= \sum_{n=0}^{\infty} g_n \rho^n, & e^{2h} &= \sum_{n=2}^{\infty} h_n \rho^n, & e^{2k} &= \sum_{n=0}^{\infty} k_n \rho^n, \\ e^{4\Phi} &= \sum_{n=0}^{\infty} f_n \rho^n, & a &= \sum_{n=0}^{\infty} w_n \rho^n, & b &= \sum_{n=0}^{\infty} v_n \rho^n. \end{aligned} \tag{3.3.8}$$

Substituting into the equations of motion (A.2.3–A.2.8) we find five independent parameters, which we take to be k_0, f_0, k_2, v_2 and w_2. We relabel $k_0 = h_1/2$ and $f_0 = e^{4\phi_0}$, so that we can recover the SUSY solution (3.2.14) by setting

$$k_2 = \frac{2h_1}{5} - \frac{8N_c^2}{h_1}, \qquad v_2 = -\frac{2}{3}, \qquad w_2 = \frac{8N_c}{3h_1} - 2. \tag{3.3.9}$$

After the relabeling, the five independent parameters are[5]

$$h_1, \qquad \phi_0, \qquad k_2, \qquad v_2, \qquad w_2, \tag{3.3.10}$$

and the expansions are qualitatively the same as the SUSY case (3.2.14):[6]

$$\begin{aligned} e^{2g} &= \frac{h_1}{2} + \frac{h_1}{2}\left(1 - \frac{k_2}{h_1} - \frac{4N_c^2}{h_1^2} - \frac{N_c^2 v_2^2}{h_1^2} + \frac{w_2^2}{4}\right)\rho^2 + O(\rho^4), \\ e^{2h} &= \frac{h_1}{2}\rho^2 - \frac{h_1}{6}\left(1 - \frac{2k_2}{h_1} - \frac{4N_c^2}{3h_1^2} + \frac{3N_c^2 v_2^2}{h_1^2} + \frac{3w_2^2}{4}\right)\rho^4 + O(\rho^6), \\ e^{2k} &= \frac{h_1}{2} + k_2\rho^2 + O(\rho^4), & e^{\Phi-\phi_0} &= 1 + \frac{N_c^2}{h_1^2}\left(\frac{4}{3} + v_2^2\right)\rho^2 + O(\rho^4), \\ a &= 1 + w_2\rho^2 + O(\rho^4), & b &= 1 + v_2\rho^2 + O(\rho^4). \end{aligned} \tag{3.3.11}$$

[5]Notice that h_1 does *not* refer to the coefficient of ρ in the expansion for e^{2h}, as would be expected from the form of (3.3.8). This unfortunate notation should not cause confusion because that term will always be zero to ensure regularity.

[6]More complete expressions, both for the IR expansions here and the UV (3.3.16), can be found in an appendix of [2].

In the UV we use a particular generalisation of the SUSY solutions (3.2.15):

$$
\begin{aligned}
e^{2g} &= \sum_{m=0}^{\infty}\sum_{n=0}^{m} G_{mn}\rho^n e^{4(1-m)\rho/3}, & e^{2h} &= \sum_{m=0}^{\infty}\sum_{n=0}^{m} H_{mn}\rho^n e^{4(1-m)\rho/3},\\
e^{2k} &= \sum_{m=0}^{\infty}\sum_{n=0}^{m} K_{mn}\rho^n e^{4(1-m)\rho/3}, & e^{4\Phi} &= \sum_{m=1}^{\infty}\sum_{n=0}^{m} \Phi_{mn}\rho^n e^{4(1-m)\rho/3},\\
a &= \sum_{m=1}^{\infty}\sum_{n=0}^{m} W_{mn}\rho^n e^{2(1-m)\rho/3}, & b &= \sum_{m=1}^{\infty}\sum_{n=0}^{m} V_{mn}\rho^n e^{2(1-m)\rho/3}.
\end{aligned}
\tag{3.3.12}
$$

This particular ansatz will not be sufficient to include all cases; for example we have seen in section 3.3.1 that the GTV solutions with $h_1 = 2N_c$ have a completely different form (3.3.5) in the UV. We will find other limits in which this is the case, and which will have to be treated separately.

As in the IR, we substitute the ansatz (3.3.12) into the equations of motion, and in this case we find nine independent parameters, which we take to be

$$
K_{00},\quad K_{30},\quad H_{10},\quad H_{11},\quad \Phi_{10},\quad \Phi_{30},\quad W_{20},\quad W_{40},\quad V_{40},
\tag{3.3.13}
$$

and which we again relabel to make contact with the SUSY case:

$$
K_{00} = \frac{2c_+}{3},\quad H_{10} = \frac{Q_o}{4},\quad \Phi_{10} = e^{4\Phi_\infty},\quad K_{30} = \frac{c_- - 64e^{4\rho_o}c_+^3}{48c_+^2},\quad W_{40} = 2e^{\rho_o}.
\tag{3.3.14}
$$

The nine relabeled independent parameters are then

$$
c_+,\quad c_-,\quad \Phi_\infty,\quad Q_o,\quad \rho_o,\quad H_{11},\quad W_{20},\quad \Phi_{30},\quad V_{40},
\tag{3.3.15}
$$

and the expansions are

$$
\begin{aligned}
e^{2g} &= c_+ e^{\frac{4}{3}\rho} - (4H_{11}\rho + Q_o + 2c_+W_{20}^2) + O\big(e^{-\frac{4}{3}\rho}\big),\\
e^{2h} &= \frac{c_+}{4}e^{\frac{4}{3}\rho} + H_{11}\rho + \frac{Q_o}{4} + O\big(e^{-\frac{4}{3}\rho}\big),\\
e^{2k} &= \frac{2c_+}{3}e^{\frac{4}{3}\rho} + \frac{c_+W_{20}^2}{3} + O\big(e^{-\frac{4}{3}\rho}\big),\\
e^{\Phi-\Phi_\infty} &= 1 - \left(\frac{3N_c^2}{2c_+^2}\rho - e^{-4\Phi_\infty}\frac{\Phi_{30}}{4}\right)e^{-\frac{8}{3}\rho} + O\big(e^{-4\rho}\big),\\
a &= W_{20}e^{-\frac{2}{3}\rho} + \left[\left(\frac{3H_{11}W_{20}}{c_+} + \frac{10W_{20}^3}{3}\right)\rho + 2e^{2\rho_o}\right]e^{-2\rho} + O\big(e^{-\frac{10}{3}\rho}\big),\\
b &= \frac{9W_{20}}{4}e^{-\frac{2}{3}\rho} + \left[\frac{10W_{20}^3}{3}\rho^2 + \left(4e^{2\rho_o} - \frac{Q_oW_{20}}{c_+} - \frac{23W_{20}^3}{6}\right)\rho\right.\\
&\qquad\left. + V_{40}\right]e^{-2\rho} + O\big(e^{-\frac{10}{3}\rho}\big).
\end{aligned}
\tag{3.3.16}
$$

The most significant difference here when compared to the SUSY expansions (3.2.15) is the presence of the new terms at leading order in the UV in a and b. This corresponds to the presence of the additional terms proportional to $\rho^{-1/2}$ in a which we saw in the GTV solutions (3.3.5), and we will see in section 3.6.1 that the

interpretation as a mass term still applies. The fact that the extra terms we obtain here are exponential rather than polynomial in ρ is related to the qualitatively different UV asymptotics in the baryonic branch (3.2.15) as opposed to the CVMN solution (3.2.19).

We can recover the SUSY case from (3.3.16) by setting

$$H_{11} = \frac{N_c}{2}, \quad W_{20} = 0, \quad \Phi_{30} = -\frac{3N_c}{4c_+^2} e^{4\Phi_\infty}(3N_c + 4Q_o), \quad V_{40} = \frac{2}{N_c} e^{2\rho_o}(N_c + Q_o). \tag{3.3.17}$$

For the regular SUSY solution (3.2.14, 3.2.15) we also need $\rho_o = 0$ and $Q_o = -N_c$.

In summary, our solutions are described by the fourteen parameters: the five from the IR (3.3.10) and nine from the UV (3.3.15). However, if we consider only solutions which match both the IR and UV expansions (3.3.8, 3.3.12) these are clearly not all independent. There can be at most five independent parameters, as the required solutions can be parametrised by the IR boundary conditions alone. However, we generically expect even fewer.

Our goal is to find a solution which smoothly interpolates between the IR and UV expansions. This will require that these two parametrisations lead to identical functions. We can express this as a system of twelve equations [7],

$$\begin{aligned}
g(h_1 \dots w_2; \rho) &= g(c_+ \dots V_{40}; \rho), & \tfrac{d}{d\rho} g(h_1 \dots w_2; \rho) &= \tfrac{d}{d\rho} g(c_+ \dots V_{40}; \rho), \\
h(h_1 \dots w_2; \rho) &= h(c_+ \dots V_{40}; \rho), & \tfrac{d}{d\rho} h(h_1 \dots w_2; \rho) &= \tfrac{d}{d\rho} h(c_+ \dots V_{40}; \rho), \\
&\vdots & &\vdots \\
b(h_1 \dots w_2; \rho) &= b(c_+ \dots V_{40}; \rho), & \tfrac{d}{d\rho} b(h_1 \dots w_2; \rho) &= \tfrac{d}{d\rho} b(c_+ \dots V_{40}; \rho).
\end{aligned} \tag{3.3.18}$$

This system can be further reduced using the constraint (appendix A.2). This means we can for instance express the derivative of one of the functions in terms of the other functions and their derivatives. This leaves us with a system of eleven independent equations which we would expect to allow us to solve for eleven of our fourteen parameters. Although in principle further redundancy in the system of equations (3.3.18) would allow for more independent parameters up to a maximum of five, the numerical analysis discussed in [2] and below appears to support this conclusion. Of the three remaining parameters, one corresponds to our ability to shift the dilaton, which has no other effect on the solution. The final two parameters we then associate with movement along the baryonic branch and finally the breaking of SUSY.

In much of the following it will be convenient to describe the solution space in terms of the parameters that appear in the IR expansions. Firstly, as in [2] the smaller number of parameters makes finding suitable numerical solutions much simpler starting from the IR. Secondly, our IR ansatz (3.3.8) imposes a comparatively natural restriction on the solutions, while the UV ansatz (3.3.12) is more arbitrary, merely being a plausible candidate for a generalisation of the most usual SUSY solution. Indeed, as discussed we know that it does not apply in several interesting special cases.

[7] We write the functions resulting from a given choice of the IR parameters $\{h_1, k_2, v_2, w_2\}$ in the form $g(h_1, k_2, v_2, w_2; \rho)$. Similarly the expressions of the form $g(c_+, c_-, Q_o, \rho_o, H_{11}, W_{20}, \Phi_{30}, V_{40}; \rho)$ refer to the functions resulting from a given choice of the UV parameters.

To allow contact with the SUSY case, we choose h_1 to parametrise the position along the baryonic branch. We could then in principle choose any combination of the remaining IR parameters v_2, w_2 and k_2 to describe the remaining degree of freedom (figure 3.6). It turns out that a description in terms of v_2 is usually simplest; we see from (3.3.9) that its SUSY value, $v_2^{\text{SUSY}} = -2/3$, is independent of h_1.

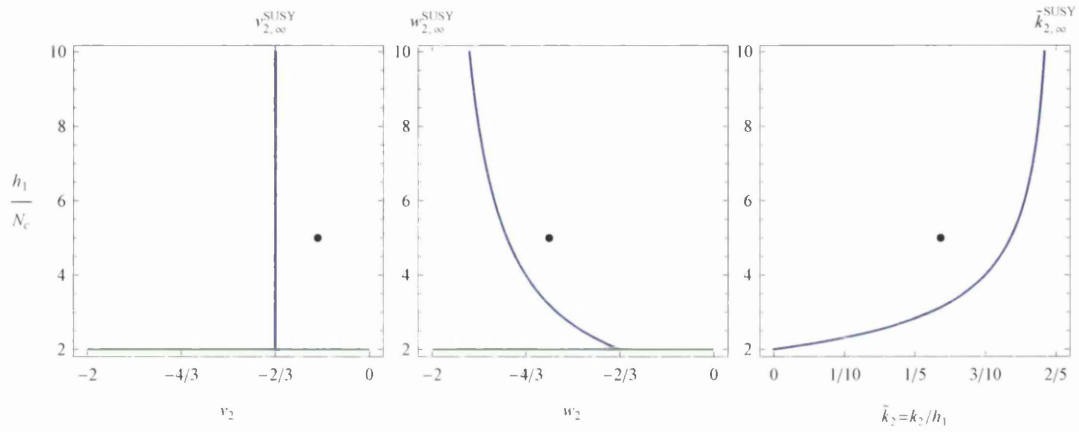

Figure 3.6: The space of solutions, seen in terms of (v_2, h_1), (w_2, h_1), and $(\tilde{k}_2, h_1)$, where $\tilde{k}_2 = k_2/h_1$. The blue curves denote the SUSY baryonic branch (section 3.2), and the green lines correspond to the GTV solutions (section 3.3.1). Note that all the GTV solutions have $k_2 = 0$, as can be seen from (3.3.3). Any solution to the equations of motion of the form (3.3.8) is represented by a point on each of these diagrams. If we require a well-behaved UV, specifying the position on one diagram is sufficient to determine the positions on the other two. For example the marked point represents schematically a generic solution of the sort presented in [2]. The values marked at the top show the SUSY values in the limit $h_1 \to \infty$, corresponding to the KS solution [12].

3.3.3 Finding globally regular solutions

In order for us to be able to conclude that the IR expansions of the form (3.3.8) and the UV expansions of the form (3.3.12) describe the same system of solutions, it is necessary to find numerical solutions interpolating between them. This was achieved in [2] for isolated examples, simply by manually searching the IR parameter space for solutions with the expected UV behaviour. However, without having a good understanding of the structure of the parameter space it was difficult to make progress. In particular, the approach was in practice limited to solutions very close to the SUSY case (i.e. $v_2 \approx -2/3$).

Fortunately, we can make use of the simpler system of GTV solutions (section 3.3.1). Just as the CVMN solution (3.2.17) can be obtained from the SUSY baryonic branch solution (3.2.15–3.2.14) in the limit $h_1 \to 2N_c$, we would expect to obtain the GTV solutions from our non-SUSY generalisation of the baryonic branch in the same limit. In the IR, this is indeed the case; by setting $w_2 = v_2$ and $k_2 = 0$ in our solution we recover (3.3.4). Of course, there is no way to obtain the GTV UV (3.3.5) from UV expansions of the form (3.3.12), but this is to be expected given that

the equivalent statement is also true in the SUSY case — the CVMN UV (3.2.19) cannot be obtained as a simple limit of the generic UV (3.2.15).

As the GTV system has no redundant parameters in the IR, it is simple to generate numerical solutions. It is then possible to deform this well-understood case by increasing h_1 and adjusting w_2 and v_2 slightly to correct the UV behaviour. More precisely, for a given value of $v_2 = \Delta v_2 - 2/3$ it is trivial to obtain a numerical solution with $h_1 = 2N_c$, for which $w_2 = v_2$ and $k_2 = 0$. We then deform this by keeping Δv_2 fixed and setting $h_1 = 2N_c + \Delta h_1$. If we use a small perturbation Δh_1, we will require corrections of the form

$$w_2 = w_2^{\text{SUSY}}(\Delta h_1) + \Delta v_2 + \delta w_2(\Delta h_1, \Delta v_2), \qquad k_2 = k_2^{\text{SUSY}}(\Delta h_1) + \delta k_2(\Delta h_1, \Delta v_2), \tag{3.3.19}$$

where δw_2 and δk_2 are extremely small.

The far UV of the solutions obtained in this way match our general ansatz (3.3.12), justifying our assumption that the GTV solutions can be viewed as a limit of our deformations of the general case.

In itself, this yields a considerable advance over using only the approach described in [2] — it gives us access to solutions with $h_1 \approx 2N_c$ and general v_2, in addition to those with $v_2 \approx -2/3$ and general h_1. More significantly, however, it allows us to understand the behaviour of solutions with generic values of both h_1 and v_2 in terms of the corresponding solutions in the two limits.

3.4 The two-dimensional solution space

3.4.1 Combining the effects of h_1 and v_2

As we have seen in section 3.3.2, the system is described by a two-dimensional parameter space, corresponding to the position along the baryonic branch and the size of the SUSY-breaking deformation. We generate numerical solutions starting from the IR, so we are led to the choice of h_1 and one of the three SUSY-breaking parameters $\{w_2, v_2, k_2\}$. Of these v_2 turns out to be most convenient because v_2^{SUSY} is independent of h_1.

In section 3.2.3 we described the effect of varying h_1 in terms of the scale ρ_{h_1}, corresponding to the transition between the CVMN behaviour (3.2.17–3.2.19) and the generic (KS-like) behaviour (3.2.15). Similarly, in section 3.3.1 we introduced the scale ρ_{SUSY}, associated with the transition between the qualitatively SUSY CVMN behaviour and the (non-SUSY) GTV UV (3.3.5).

In the case of a generic solution, with $h_1 > 2N_c$ and $v_2 \neq -2/3$, we find that these features survive and both scales are present. The sequence then depends on the ordering of the two scales. If $\rho_{h_1} < \rho_{\text{SUSY}}$, the sequence is (figure 3.7 (i)):

$$\begin{aligned}
\rho < \rho_{h_1} &: \quad k \approx g \sim \text{constant}, \quad a \approx b \sim e^{-2\rho} \quad \text{(SUSY, CVMN-like)} \\
\rho_{h_1} < \rho < \rho_{\text{SUSY}} &: \quad k \sim g \sim 2\rho/3, \quad a \sim b \sim e^{-2\rho} \quad \text{(SUSY, KS-like)} \\
\rho > \rho_{\text{SUSY}} &: \quad k \sim g \sim 2\rho/3, \quad a \sim b \sim e^{-2\rho/3} \quad \text{(non-SUSY, KS-like)}
\end{aligned}$$

On the other hand, if $\rho_{\text{SUSY}} < \rho_{h_1}$ we have (figure 3.7 (ii))

$$\begin{aligned}
\rho < \rho_{\text{SUSY}} &: \quad k \approx g \sim \text{constant}, \quad a \approx b \sim e^{-2\rho} \quad \text{(SUSY, CVMN-like)} \\
\rho_{\text{SUSY}} < \rho < \rho_{h_1} &: \quad k \approx g \sim \text{constant}, \quad a \approx b \sim \rho^{-1/2} \quad \text{(non-SUSY, GTV-like)} \\
\rho > \rho_{h_1} &: \quad k \sim g \sim 2\rho/3, \quad a \sim b \sim e^{-2\rho/3} \quad \text{(non-SUSY, KS-like)}
\end{aligned}$$

It appears that ρ_{h_1} is almost independent of v_2, and that $\rho_{\rm SUSY}$ is almost independent of h_1, although this may break down for sufficiently large h_1 and v_2, depending on the precise definition used for the scales. In fact the presence of the two scales becomes less clear as they move into the IR for large h_1 and v_2. This reflects the reduced gradient far from the CVMN solution ($h_1 = 2N_{\rm c}, v_2 = -2/3$) in figures 3.2 and 3.4. We show the behaviour of the functions for some generic solutions in figure 3.8. In this case h_1 is large enough that ρ_{h_1} is not visible.

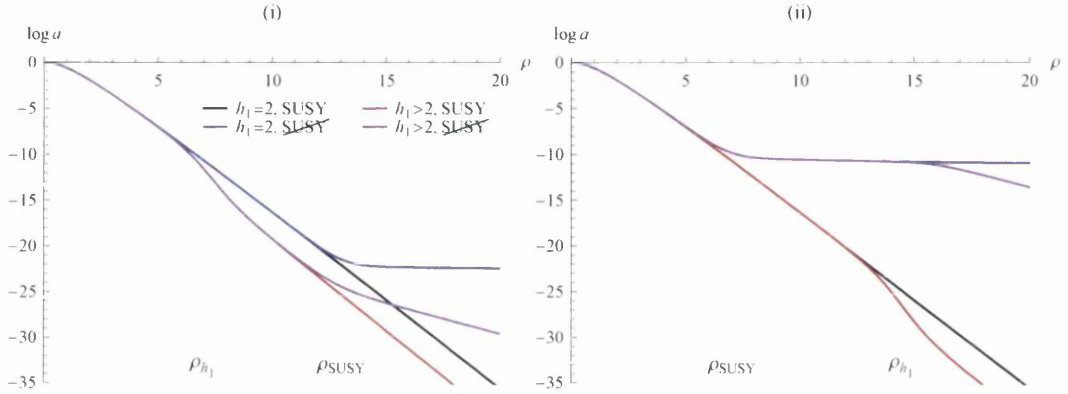

Figure 3.7: Plots of $\log a$ against ρ comparing the solutions obtained for each combination of $h_1 = 2N_{\rm c}$, $h_1 = 2N_{\rm c} + \Delta h_1$, $v_2 = -2/3$ and $v_2 = -2/3 + \Delta v_2$.
(i) $\Delta h_1 = 10^{-5}$, $\Delta v_2 = 10^{-9}$, with $N_{\rm c} = 1$. Here $\rho_{h_1} < \rho_{\rm SUSY}$. In the IR we see the CVMN-like behaviour, with $a \approx 2\rho/\sinh 2\rho$. At ρ_{h_1} the solutions with $h_1 > 2$ deviate from this, but after the transition the gradient is unchanged as we still have $a \sim e^{-2\rho}$. Then at $\rho_{\rm SUSY}$ the non-SUSY solutions switch to the slower decaying behaviour.
(ii) $\Delta h_1 = 10^{-11}$, $\Delta v_2 = 10^{-4}$, again with $N_{\rm c} = 1$. Here $\rho_{\rm SUSY} < \rho_{h_1}$. The IR still shows the CVMN-like behaviour. At $\rho_{\rm SUSY}$ the non-SUSY solutions switch to the GTV-like behaviour, with $a \sim \rho^{-1/2}$. Then at ρ_{h_1} the solutions with $h_1 \neq 2$ show a transition. In the SUSY case the gradient is the same after the transition, but in the non-SUSY solution the gradient increases. This corresponds to the transition between $a \sim \rho^{-1/2}$ and $a \sim e^{-2\rho/3}$.

3.4.2 The boundaries of the parameter space

A notable feature of the GTV solutions is the restriction to $-2 < v_2 < 0$ for solutions with a regular UV. There is no obvious way to determine whether an equivalent condition holds for $h_1 > 2N_{\rm c}$, or to find the correct generalisation.

However, numerical observations suggest that $w_2(h_1, v_2)$ becomes independent of h_1 for for $v_2 \to 0$, and that in particular there is a family of solutions with $a = b = 1$ and $g = k$ even for $h_1 > 2N_{\rm c}$. This corresponds in our IR expansions (3.3.11) to setting

$$w_2 = v_2 = 0, \qquad k_2 = \frac{h_1}{3} - \frac{4N_{\rm c}^2}{3h_1} = \frac{5}{6}k_2^{\rm SUSY}, \tag{3.4.1}$$

which agrees with the values obtained numerically. Setting $v_2 > 0$ (so that $a > 1$ for small ρ) appears numerically to result in a divergent UV, and it seems likely that

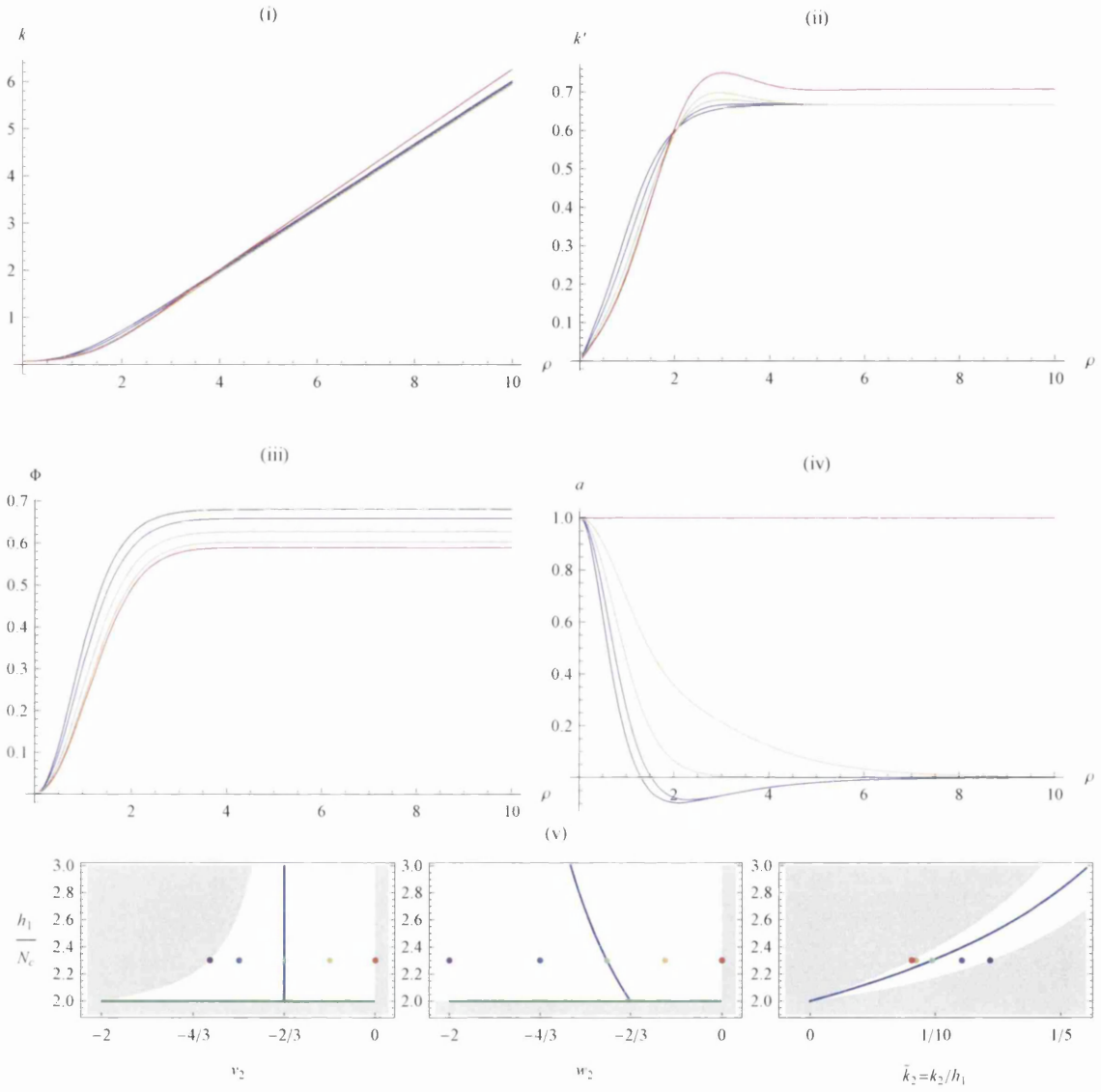

Figure 3.8: Plots of some of the metric functions for different v_2, having set $h_1 = 2.3$ with $N_c = 1$ and $\phi_0 = 0$. In (i) we plot k, showing that the SUSY-breaking parameter v_2 has little effect on the qualitative behaviour except in the case $v_2 = 0$. This transition between the generic $k \sim 2\rho/3$ and $k \sim \rho/\sqrt{2}$ is shown clearly in (ii), in which we plot the derivative. The UV behaviour, and effect of v_2, is very similar in g and h. In (iii) we plot the dilaton, showing that Φ_∞ is a function of v_2 for constant h_1, and (iv) shows the effect on a. The values of v_2 used, and the corresponding values of w_2 and k_2, are shown as coloured points on the solution space diagrams in (v). The colours correspond to those of the curves in (i)–(iv). As in figure 3.6, in (v) the blue curves are the SUSY solutions and the green lines are the GTV solutions. The shaded areas are the regions which are excluded according to the discussion of sections 3.4.2–3.4.3. As we will explain in section 3.4.3, we can restrict our attention to $w_2 > -2$ without loss of generality.

this is indeed the correct generalisation of the boundary. This corresponds to the solid red curves in figure 3.10.

Setting $a = b = 1$ and $g = k$ in the equations of motion, we find that our UV ansatz (3.3.12), (expansions in powers of $e^{4\rho/3}$) is not suitable. However, using equivalent expansions in powers of $e^{\sqrt{2}\rho}$ does lead to a solution:

$$\begin{aligned}
e^{2h} &= \frac{K_{00}}{2}e^{\sqrt{2}\rho} + \left(\frac{K_{00}K_{20}+N_c^2}{2K_{00}} + \frac{N_c^2}{2\sqrt{2}K_{00}}\rho\right)e^{-\sqrt{2}\rho} + O\big(e^{-3\sqrt{2}\rho}\big) \\
e^{2k} &= K_{00}e^{\sqrt{2}\rho} + \left(K_{20} + \frac{N_c^2}{\sqrt{2}K_{00}}\rho\right)e^{-\sqrt{2}\rho} + O\big(e^{-3\sqrt{2}\rho}\big) \\
e^{4\Phi-4\Phi_\infty} &= 1 - \frac{1}{K_{00}^2}\left(4K_{00}K_{20} + N_c^2 + 2\sqrt{2}N_c^2\rho\right)e^{-2\sqrt{2}\rho} + O\big(e^{-4\sqrt{2}\rho}\big)
\end{aligned} \tag{3.4.2}$$

It is important to emphasise that although the form of (3.4.2) is simply the original ansatz (3.3.12) with the replacement $4\rho/3 \to \sqrt{2}\rho$, we cannot obtain these expansions from the generic UV (3.3.16) simply by a change of coordinates. For example, here we have $e^{2k} = e^{2g}$, whereas in (3.3.16) we have $e^{2k} \sim 2e^{2g}/3$ for large ρ. This is why we have not attempted to match the parameters in (3.4.2) to the usual set $\{c_+, c_-, \dots\}$. Instead, we denote the two free parameters by K_{00} and K_{20}, the leading parameter (roughly corresponding to c_+) being K_{00}. Note that, as we have set $v_2 = 0$, the two parameters K_{00} and K_{20} cannot be independent once we match to the IR. This is analogous to the SUSY solutions, in which there are two UV parameters c_+ and c_-, which are related by the requirement to match to the (one-parameter) IR solutions.

Actually, we will see in chapter 4 that this picture is incomplete. If we use a more general ansatz for the UV expansions we find additional (sub-leading) terms, besides those in (3.4.2). As always, the values of the various UV parameters are not independent once we match to the IR, and so we cannot expect (3.4.2) to go to the correct (i.e. regular) behaviour in the IR. As we will see, this is confirmedwhen numerical calculations are carried out sufficiently carefully to be sensitive to the sub-leading terms.

In section 3.3.1 we noted that the 'twist' which mixes the S^2 and the S^3 could be removed by a change of coordinates when $a = b = 1$. As we still have $g = k$ here, the same coordinate transformation still works, leading to a simplified system. With C_4 and F_5 unchanged from (3.2.9), we now find

$$\begin{aligned}
ds_E^2 &= e^{\Phi/2}\left[\hat{h}^{-1/2}dx_{1,3}^2 + \hat{h}^{1/2}\left(e^{2k}d\rho^2 + e^{2h}d\Omega_2 + \frac{e^{2k}}{4}d\Omega_3\right)\right], \\
F_3 &= -\frac{N_c}{4}\tilde{\omega}_1 \wedge \tilde{\omega}_2 \wedge \tilde{\omega}_3, \\
H_3 &= 2N_c e^{2h-2k+2\Phi-\Phi_\infty}\sin\theta\; d\rho \wedge d\theta \wedge d\varphi.
\end{aligned} \tag{3.4.3}$$

Unfortunately the boundary for $v_2 < -2/3$, corresponding to $v_2 = -2$ in the GTV solutions, seems to be much less accessible numerically, in part due to the presence of changes of the sign of a and b. However, in the next section we will shed some light on this matter.

3.4.3 A $\mathbb{Z}_2$ symmetry

The system we describe in section 3.2.1, which applies to all the solutions we consider, exhibits a $\mathbb{Z}_2$ symmetry $\mathcal{I}$ which exchanges the two 2-spheres of the conifold and changes the sign of the 3-forms F_3 and H_3 in (3.2.9). To see this, we make use of the fact that all the systems we consider can be described by the Papadopoulos-Tseytlin ansatz [62]. This can be written in the form

$$\begin{aligned} ds_E^2 &= e^{\Phi/2}(\hat{h}^{-1/2}dx_{1,3}^2 + \hat{h}^{1/2}ds_6^2), \\ ds_6^2 &= \frac{2}{3}e^{-8p+3q}(4d\rho^2 + g_5^2) + e^{2p+3q}\Big\{\cosh y\,\left[e^z(\omega_1^2+\omega_2^2) + e^{-z}(\tilde{\omega}_1^2+\tilde{\omega}_2^2)\right] \\ &\qquad - 2\sinh y\,(\omega_1\tilde{\omega}_1 + \omega_2\tilde{\omega}_2)\Big\}, \end{aligned} \tag{3.4.4}$$

where the angular forms g_5 and ω_i are given by

$$\omega_1 = d\theta, \qquad \omega_2 = -\sin\theta d\varphi, \qquad g_5 = \tilde{\omega}_3 + \cos\theta d\varphi. \tag{3.4.5}$$

We use here the notation of [32], in anticipation of making contact with their results in section 3.4.4.[8] By comparing the metrics in the two cases we can write an explicit relation between our original functions and those used in (3.4.4):

$$\begin{aligned} e^{10p} &= \frac{4}{3}e^{g+h-2k}, & e^{15q} &= \frac{3}{8}e^{4g+4h+2k}, \\ e^{y} &= \frac{1}{2}e^{-h}\left(\sqrt{4e^{2h}+e^{2g}a^2} - ae^{g}\right), & e^{z} &= e^{-g}\sqrt{4e^{2h}+e^{2g}a^2}. \end{aligned} \tag{3.4.6}$$

It is then possible to show that the metric and fields are unchanged (up to a change of sign) if we exchange $(\theta,\varphi) \leftrightarrow (\tilde{\theta},\tilde{\varphi})$ and relabel $z \leftrightarrow -z$. In the KS solution [12] which we obtain by taking the limit $h_1, c_+ \to \infty$ in the SUSY solutions (section 3.2), $z = 0$ and the transformation $\mathcal{I}$ reduces to a simple change of coordinates. This is the $N_f = 0$ version of the Seiberg duality discussed in [48, 49, 50].

We now consider the effect of $\mathcal{I}$ on a generic globally regular solution of the sort we have discussed, for which $z \neq 0$. Inverting (3.4.6) we find

$$\begin{aligned} e^{2g} &= 2^{6/5}e^{2p+3q-z}\cosh y, & e^{2h} &= 2^{-4/5}e^{2p+3q+z}\,\mathrm{sech}\, y, \\ e^{2k} &= \frac{2^{11/5}}{3}e^{-8p+3q}, & a &= e^{z}\tanh y. \end{aligned} \tag{3.4.7}$$

It is then clear that the effect of taking $z \to -z$ can be written as

$$e^{2g} \to e^{2g+2z}, \qquad e^{2h} \to e^{2h-2z}, \qquad a \to e^{-2z}a. \tag{3.4.8}$$

Referring to our expansions (3.3.11, 3.3.16), we find

$$e^z = \begin{cases} 1 + (2+w_2)\rho^2 + O(\rho^4) & \text{for } \rho \to 0 \\ 1 + \dfrac{1}{c_+}\left(4H_{11}\rho + Q_o + \dfrac{3}{2}c_+W_{20}^2\right)e^{-4\rho/3} + O\big(e^{-4\rho/3}\big) & \text{for } \rho \to \infty. \end{cases} \tag{3.4.9}$$

[8] We adapt the notation slightly to avoid confusion with the vielbeins (3.2.8). The relationship with [32] is $\omega_i^{\text{here}} = e_i^{[32]}$ and $\tilde{\omega}_i^{\text{here}} = \epsilon_i^{[32]}$. We also have $\rho_{\text{here}} = \tau_{[32]}/2$.

This means that the transformation (3.4.8) has only subleading effects on g, h and a, and in particular the transformed functions are still compatible with the form of our expansions (3.3.8, 3.3.12). More specifically, we can see from (3.4.9) that for $z \to -z$ we need to take

$$w_2 \to -4 - w_2, \tag{3.4.10}$$

corresponding to a reflection in the line $w_2 = -2$. As (3.3.9) implies that $w_2^{\text{SUSY}} \to -2$ for $h_1 \to \infty$, this is compatible with the fact that the KS solution has $z = 0$. Note that because k and b do not appear in (3.4.8) we can conclude that k_2 and v_2 are unchanged under $\mathcal{I}$.

This gives us a simple procedure whereby for each solution discussed in 3.4.1, specified by values of (h_1, v_2), we can obtain different solution, with a different value of w_2. Because of the way that $\mathcal{I}$ acts only on the subleading terms in the UV expansion we can be sure that the 'reflected' solution will also be globally regular and compatible with our ansatz (3.3.12). This can be seen numerically. For a given pair of values of (h_1, v_2), the requirement of UV regularity gives us values of w_2 and k_2 as described in section 3.3.3. If we then take $w_2 \to -4 - w_2$ we immediately find another solution with the correct UV behaviour, without having to adjust v_2 or k_2. The two types of solutions are compared in figure 3.9.

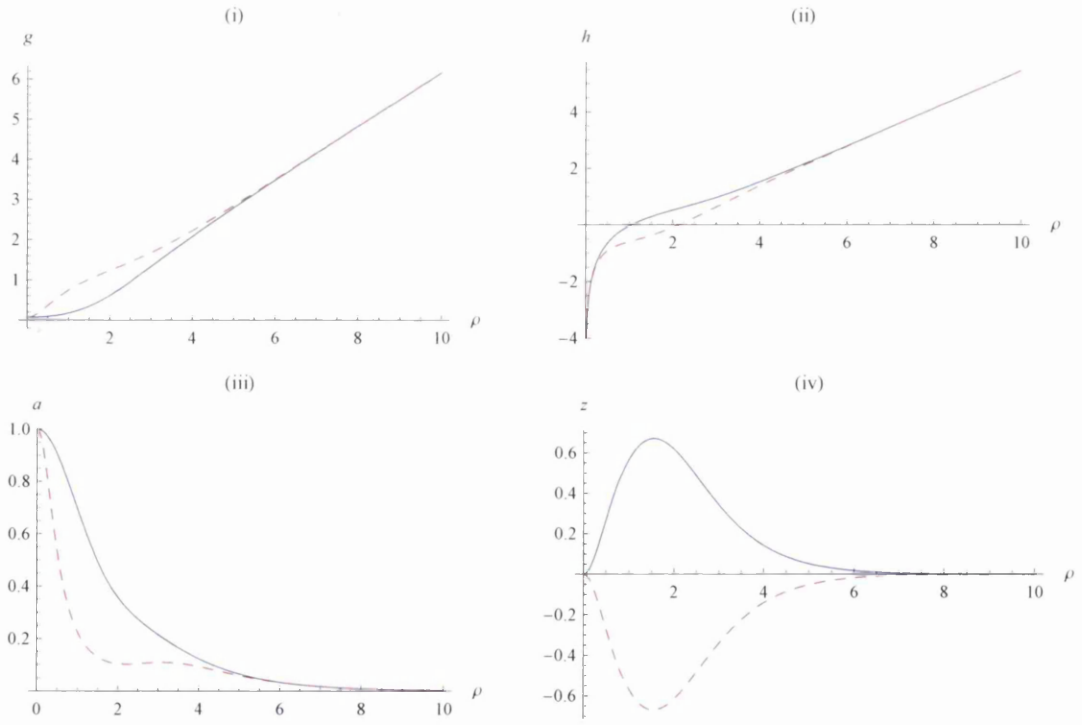

Figure 3.9: Comparison of the solutions before and after the transformation (3.4.8). The blue solid curves correspond to the original description with $w_2 > -2$, and the red dashed curves to the 'reflected' solutions with $w_2 < -2$. In (i)–(iii) we plot the three functions $\{g, h, a\}$ which are affected by the transformation, and in (iv) we show z, as defined in (3.4.6), for which the transformation is simply a change of sign. These solutions have $h_1 = 2.3$ (with $N_c = 1$) and $v_2 = -1/3$, resulting in $k_2 \approx 0.195$ and $w_2 \approx -2 \pm 1.58$ (corresponding to the yellow plots in figure 3.8).

We should emphasise, however, that although this results in a distinct solution to the equations of motion (A.2.3–A.2.8), it does not actually correspond to a different background — $\mathcal{I}$ is simply a relabeling, which is obscured by our choice of basis for the functions.

By demanding that $z \to -z$ while the other functions are unchanged, we can also write down the effect on the UV parameters equivalent to (3.4.10):

$$\begin{aligned}
&\frac{c_-}{c_+^3} \to \frac{c_-}{c_+^3} - 32W_{20}\left(2\frac{Q_o}{c_+} + 3W_{20}^2\right)\left(2e^{2\rho_o} - \frac{Q_o}{c_+}W_{20} - \frac{3}{2}W_{20}^3\right), \\
&\frac{Q_o}{c_+} \to -\frac{Q_o}{c_+} - 3W_{20}^2, \qquad e^{2\rho_o} \to e^{2\rho_o} - \frac{Q_o}{c_+}W_{20} - \frac{3}{2}W_{20}^3, \qquad \frac{H_{11}}{c_+} \to -\frac{H_{11}}{c_+},
\end{aligned} \tag{3.4.11}$$

while keeping the remaining parameters $\{c_+, \Phi_\infty, W_{20}, \Phi_{30}, V_{40}\}$ fixed. We retain the factors of $1/c_+$ in anticipation of taking the limit $c_+ \to \infty$.

For solutions with $w_2 = -2$, the IR expansion (3.4.9) appears to vanish at all orders. We would therefore expect that these solutions have $z = 0$ for all ρ, meaning that as in the KS solution $\mathcal{I}$ is a symmetry of the geometry. Our numerical calculations support this assumption — for these solutions we find that z is indeed essentially zero everywhere (we find $z \lesssim 10^{-14}$ for all $\rho \lesssim 30$).

This family of solutions consists of a line in the (h_1, w_2) plane (see figure 3.10), and it would be interesting to determine the corresponding curves in the (h_1, v_2) and (h_1, k_2) planes. We have not been able to determine exact expressions for these functions, but for large h_1 we find numerically that $\Delta v_2(h_1) = v_2(h_1) + 2/3 \sim -1/h_1^2$, and

$$\Delta k_2(h_1) = k_2(h_1) - k_2^{\text{SUSY}}(h_1) = \frac{16}{45h_1} - \epsilon(h_1), \tag{3.4.12}$$

where the higher-order corrections $\epsilon > 0$ to this last expression are extremely suppressed. For example, with $h_1 \approx 10^3$ we find that using $\Delta k_2 = 16/45h_1$ gives the correct value up to around eleven significant digits. In figure 3.10 the curves $v_2(w_2 = -2)$ and $k_2(w_2 = -2)$ were obtained from expansions in powers of $1/h_1$ fitted to eight solutions determined numerically.

If these solutions are indeed symmetric under $\mathcal{I}$ for all ρ then we can write down a relationship between some of the UV parameters, analogous to the requirement that $w_2 = -2$. Specifically, referring to (3.4.11), we find[9]

$$W_{20}^2 = -\frac{2Q_o}{3c_+}, \qquad \frac{H_{11}}{c_+} = 0. \tag{3.4.13}$$

As expected, this is satisfied by the SUSY values (3.3.17) in the limit $c_+ \to \infty$, corresponding to the KS solution.

In section 3.4.2 we considered the generalisation to $h_1 > 2N_c$ of the upper bound $v_2 = 0$ in the GTV solutions (section 3.3.1). It is suggestive that the line of solutions in which the geometry possesses a $\mathbb{Z}_2$ symmetry passes through the lower bound, $v_2 = -2$. In the light of the discussion in this section, we should reinterpret this boundary in the GTV solutions. If we parametrise the solutions by w_2, we see

[9]Of course, we still have the usual undetermined relationships between the UV parameters, so that we are left with only one degree of freedom corresponding to the position on the line $w_2 = -2$.

that there is no lower bound on w_2, but $v_2(w_2)$ has a minimum at $w_2 = -2$. This description was not possible in the context of [24], in which all solutions had $a = b$ (so that $v_2 = w_2$).

Interpreting the boundary as a minimum of $v_2(w_2)$ would imply that the line $w_2 = -2$ is the right generalisation to $h_1 > 2N_c$. This is supported by our numerical analysis. It appears not to be possible to tune to a regular UV for values of v_2 smaller than that which gives $w_2 = -2$.

Of course, we must be cautious here — our inability to find a solution with $w_2 < -2$ could simply be the result of a significant discontinuity in the values of the other parameters across the line $w_2 = -2$.

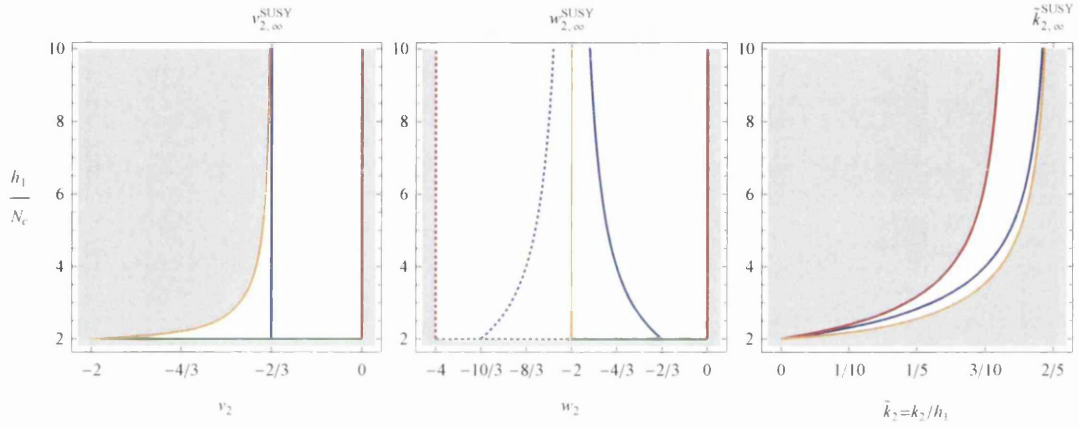

Figure 3.10: The space of solutions, as in figure 3.6. Again, the blue and green curves are the SUSY and GTV solutions respectively. The red curves correspond to the case $a = b = 1$ discussed in section 3.4.2, while the orange curves correspond to the solutions which are invariant under $\mathcal{I}$, and so have a $\mathbb{Z}_2$ symmetry of the geometry (section 3.4.3). The dotted curves are the equivalents with $w_2 \to -4 - w_2$. Under the assumption that these two cases constitute the correct generalisation of the requirement $-2 \leq v_2 \leq 0$ in the GTV solutions, the gray shaded areas show the regions where no regular solutions exist.

3.4.4 The limit $h_1, c_+ \to \infty$

Having discussed a non-SUSY generalisation of the baryonic branch, it is natural to consider the generalisation of the Klebanov-Strassler solution [12] itself, which in the SUSY case occurs in the limit $h_1 \sim c_+ \to \infty$. In terms of the functions $\{p, q, y, z\}$ which we introduced in section 3.4.3, the SUSY KS solution has a simple exact description: with $\Phi =$ constant and $z = 0$, we have

$$e^{10p} = K^3 \sinh 2\rho, \qquad e^{15q} = \frac{3^{5/4}}{2^{15/2}} K^2 \sinh^4 2\rho, \qquad e^y = \tanh \rho, \tag{3.4.14}$$

where we have defined

$$K \equiv \frac{(\sinh 4\rho - 4\rho)^{1/3}}{2^{1/3} \sinh 2\rho}. \tag{3.4.15}$$

The remaining function $b = 2\rho/\sinh 2\rho$ is the same as in the whole SUSY baryonic branch. As we have seen in section 3.4.3, the fact that $z = 0$ implies that the geometry itself possesses a $\mathbb{Z}_2$ symmetry.

Of course, in order for the concept of a non-SUSY generalisation to be meaningful, we have to choose which characteristics of the SUSY KS solution we want to keep in the non-SUSY solution. One natural possibility would be to require that the geometry retains the $\mathbb{Z}_2$ symmetry, in which case the we obtain the family of solutions with $w_2 = -2$ which we discussed in section 3.4.3.

However in [32], Dymarsky and Kuperstein (DK) followed a different approach. They noted that the KS background has several simplifying features which are retained in the linear deformations studied in [63, 14], but not in the generic baryonic branch:

(i) A constant dilaton, $e^{\Phi} = g_s$

(ii) An imaginary self-dual 3-form flux[10], $iG_3 = *_6 G_3$, where $G_3 \equiv F_3 + \frac{i}{g_s} H_3$

(iii) An RR 4-form satisfying $C_4 = H^{-1}\mathrm{Vol}_{1,3}$, where $ds^2 = H^{-1/2} dx^2_{1,3} + H^{1/2} ds^2_6$

(iv) A Ricci-flat 6d unwarped metric

As noted in [32], these are particularly convenient because they mean that the fluxes completely decouple from the equations which determine the metric. It should be noted that in our solutions (ii) and (iii) are satisfied automatically once (i) is imposed.

By imposing that these properties are retained, DK found a one-dimensional family of solutions which break both SUSY and the $\mathbb{Z}_2$ symmetry of the geometry (although the full symmetry including the exchange $z \leftrightarrow -z$ is of course retained). It seems natural to assume that this corresponds to a line of solutions in the two-dimensional solution space described above.

To see that this is indeed the case, we first need to identify the appropriate limit. Referring to our generic IR expansions (3.3.11), we see that we obtain a constant dilaton in the limit $h_1 \to \infty$, as in the SUSY case. This means that conditions (i)–(iii) are satisfied. It is also possible to check that this results in the IR expansion for the 6d Ricci scalar vanishing, as required by condition (iv).

We now look to relate our three SUSY-breaking parameters $\{w_2, k_2, v_2\}$ to the parameters $\{\zeta_1, \zeta_2, \zeta_3\}$ used in [32]. Looking then at the IR expansion for z, we find by substituting our IR expansions (3.3.11) into (3.4.6)

$$z = (2 + w_2)\rho^2 + O(\rho^4), \tag{3.4.16}$$

meaning we can compare with the expression given in [32] and conclude that

$$w_2 = 4\zeta_1 - 2. \tag{3.4.17}$$

To gain the relation for k_2 we look at the expansion for e^y and upon taking the limit $h_1 \to \infty$ we find

$$e^y = \rho - \left(\frac{2}{3} + 4\zeta_1^2\right)\rho^3 + O(\rho^5). \tag{3.4.18}$$

[10]Here $*_6$ is the six-dimensional Hodge dual

This does not have enough freedom in the ρ^3 term when compared to [32]. To fix this, it is possible to take $k_2 \to \infty$ while keeping fixed $\tilde{k}_2 \equiv k_2/h_1$. This then gives

$$e^y = \rho - \left(\frac{2}{3} + 4\zeta_1^2 - \frac{5}{6}\tilde{k}_2\right)\rho^3 + O(\rho^5), \tag{3.4.19}$$

which we can match to the result of [32] by setting

$$\tilde{k}_2 \equiv \frac{k_2}{h_1} = \frac{2}{65}(13 - 90\zeta_2). \tag{3.4.20}$$

We finally need to determine the relationship between v_2 and ζ_3. This can be achieved by comparing our expansion for b with that for $F = (1-b)/2$ in [32], from which we obtain

$$v_2 = -\frac{2}{3}(\zeta_3 + 1). \tag{3.4.21}$$

In summary, in the limit $h_1 \to \infty$ we find the following relationships between our three SUSY-breaking IR parameters and those used in [32]:

$$w_2 = 4\zeta_1 - 2, \qquad \tilde{k}_2 \equiv \frac{k_2}{h_1} = \frac{2}{65}(13 - 90\zeta_2), \qquad v_2 = -\frac{2}{3}(\zeta_3 + 1). \tag{3.4.22}$$

Of course, setting the ζ_i to zero we recover (the large-h_1 limit of) the SUSY values (3.3.9). In fact, defining for example $\Delta w_2(h_1) = w_2 - w_2^{\text{SUSY}}(h_1)$, we obtain

$$\zeta_1 = \frac{1}{4}\Delta w_2, \qquad \zeta_2 = -\frac{13}{36}\Delta\tilde{k}_2, \qquad \zeta_3 = -\frac{3}{2}\Delta v_2. \tag{3.4.23}$$

In the UV we are less sure how to find similar relationships between parameters. It is clear from the numerical analysis that the relevant limit is still $c_+ \to \infty$ (even if the precise relation (3.2.16) may no longer hold in the non-SUSY case), and we know we will need $\Phi_\infty \to \phi_0$ in order to get a constant dilaton. However, it is not obvious how the other parameters in (3.3.15) behave in this limit. One possibility is suggested by the fact that in the case of the IR parameters we could have guessed the correct behaviour ($v_2 \sim w_2 \sim$ constant, $k_2 \sim h_1$) from the h_1-dependence of the SUSY values (3.3.9) in the limit. Using the same approach in the UV would imply that we should consider all the remaining parameters fixed except for $\Phi_{30} \sim 1/c_+^2$.

Looking at the UV expansions for the 6d Ricci scalar and the dilaton we find that in fact the limit $c_+ \to \infty$ is itself sufficient for Ricci-flatness, and taking both $c_+ \to \infty$ and $\Phi_{30} \to 0$ gives a constant dilaton. This can be seen for the SUSY baryonic branch in figure 3.1 (iv); the non-SUSY solutions show qualitatively the same behaviour.

Unlike in the case $h_1 \to 2N_c$, our numerical approach does not allow us to take the limit $h_1 \to \infty$ explicitly. However, we can probe sufficiently large values of h_1 to yield solutions which appear to have many of the characteristics we expect from the true limit. For example, we do not have to take h_1 very large before the dilaton is very close to constant. Notice in figure 3.1 (iv) the curve for $h_1 = 12$ appears to lie on the axis.

3.5 Energy

In this section we study the energy of the non-SUSY solutions found above. For any stationary spacetime admitting foliations by a spacelike hypersurface Σ_t, the free energy and the energy are related via the thermodynamic relation $F = E - TS$. Here we are considering $T = 0$ backgrounds and so we expect $F = E$. In this section we will first calculate the ADM energy E, for the solutions before the U-duality — we will refer to the U-duality of reference [47] as 'rotation'. We will then repeat this calculation for the solutions after rotation and show that the energies before and after rotation are equal. As a check of our results, in Appendix B.1 we obtain the free energy using the on-shell action method and show that $F = E$.

3.5.1 ADM energy

Consider a non-asymptotically flat 10-dimensional background. Let Σ_t be a 9-dimensional constant-time slice whose 8 dimensional boundary is a constant-radius surface S_t^∞. The regularized internal energy E is defined as [64],

$$E = -\frac{1}{8\pi}\int_{S_t^\infty}\left[N_t\left({}^8K - {}^8K_0\right) + N_t^\mu p_{\mu\nu}n^\nu\right]dS_t^\infty. \tag{3.5.1}$$

N_t is the lapse function, N_t^μ is the shift vector, $p_{\mu\nu}$ the momentum conjugate to the time derivative in the constant time-slice, ${}^8K$ and ${}^8K_0$ are the extrinsic curvatures of the 8 dimensional boundary S_t^∞, for the background under consideration and the reference background respectively. Finally n^ν is the spatial unit vector normal to the constant radius-surface S_t^∞. It is required that both geometries induce the same metric on ${S_t}^\infty$. The matter fields should also agree at S_t^∞ or at least the difference should tend to zero as S_t^∞ goes to infinity. We will choose a SUSY background as a reference geometry.

For the metrics before rotation (3.2.4–3.2.6) we have $N_t^\mu = 0$, $N_t = \sqrt{|g_{00}|} = e^{\Phi/4}$, $dS_t^\infty = \frac{1}{8}e^{2(\Phi+g+h)+k}$, $n^\mu = \sqrt{g^{rr}}\delta_r^\mu = e^{-\Phi/4}e^{-k}$. The extrinsic curvature is

$${}^8K = \nabla_\mu n^\mu = \frac{1}{\sqrt{g_9}}\partial_\mu(\sqrt{g_9}n^\mu) = e^{-\Phi/4-k}\Big[2(\Phi' + g' + h') + k'\Big], \tag{3.5.2}$$

where g_9 denotes the determinant of the 9-dimensional constant time slice Σ_t. The requirement that the induced metrics on ${S_t}^\infty$ agree at the boundary implies[11],

$$e^{\frac{\Phi_{ns}}{2}}e^{2g_{ns}} = e^{\frac{\Phi_{su}}{2}}e^{2g_{su}}, \quad e^{\frac{\Phi_{ns}}{2}}e^{2h_{ns}} = e^{\frac{\Phi_{su}}{2}}e^{2h_{su}}, \quad e^{\frac{\Phi_{ns}}{2}}e^{2k_{ns}} = e^{\frac{\Phi_{su}}{2}}e^{2k_{su}}, \tag{3.5.3}$$

and the g_{00} component agrees if

$$e^{-\frac{\Phi_{ns}}{2}} = e^{-\frac{\Phi_{su}}{2}}. \tag{3.5.4}$$

All the quantities in (3.5.3) and (3.5.4) are evaluated at some large but finite r_c that acts as a cutoff. Using (3.5.1), the energy is

$$E = -\frac{vol_8}{64\pi}\lim_{r_c\to\infty}\left\{e^{-k_{ns}}\left(e^{2\Phi_{ns}+2g_{ns}+2h_{ns}+k_{ns}}\right)' - e^{-k_s}\left(e^{2\Phi_s+2g_s+2h_s+k_s}\right)'\right\}. \tag{3.5.5}$$

[11]The subscripts ns and su stand for non-supersymmetric and supersymetric respectively.

Before evaluating (3.5.5) we have to satisfy the matching conditions at the boundary, (3.5.3) and (3.5.4). In order to do this we have to use the most general asymptotics of a supersymmetric solution. As discussed in eq.(3.3.17), analyzing the BPS equations (see Appendix A in reference [48]) we see that the most general supersymmetric UV asymptotics is obtained by replacing

$$W_{20} \to 0,\ V_{40} \to 2e^{2\rho_o}(1+Q_o),\ H_{11} \to 1/2,\ \Phi_{30} \to -3\frac{(3+4Q_o)}{4c_+^2}e^{4\Phi_\infty} \tag{3.5.6}$$

in the non-supersymmetric expansion (3.3.12). Notice that this substitution restores the integration constants Q_o, ρ_0 and e^{Φ_∞} that are usually set to -1, 0 and 1 respectively [50]. Reintroducing the integration constants is equivalent to using the shift invariance of the r coordinate (encoded in Q_0 and ρ_0) and the dilaton [65]. Adjusting these constants will allow us to satisfy the matching conditions at the boundary and cancel divergences in the energy. Given the complexity of the UV expansions the matching procedure is cumbersome but straightforward. Working to linear order in W_{20} we obtain,

$$E = \frac{1}{24\pi}c_+^2 e^{2\rho_0+2\Phi_\infty}W_{20}. \tag{3.5.7}$$

After the duality transformations the UV asymptotics changes drastically. In this case we have $N_t^\mu = 0$, $N_t = \sqrt{|g_{00}|} = \frac{e^{-\Phi/4}}{H^{1/4}}$, $dS_t^\infty = \frac{1}{8}e^{3\Phi+2g+2h+k}H^{1/2}$, $n^\mu = e^{-3\Phi/4}e^{-k}H^{-1/4}$ and

$${}^8K = \nabla_\mu n^\mu = \frac{1}{\sqrt{g_9}}\partial_\mu(\sqrt{g_9}n^\mu) = \frac{e^{-\frac{3\Phi}{4}-k}}{2H^{5/4}}\left[H' + 2H(3\Phi' + 2g' + 2h' + k')\right]. \tag{3.5.8}$$

Note that here we defined $H = e^{-2\Phi} - e^{-2\Phi_\infty}$. The regularized energy after the rotation is

$$E = -\frac{vol_8}{64\pi^2}\lim_{r\to\infty}\{\Delta_{ns} - \Delta_{su}\} \tag{3.5.9}$$

where

$$\Delta \equiv \frac{e^{-\Phi-k}}{\sqrt{H}}\left(\sqrt{H}e^{3\Phi+2g+2h+k}\right)'. \tag{3.5.10}$$

The matching conditions now read,

$$\begin{aligned} H_{ns}^{1/2}e^{\frac{3\Phi_{ns}}{2}+2g_{ns}} &= H_{su}^{1/2}e^{\frac{3\Phi_{su}}{2}+2g_{su}}, \qquad H_{ns}^{1/2}e^{\frac{3\Phi_{ns}}{2}+2h_{ns}} = H_{su}^{1/2}e^{\frac{3\Phi_{su}}{2}+2h_{su}}, \\ H_{ns}^{1/2}e^{\frac{3\Phi_{ns}}{2}+2k_{ns}} &= H_{su}e^{\frac{3\Phi_{su}}{2}+2k_{su}}, \qquad H_{ns}^{-\frac{1}{2}}e^{-\frac{\Phi_{ns}}{2}} = H_{su}^{-1/2}e^{-\frac{\Phi_{su}}{2}}. \end{aligned} \tag{3.5.11}$$

Note that

$$\begin{aligned} \Delta &= e^{-k}\left(e^{2\Phi+2g+2h+k}\right)' + \frac{e^{\Phi+2g+2h}}{\sqrt{H}}\left(e^{\Phi}\sqrt{H}\right)' \\ &= \Delta^{before} + \Delta^{extra} \end{aligned} \tag{3.5.12}$$

where $\Delta^{before} \equiv e^{-k}\left(e^{2\Phi+2g+2h+k}\right)'$ and $\Delta^{extra} \equiv \frac{e^{\Phi+2g+2h}}{\sqrt{H}}\left(e^{\Phi}\sqrt{H}\right)'$. We have

$$E = -\frac{vol_8}{64\pi^2}\lim_{r_c\to\infty}\left\{(\Delta_{ns}^{before} - \Delta_s^{before}) - (\Delta_{ns}^{extra} - \Delta_s^{extra})\right\}, \tag{3.5.13}$$

where all the functions are evaluated at some large but finite cutoff r_c. After adjusting the parameters to ensure that the induced metrics at the boundaries are the same, as required in (3.5.11), we take the cutoff to infinity. The first two terms in (3.5.13) are the same as in the energy before rotation (3.5.5). We find that — to first order in W_{20} — the matching conditions are satisfied using the same set of integration constants as before the rotation. Thus, the first two terms in (3.5.13) give exactly the energy before rotation. Any difference in energies will come from the *extra* terms (3.5.13). However, it can be shown that using the integration constants necessary to satisfy (3.5.11),

$$\lim_{r_c\to\infty}\left\{(\Delta_{ns}^{extra}-\Delta_{s}^{extra})\right\}=0. \tag{3.5.14}$$

Thus the energy before and after rotation are the same[12]. Indeed, plugging in the UV expansions directly in (3.5.9) we obtain,

$$E=\frac{1}{24\pi}c_+^2e^{2\rho_0+2\Phi_\infty}W_{20}. \tag{3.5.15}$$

A couple of comments are in order. First, note that the overall constant that appears in the energy can be changed by shifting the value of the dilaton at infinity. Thus, the physically meaningful statement is that the energies before and after rotation have the same functional dependence on the parameters,

$$E_{before}\sim E_{after}\sim c_+^2e^{2\rho_0+2\Phi_\infty}W_{20}. \tag{3.5.16}$$

Second, this calculation can be carried out to higher order in the SUSY breaking parameter W_{20}. The divergences in the energy can be cancelled by subtracting an appropiate SUSY background. However, at higher orders there will always be a discrepancy of order W_{20}^2 of the metrics at the boundary. This clearly indicates that the treatment presented in this section is valid only for soft supersymmetry breaking with small breaking parameter, W_{20}. Had we not expanded around $W_{20}\sim 0$ the mismatch at the boundary could be arbitrarily large indicating that the non-supersymmetric solution does not approach the SUSY solution fast enough for the energy to be finite, indicating that one should find another reference background to subtract. Note that this substantiates the smallness of W_{20} seen numerically in the previous section where the solutions found have $W_{20}\sim\mathcal{O}(10^{-5})$.

3.6 Field Theory Aspects

In this section we will analyze various field theory aspects of a non-SUSY version of the quiver that we called field theory B and described below eq.(3.2.2) To this end, we will use the non-SUSY background one obtains when plugging our numerical solutions in the background of eq.(3.2.9) dual to the field theory B.

To begin with, notice that in eq.(3.2.9) we did not specify the NS potential B_2. Since this will be useful below, we discuss it here (the result is different from the SUSY one).

[12]This suggests that the ADM Energy is 'uncharged' under the U-duality, like probably are also uncharged various thermodynamical quantities.

Following the intuition gained in the SUSY example, we propose a B_2 of the form

$$B_2 = b_1(\rho)e^{\rho 3} + b_2(\rho)e^{\theta\varphi} + b_3(\rho)e^{12} + b_4(\rho)e^{\theta 2} + b_5(\rho)e^{\varphi 1}, \tag{3.6.1}$$

by imposing that $dB_2 = H_3$ and that the Page charge vanishes $Q_{\text{Page, D3}} = 0$ (see below) we obtain — all details are discussed in Appendix B.2 —

$$\begin{aligned}
b_1 &= \frac{e^{2g-2k}}{4\hat{h}}\left[2b_3\Phi' - 3\hat{h}b_3\Phi' - 4\hat{h}b_3g' - 2\hat{h}b_3' + \kappa N_c e^{\frac{3\Phi}{2}-2h}\hat{h}^{\frac{1}{2}}\left(a^2 - 2ab + 1\right)\right] \\
b_2 &= \frac{e^{-2h}}{4\hat{h}^{1/2}}\left\{e^{2g}\hat{h}^{\frac{1}{2}}\left(1-a^2\right)b_3 - \frac{\kappa}{N_c}e^{\frac{3\Phi}{2}}\left[N_c^2(a-b)b' + 4e^{2(g+h)}\Phi'\right]\right\} \\
b_4 &= b_5 = -\frac{1}{2}e^{g-h}ab_3 - \frac{\kappa N_c e^{\frac{3\Phi}{2}-g-h}b'}{4\hat{h}^{1/2}},
\end{aligned} \tag{3.6.2}$$

with $b_3(\rho)$ an undetermined function. This freedom corresponds to a gauge transformation. A general B_2 can be expressed as

$$B_2 = (B_2)_{b_3=0} - \frac{1}{2}d\Big(e^{2g-k+\Phi/4}\hat{h}^{1/4}b_3\ e^3\Big). \tag{3.6.3}$$

Before computing various observables of the strongly coupled non-SUSY field theory I, we will quote another quantity that will appear frequently in the analysis. This is a periodic quantity in the string theory. Given the two cycle defined as,

$$\Sigma_2 = [\theta = \tilde{\theta}, \varphi = 2\pi - \tilde{\varphi}, \psi = \psi_0], \tag{3.6.4}$$

we define

$$b_0 = \frac{1}{4\pi^2}\int_{\Sigma_2} B_2. \tag{3.6.5}$$

When computed explicitly using the form of the B_2 potential in eqs.(3.6.1-3.6.2), we obtain

$$b_0(\psi_0) = \frac{\kappa N_c}{4\pi}e^{2\Phi}b'(b + \cos\psi_0) - \frac{\kappa}{\pi N_c}e^{2\Phi+2h+2g}\Phi' \tag{3.6.6}$$

These quantities together with those appearing in the background of eq.(3.2.9) will be important in the study of the non-perturbative field theory dynamics.

3.6.1 General remarks on the dual field theory

Here we shall discuss a little about how the structure of the solution space described above relates to the dual field theories to the gravity backgrounds we have presented.

We will only consider the solutions with $h_1 > 2N_c$. In this case the geometry is 'almost' asymptotically AdS_5. More precisely, for large ρ we can write the metric in the form

$$\begin{aligned}
ds^2 &\sim \frac{u^2}{H(u)^{1/2}}dx_{1,3}^2 + \frac{H(u)^{1/2}}{u^2}du^2 + ds_5^2, \\
H(u) &\sim \log u + \text{constant} + O(u^{-2}),
\end{aligned} \tag{3.6.7}$$

where we have defined a suitable radial coordinate u (increasing with ρ). For the generic solutions satisfying the ansatz (3.3.12) (including the SUSY solutions), the definition which results in (3.6.7) is $u = e^{2\rho/3}$. For the solutions with $v_2 = 0$ discussed in section 3.4.2 we instead need $u = e^{\rho/\sqrt{2}}$. The term of order $\log u$ in the correction $H(u)$ results from the sub-leading behaviour of the dilaton (3.3.16, 3.4.2).

There are three different field combinations which are invariant under the rotation which are of interest [7]. The first is the dilaton Φ, and the others are defined as

$$M_1 = e^{2z} - 1 = a^2 + 4e^{2h-2g} - 1, \qquad M_2 = e^{2h+2g-4k}. \tag{3.6.8}$$

In the case of the generic solutions described by (3.3.16), these functions have UV expansions

$$\begin{aligned} e^{\Phi-\Phi_\infty} &= 1 - \left(\frac{3N_c^2}{2c_+^2}\rho - e^{-4\Phi_\infty}\frac{\Phi_{30}}{4}\right)e^{-\frac{8}{3}\rho} + O\big(e^{-4\rho}\big), \\ M_1 &= \big(8H_{11}\rho + 3c_+W_{20}^2 + 2Q_0\big)\frac{e^{-4\rho/3}}{c_+} + O(e^{-8\rho/3}), \\ M_2 &= \frac{9}{16} - \frac{27}{16}W_{20}^2 e^{-4\rho/3} + O(e^{-8\rho/3}). \end{aligned} \tag{3.6.9}$$

By looking at the asymptotic behaviour of fields (and combinations of them) it is possible to think of our constants in terms of the operators which are deforming a fixed point. We may do this as it is understood that a generic field $\mathcal{M} \sim u^{-\Delta}$ as $u \to \infty$ behaves in the following manner. If $\Delta > 0$ (or $\Delta = 0$) it is either an indication of a relevant (or marginal) operator in the Lagrangian or the VEV for an operator of dimension Δ. If instead, $\Delta < 0$, then it indicates the insertion of an irrelevant operator of dimension $(4 - \Delta)$ in the Lagrangian.

Using this analysis it can be seen, from the UV expansion above, that the dilaton falls into the marginal operator category as it has scaling dimension $\Delta = 4$ (this can be associated with a certain combination of gauge couplings discussed in [2]).

We can further use this analysis on the expansion of the function $b(\rho)$ presented here for convenience

$$b = \frac{9W_{20}}{4}e^{-\frac{2}{3}\rho} + \left[\frac{10W_{20}^3}{3}\rho^2 + \left(4e^{2\rho_o} - \frac{Q_oW_{20}}{c_+} - \frac{23W_{20}^3}{6}\right)\rho + V_{40}\right]e^{-2\rho} + O\big(e^{-\frac{10}{3}\rho}\big). \tag{3.6.10}$$

Here we can see that W_{20}, which we could consider to be our 'SUSY-breaking constant', corresponds to an operator of dimension three being inserted in the Lagrangian. We anticipated in section 3.3.2 that we can associate this operator with the mass of the gaugino, as in [2]. Following the SUSY case we also associate $e^{2\rho_0}$, which appears at next-to-leading order in M_1, with the VEV of the gaugino. From this we can write schematically

$$W_{20} \to m\lambda\lambda, \qquad e^{2\rho_0} \to \langle\lambda\lambda\rangle \sim \Lambda_{\rm YM}^3. \tag{3.6.11}$$

It should be noted that this association is not exact once we have broken SUSY — the SUSY-breaking parameter can generically also deform the gaugino VEV, as indicated by the contributions from W_{20} and V_{40} to M_1 in (3.6.9).

As discussed in appendix A.5, it appears that $W_{20} \to \infty$ as we approach the boundary at $v_2 = w_2 = 0$ (figure A.1). This suggests that we can interpret the solution *on* the boundary, with $a = b = 1$ for all ρ (section 3.4.2) as corresponding to a field theory in which the gaugino has been given infinite mass. We therefore no longer have soft SUSY breaking — the theory is non-SUSY all the way into the UV. Presumably, by sending the mass to infinity we effectively remove the gaugino entirely, obtaining a completely non-SUSY theory.

We can now look to the field combination M_1 and see that it can be thought of as corresponding to the VEV of a dimension two operator $\mathcal{U}$. In the SUSY case we can identify [66]

$$\mathcal{U} \sim \mathrm{tr}[AA^\dagger - B^\dagger B], \tag{3.6.12}$$

and this operator getting a VEV is the exact thing which allows us to explore the baryonic branch. Notice that in the SUSY case $W_{20} = 0$ and the leading term of M_1 vanishes for $c_+ \to \infty$, when we recover KS. This is also the limit in which the geometry is invariant under the $\mathbb{Z}_2$ symmetry $\mathcal{I}$ which we discussed in section 3.4.3. In fact, from the point of view of the field theory, the transformation $\mathcal{I}$ can be identified with swapping $A \leftrightarrow B$ [63].

As soon as we move away from the SUSY solutions we can no longer make the identification (3.6.12). However, it is still instructive to consider the behaviour of the operator $\mathcal{U}$ associated with M_1. From (3.6.9) it is clear that we can expect $\mathcal{U}$ to be changed when we break SUSY while keeping c_+ fixed. Indeed, referring to the definition (3.6.8), we see that $M_1 = 0$ when $z = 0$. This applies at all ρ in all the solutions on the line $w_2 = -2$. (As required, we see that the combination of parameters appearing in the UV expansion (3.6.9) vanishes when (3.4.13) is satisfied.) It is interesting that the presence of the $\mathbb{Z}_2$ symmetry still corresponds to the vanishing of this operator, even in the non-SUSY case. This is perhaps indicative of the extent to which the structure of the SUSY system survives in the generic case.

As we move in the opposite direction from the SUSY solutions, increasing v_2 (and W_{20}) we find numerically (appendix A.5) that both terms at leading order in M_1 diverge. However, in the limit we obtain the solutions described in section 3.4.2 and the expansions (3.6.9) are no longer valid. Instead, for large ρ

$$M_1 = 2 + \frac{2N_c^2}{K_{00}^2} e^{-2\sqrt{2}\rho} + O\big(e^{-4\sqrt{2}\rho}\big). \tag{3.6.13}$$

This is qualitatively different to the generic case. Firstly, we now have $M_1 \to 2$ in the UV, as opposed to $M_1 \to 0$. This indicates that these solutions do not recover the $\mathbb{Z}_2$ symmetry in the UV. Secondly, the next-to-leading term is now of order u^{-4}, meaning that we can no longer associate this field with a dimension two operator.

There is some subtlety here in the fact that unlike in [2] we have allowed our deformations of the SUSY solutions to become large. It is then not clear that any deductions based on analogy with the SUSY solutions remains valid. In particular, we cannot not necessarily expect to find stable solutions for all values of W_{20}. However, the similarities between the SUSY and non-SUSY solutions are interesting. It should be noted that we still find a continuous and smooth deformation of the SUSY solutions between smaller and larger values of the non-SUSY deformations in the IR. We only find a different UV expansion in the limiting cases (or boundaries of our solution space).

3.6.2 Calculation of observables

We now move into the calculation of observables that will help us understand the field theory interpretation of our solution. In this section we will generally assume that the SUSY-breaking parameters are small. In other words, we are restricting our attention to the region of the parameter space close to the (SUSY) baryonic branch (close to the blue curves in figure 3.10). However, at least some the quantities calculated here may have significance even outside that region.

Energy

We take the expressions for the ADM Energy of the non-SUSY backgrounds as derived in eqs.(3.5.7) and (3.5.16) and we use the map described in eq.(3.6.11), we obtain that

$$E_{ADM} \sim c_+^2 e^{2\Phi(\infty)} e^{2\rho_0} W_{20} \sim m\Lambda_{YM}^3. \tag{3.6.14}$$

Then the energy is proportional to the gaugino mass and the strong coupling scale, as expected. The result in eq.(3.6.14) was first obtained in [67].

Charges

We will define the Maxwell and Page Charges

$$\begin{aligned} Q_{\text{Maxwell, D3}} &= \frac{1}{16\pi^4}\int_{X_5} F_5, \qquad Q_{\text{Maxwell, D5}} = \frac{1}{4\pi^2}\int_{X_3} F_3, \\ Q_{\text{Page, D3}} &= \frac{1}{16\pi^4}\int_{X_5} F_5 - B_2 \wedge F_3, \end{aligned} \tag{3.6.15}$$

where the manifold $X_5 = [\theta, \varphi, \tilde{\theta}, \tilde{\varphi}, \psi]$ and $X_3 = [\tilde{\theta}, \tilde{\varphi}, \psi]$. As in the SUSY case we have that

$$Q_{\text{Maxwell, D3}} = \frac{\kappa}{\pi} e^{2g+2h+2\Phi}\Phi', \qquad Q_{\text{Maxwell, D5}} = N_c. \tag{3.6.16}$$

We have also imposed that $Q_{\text{Page, D3}} = 0$ in determining the B_2 field of eq.(3.6.1) — see Appendix B.2 for details. The vanishing of the D3-Page charge is a feature of the SUSY non-singular solutions; this is the reason why we imposed it here. It would be interesting to see if one can obtain a regular non-SUSY solution in the presence of sources indicated by a non-vanishing Page charge. Using the UV expansions, the Maxwell charge for D3 branes is

$$\begin{aligned} Q_{\text{Maxwell, D3}} = \frac{e^{\Phi_\infty}}{\pi}\rho - \frac{1}{24\pi}\left(9e^{\Phi_\infty} + 4c_+^2 e^{-3\Phi_\infty}\Phi_{30}\right) \\ + \frac{33e^{\Phi_\infty}W_{20}^2}{32\pi} e^{-4\rho/3} + O\left(e^{-8\rho/3}\right). \end{aligned} \tag{3.6.17}$$

So, we see that W_{20}, the same number that determines the mass of the gaugino according the discussion above, changes the large energy value of the Maxwell charge (correspondingly of the c-function — see below) in a subleading way, as expected.

Gauge couplings and beta functions

Let us review briefly what happens in the SUSY case. In the $SU(N_c+n)\times SU(n)$ SUSY quiver, we have two couplings g_1, g_2. Close to the Klebanov-Witten conformal point (in the UV), the anomalous dimensions are $\gamma_{A,B}\sim -\frac{1}{2}$. This implies that the beta functions for the diagonal combinations

$$\beta_{\frac{8\pi^2}{g_-^2}}=\beta_{\frac{8\pi^2}{g_1^2}}-\beta_{\frac{8\pi^2}{g_2^2}}=6N_c,\quad \beta_{\frac{8\pi^2}{g_+^2}}=\beta_{\frac{8\pi^2}{g_1^2}}+\beta_{\frac{8\pi^2}{g_2^2}}=0. \tag{3.6.18}$$

As in the SUSY case, we will adopt the definitions[13]

$$\frac{4\pi^2}{g_+^2}=\pi e^{-\Phi},\qquad \frac{4\pi^2}{g_-^2}=2\pi e^{-\Phi}\left[1-b_0(\pi)\right] \tag{3.6.19}$$

where $b_0(\psi_0)$ is defined in eq. (3.6.5)-(3.6.6). We obtain

$$\frac{4\pi^2}{g_-^2}=2e^{-\Phi}\left(\pi+\frac{\kappa}{N_c}e^{2g+2h+2\Phi}\Phi'\right)-\frac{\kappa N_c}{2}e^{\Phi}(b-1)b', \tag{3.6.20}$$

Notice that the result is independent of the gauge artifact function $b_3(\rho)$. In the UV, these formulas are typically trustable. The explicit expansions are

$$\frac{4\pi^2}{g_+^2}=e^{-\Phi_\infty}\pi+\left(\frac{3e^{-\Phi_\infty}\pi}{2c_+^2}\rho-\frac{1}{4}e^{-5\Phi_\infty}\pi\Phi_{30}\right)e^{-8\rho/3}+O\big(W_{20}^2e^{-4\rho}\big) \tag{3.6.21}$$

and

$$\frac{4\pi^2}{g_-^2}=\left(2\rho-\frac{1}{3}c_+^2\Phi_{30}e^{-4\Phi_\infty}+2\pi e^{-\Phi_\infty}-\frac{3}{4}\right)-\frac{3}{4}W_{20}e^{-2\rho/3}+O\big(e^{-4\rho/3}\big). \tag{3.6.22}$$

Let us now compute the beta functions as read from the geometry. We will use the radius/energy relation

$$r=e^{2\rho/3}=\frac{\mu}{\Lambda} \tag{3.6.23}$$

where μ is the energy scale at which we probe the process and Λ the reference or strong coupling scale of the given gauge group. Notice that this choice is arbitrary, just reflecting the possibility of choosing a scheme. Other monotonic relations $\rho(\mu)$ would express the beta function in other schemes. To calculate the beta functions we perform

$$\begin{aligned}\beta_{\frac{8\pi^2}{g_-^2}}&=\frac{d}{d\rho}\left(\frac{8\pi^2}{g_-^2}\right)\frac{d\rho}{d\log(\mu/\Lambda)}=6N_c+W_{20}N_c\frac{\Lambda}{\mu},\\ \beta_{\frac{8\pi^2}{g_+^2}}&=\frac{d}{d\rho}\left(\frac{8\pi^2}{g_+^2}\right)\frac{d\rho}{d\log(\mu/\Lambda)}=O\left(\log\left(\frac{\Lambda}{\mu}\right)\frac{\Lambda^4}{\mu^4}\right).\end{aligned} \tag{3.6.24}$$

We have reinstated the factor of N_c in the expansions. With a naive use of the NSVZ expression for the Wilsonian beta functions one may have interpreted this result for β_- as the SUSY breaking parameter W_{20} changing slightly the value of the anomalous dimensions $\gamma_{A,B}\sim -\frac{1}{2}+O\left(W_{20}\frac{\Lambda}{\mu}\right)$. But this is not matching with

[13]These are strictly correct in the $N=2$ examples and the KW fixed point. We adopt the definition here to get a handle on the non-SUSY dynamics.

the analogous calculation for β_+. Hence this solution does not respect the NSVZ expression (as expected). Also, notice that while in the SUSY case, the beta functions receive corrections $O\left(\frac{\Lambda^3}{\mu^3}\right)$, we have here an example where the SUSY breaking parameters produce lower order corrections $O\left(\frac{\Lambda}{\mu}\right)$. Let us move now to IR observables.

K-Strings

We will follow the treatment in [19]. We need to evaluate the action for a D3 brane that extends on the manifold $\Sigma = [t, x_1, \theta = \tilde{\theta}, \varphi = 2\pi - \tilde{\varphi}]$. The D3 brane is sitting at $\rho = 0$ but can move on the angle ψ, so that it will minimize its energy. The (string frame) metric seen by such a D3 brane is

$$ds^2_{ind} = \frac{e^{\phi_0}}{\sqrt{\hat{h}_0}}\left\{dx^2_{1,1} + N_c\hat{h}_0\frac{h_1}{2}\left[d\chi^2 + \sin^2\chi\left(d\theta^2 + \sin^2\theta d\varphi^2\right)\right]\right\} \tag{3.6.25}$$

where we have written $\psi = 2\chi + \pi$, and used the values of the functions at $\rho = 0$:

$$e^{2g(0)} = e^{2k(0)} = \frac{h_1}{2}, \qquad e^{2h(0)} = 0, \qquad \Phi(0) = \phi_0, \qquad a(0) = 1. \tag{3.6.26}$$

We have additionally written $\hat{h}_0 \equiv \hat{h}(0) = 1 - e^{2\phi_0 - 2\Phi_\infty}$.

The RR field and its potential are,

$$\begin{aligned} &F_3|_\Sigma = 2N_c\sin^2\chi\,\Omega_2\wedge d\chi, \quad C_2|_\Sigma = N_c\left(\chi - \frac{\sin 2\chi}{2}\right)\Omega_2, \\ &\Omega_2 = \sin\theta\; d\theta\wedge d\varphi. \end{aligned} \tag{3.6.27}$$

Using eqs.(3.6.1–3.6.2) and the fact that $b'(0) = \Phi'(0) = 0$ we find that the NS potential B_2 vanishes.

We will turn on an electric field $F_2 = F_{tx}\; dt\wedge dx$ in the space-time directions. Then the Born-Infeld-Wess-Zumino action gives an effective one dimensional lagrangian,

$$L_{\text{eff}} = -4\pi T_{D3}N_c\left[\frac{h_1}{2}\sqrt{e^{2\phi_0} - \hat{h}_0\frac{F^2_{tx}}{4}}\;\sin^2\chi - \left(\chi - \frac{\sin 2\chi}{2}\right)F_{tx}\right]. \tag{3.6.28}$$

This is equivalent to eq. (9.8) of [19], with modifications which result from the U-duality,

$$\beta = \frac{h_1}{2} \to \frac{h_1}{2}\sqrt{\hat{h}_0}, \qquad e^{2\Phi(0)} \to \frac{e^{2\phi_0}}{\hat{h}_0}. \tag{3.6.29}$$

The rest of the discussion then proceeds as in [19]. We impose the equation of motion for F_{tx} and quantize it to be an integer multiple of the tension of the fundamental string, $\frac{\partial L_{\text{eff}}}{\partial F_{tx}} = \frac{kT_f}{2}$. The resulting tension follows an *approximate* sine-law, as in the whole baryonic branch, including the KS solution. This also happens for D5 solutions in section 8 of reference [48].

The influence from the SUSY breaking parameters enters only through the modifications (3.6.29).

The Non-SUSY Seiberg-like duality.

We will follow the treatment in the SUSY case, as developed in [68]. The basic idea is go back to the quantity $b_0(\psi)$, computed as specified around eq.(3.6.6) and compare with what occurs in the SUSY case. The Seiberg duality is identified with a large gauge transformation such that $b_0 \to b_0 \pm 1$ and the charge of D3 branes changes by $\pm N_c$.

Consider the Page charge of Section 3.6.2; a large gauge transformation on B_2 will change b_0 by one unit. This translates in the change of N_c units in the Page charge. This works exactly as in [68].

Let us now study how the Maxwell charge 'sees' the Seiberg duality. We will focus on the UV part of the background, where the cascade is known to work in the SUSY case. Following the steps described in Appendix B.3, we have

$$b_0 = \frac{\hat{h}^{1/2}e^{\Phi/2}}{\pi}\Big[b_2 e^{2h} - b_4(a+\cos\psi_0)e^{h+g}\Big] = \frac{N_c}{\pi}[(f+\tilde{k}) + (\tilde{k}-f)\cos\psi_0] \quad (3.6.30)$$

with (using the explicit values for b_2, b_4)

$$\begin{aligned} f &= \frac{e^{\Phi/2}\hat{h}^{1/2}}{2N_c}[b_2 e^{2h} - b_4 e^{g+h}(a-1)] = \kappa\frac{e^{2\Phi}}{8}[b'(b-1) - \frac{4}{N_c^2}e^{2g+2h}\Phi'], \\ \tilde{k} &= \frac{e^{\Phi/2}\hat{h}^{1/2}}{2N_c}[b_2 e^{2h} - b_4 e^{g+h}(a+1)] = \kappa\frac{e^{2\Phi}}{8}[b'(b+1) - \frac{4}{N_c^2}e^{2g+2h}\Phi'], \\ \to b_0 &= \frac{\kappa N_c e^{2\Phi}}{4\pi}b'(b+\cos\psi_0) - \frac{\kappa e^{2\Phi+2h+2g}}{\pi N_c}\Phi'. \end{aligned} \quad (3.6.31)$$

Now, it is interesting to notice that — far in the UV — the Maxwell charge

$$Q_{Max,D3} = \frac{\kappa}{\pi}e^{2g+2h+2\Phi}\Phi' = \frac{\kappa N_c^2 e^{2\Phi}}{4\pi}b'(b+\cos\psi_0) - N_c b_0 \quad (3.6.32)$$

changes under a change in b_0 as,

$$b_0 \sim b_0 \pm 1 \to Q_{Max,D3} \sim Q_{Max,D3} \mp N_c. \quad (3.6.33)$$

Specially, notice that for large values of ρ the 'correction-term' $b'(b+\cos\psi_0)$ is quite suppressed. This 'correction' is more suppressed in the SUSY case, where $b' \sim e^{-2\rho}$, in contrast to our non-SUSY solutions, where $b' \sim e^{-2\rho/3}$. The 'Seiberg duality', associated with a large gauge transformation of index k that changes the Maxwell charge in kN_c units is better approximated in the SUSY than in the non-SUSY case. Nevertheless, in both cases, the transformation is good at leading order.

So, as expected, far in the UV we could think that the decrease in the Maxwell charge is interpreted as a non-SUSY version of Seiberg duality that is at work here.

Domain Walls

Let us compute the tension of a domain wall as the effective tension of a five brane that sits at $\rho = 0$ and is extended along $\Sigma_6 = [t, x_1, x_2, \tilde{\theta}, \tilde{\varphi}, \psi]$. Before the U-duality for field theories of type A, we use the background in eq.(3.2.6) and obtain that the induced metric on such five brane is (in string frame)

$$ds^2_{ind} = e^{\Phi}\Big[dx^2_{1,2} + \frac{e^{2g}}{4}(d\tilde{\theta}^2 + \sin^2\tilde{\theta}d\tilde{\varphi}^2) + \frac{e^{2k}}{4}(d\psi + \cos\tilde{\theta}d\tilde{\varphi})^2\Big] \quad (3.6.34)$$

The induced tension on the three dimensional wall is

$$T_{eff} = 2\pi^2 T_{D5} e^{2\Phi+2g+k}\big|_{\rho=0} = \frac{\pi^2 T_{D5} e^{2\phi_0} h_1^{3/2}}{\sqrt{2}}, \tag{3.6.35}$$

which is unchanged from the SUSY result.

After the U-duality, in the background of eq.(3.2.9), we place a similar five brane, the induced metric is,

$$ds^2_{ind} = e^{\Phi}\Big[\frac{1}{\sqrt{\hat{h}}}dx^2_{1,2} + \sqrt{\hat{h}}\Big(\frac{e^{2g}}{4}(d\tilde{\theta}^2 + \sin^2\tilde{\theta}d\tilde{\varphi}^2) + \frac{e^{2k}}{4}(d\psi + \cos\tilde{\theta}d\tilde{\varphi})^2\Big)\Big]. \tag{3.6.36}$$

There is also an induced B_2 field,

$$B_2 = \frac{1}{4}\sqrt{\hat{h}}e^{2g+\Phi/2}b_3(\rho)\sin\tilde{\theta}d\tilde{\theta}\wedge d\tilde{\varphi}. \tag{3.6.37}$$

In order to have a gauge invariant Born-Infeld Action, we must add the F_2 field on the world-volume of the brane. Indeed, the change due to a gauge transformation of the B_2 field is cancelled by a (non-gauge)-transformation on F_2[14],

$$B_2 \to B_2 + d\Lambda_1, \quad F_2 \to F_2 - d\Lambda_1. \tag{3.6.38}$$

Hence, we need to turn on gauge field strength on the world-volume of the brane,

$$F_{\tilde{\theta}\tilde{\varphi}} = -\frac{\sqrt{\hat{h}}}{4}e^{2g+\Phi/2}b_3(\rho)\sin\tilde{\theta}. \tag{3.6.39}$$

This implies that the BIWZ action will be

$$S = -T_{D5}(4\pi)^2\frac{e^{2g+k+2\Phi}}{8}\int d^{2+1}x \tag{3.6.40}$$

which gives the same effective tension as in eq.(3.6.35) and the same as in the SUSY case [15]. Then the tension before and after the U-duality is the same. As a side remark, one may wonder if it is possible to fix the value of b_3 at $\rho = 0$ using some physical criterium. Though it is not an invariant quantity, the small ρ expansion of

$$B_{\mu\nu}B^{\mu\nu} \sim \frac{b_3(0)^2}{\rho^2} + \cdots \tag{3.6.42}$$

suggests that we should take $b_3(0) = 0$ as in the SUSY case.

[14] One can also add a field strength F_2 such that aside from cancelling the gauge-variance of B_2 adds a kind of 'magnetic charge' to the domain wall or a Maxwell-like term in the Minkowski directions. We will not consider the addition of these extra components of F_2 as they will typically raise the energy of the wall.

[15] Notice, that in the SUSY case we have (using eq. B.2.1)

$$b_3 = -\kappa e^{3\Phi/2}\hat{h}^{-1/2}\cos\alpha, \tag{3.6.41}$$

which vanishes for $\rho = 0$.

Central charge

We will calculate the central charge of this non-susy solution. We should follow the usual procedure of [69], that requires a reduction to five dimensions. However, an equivalent treatment presented in [70] indicates that for any string-frame metric of the form

$$ds^2 \sim \alpha(\rho)dx_{1,d}^2 + \alpha(\rho)\beta(\rho)d\rho^2 + g_{ij}(\rho,y)dy^i dy^j \tag{3.6.43}$$

we define

$$V_{int} = \int d\vec{y}\sqrt{\det g_{ij}}, \quad H = e^{-4\Phi}\alpha^d V_{int}^2. \tag{3.6.44}$$

and the central charge (for $d=3$) is given by $c \sim \frac{\beta^{3/2}H^{7/2}}{(H')^3}$, in our case

$$c \sim \frac{e^{2h+2g+2\Phi+4k}\hat{h}^2}{(2h'+2g'+2\Phi'+k'+\frac{\hat{h}'}{2\hat{h}})^3} \tag{3.6.45}$$

In the IR, the explicit expansion for the central charge is

$$\begin{aligned} c \sim\ & e^{2\phi_0-4\Phi_\infty}\left(e^{2\Phi_\infty}-e^{2\phi_0}\right)^2 h_1^4\rho^5 \\ & + \frac{1}{9}e^{2\phi_0-4\Phi_\infty}\left(e^{2\Phi_\infty}-e^{2\phi_0}\right)h_1^2\Big[e^{2\Phi_\infty}\left(-16-15h_1k_2+12h_1^2\right) \\ & + e^{2\phi_0}\left(28+15h_1k_2-12h_1^2+9v_2^2\right)\Big]\rho^7 + O(\rho^9), \end{aligned} \tag{3.6.46}$$

and in the UV we have

$$c \sim e^{2\Phi_\infty}\rho^2 - \left(\frac{3}{4}e^{2\Phi_\infty} + \frac{1}{3}c_+^2 e^{-2\Phi_\infty}\Phi_{30}\right)\rho + O\left(\frac{1}{\rho}\right). \tag{3.6.47}$$

It is immediately clear that the SUSY-breaking parameters have no effect at the leading order in the UV. However, in the IR the question is more subtle. Although none of the explicit SUSY-breaking parameters appear in the leading term there is an effect. This is because in the SUSY case there are only two independent parameters, so that fixing h_1 and ϕ_0 is sufficient to determine Φ_∞. In the non-SUSY case we have seen that there is one more parameter, which breaks SUSY. This means that even with fixed h_1 and ϕ_0 we can expect that Φ_∞ varies as a function of the SUSY-breaking parameter. Indeed, when in appendix A.4 we compare SUSY and non-SUSY numerical solutions with the same h_1 and ϕ_0, we find that Φ_∞ changes.

Force on a probe $D3$-brane

We will now consider a D3 probe brane that extends in the Minkowski directions and is free to move in the radial direction as suggested in [66],

$$D3 : [t, x_1, x_2, x_3], \quad \rho(t). \tag{3.6.48}$$

the induced metric and RR four form field are obtained from the string frame version of eq. (3.2.9),

$$\begin{aligned} ds_{ind}^2 &= e^{\Phi}\hat{h}^{-1/2}\Big[-dt^2(1-\hat{h}e^{2k}\rho'^2) + dx_1^2 + dx_2^2 + dx_3^2\Big], \\ C_4 &= -\kappa\frac{e^{2\Phi}}{\hat{h}}dt\wedge dx_1\wedge dx_2\wedge dx_3. \end{aligned} \tag{3.6.49}$$

this gives an action for the D3 brane[16],

$$S_{BIWZ} = -T_{D3}V_3 \int dt \left(\frac{e^{\Phi}}{\hat{h}} \sqrt{1 - \hat{h} e^{2k} \rho'^2} - \kappa \frac{e^{2\Phi}}{\hat{h}} \right). \tag{3.6.50}$$

We then approximate this for small velocities and change to the variable $dr = e^{k+\Phi/2} d\rho$ and get

$$S = T_{D3}V_3 \int dt \left(\frac{r'^2}{2} - \frac{e^{\Phi}}{1 + \kappa e^{\Phi}} \right). \tag{3.6.51}$$

the force on this probe is then

$$f = \frac{e^{\Phi/2-k}}{(1 + \kappa e^{\Phi})^2} \Phi'. \tag{3.6.52}$$

In the IR, the explicit expansion for this force is

$$f = \frac{2\sqrt{2}}{3} \frac{e^{\frac{\phi_0}{2} + 2\Phi_\infty} (4 + 3v_2^2)}{(e^{\phi_0} + e^{\Phi_\infty})^2 h_1^{5/2}} \rho + O(\rho^2), \tag{3.6.53}$$

and in the UV we have

$$f = \left[\sqrt{\frac{3}{2}} \frac{e^{\frac{\Phi_\infty}{2}}}{c_+^{5/2}} \rho - \frac{e^{\frac{-7\Phi_\infty}{2}} \left(9 e^{4\Phi_\infty} + 4 c_+^2 \Phi_{30} \right)}{8\sqrt{6} c_+^{5/2}} \right] e^{-10\rho/3} + O(e^{-14\rho/3}). \tag{3.6.54}$$

As expected, the force vanishes quickly in the far UV, where the solution approaches the KS background. Also, notice that in the radial coordinate $r \sim e^{-2\rho/3}$, the force is $f \sim \frac{\log r}{r^5}$ as obtained in [71]. The SUSY breaking parameters do not enter explicitly in the expression for this (small) force at leading order. In the other hand, the breaking of SUSY explicitly changes the value of the force in the IR, as expected.

3.6.3 Field theory comments

This section relies on the ideas of [72]-[73], but most fundamentally on the analysis of the paper [73]. Similar ideas that may be useful in thinking about our string backgrounds have been put forward for example in [74]. This paper studies non-SUSY deformations of $\mathcal{N} = 1$ SQCD. We use this to analyze the quiver field theory of type B. This is as we discussed, a non-SUSY deformation of the KS-quiver. In the SUSY case, the Dymarsky:2011ve-field theory can be understood as $\mathcal{N} = 1$ SQCD with gauged flavor group and a quartic superpotential (see for example [75]) and due to this, the results of [73] are important to us. The qualitative results of the paper [73] become quantitatively accurate once we take the SUSY breaking parameters much smaller than the relevant scale of the problem, namely Λ_{SQCD}[17]. In our case, this is reflected in the small size of the coefficient W_{20}.

In this case, lots of the structure of Seiberg's SQCD [77] remains. Particularly interesting to us is the fact that for $SU(N_c)$ SQCD with N_f flavors and with $N_f = N_c$, there exists a vacuum which breaks spontaneously the $U(1)$-baryonic symmetry

[16]Notice that in the way things have been defined, the action for a D3 has the WZ term with the same sign as the BI term. See eq.(2.13) in the paper [17].

[17]Ofer Aharony explained us that the soft breaking mass terms for squarks could have different signs under a Seiberg Duality, see [76]. This technical subtlety seems to play no role in our analysis

and this vaccum persists in the non-SUSY analysis of [73]. This will be relevant for us as the case $N_f = N_c$ is associated in the SUSY case with the last step of the cascade. We then argue that our geometry describes a situation where SUSY is broken by gaugino masses and other VEV's and the baryonic symmetry is broken by the vacuum state.

In a bit more detail, the authors of [73], added to the SQCD lagrangian a term of the form

$$\begin{aligned} L &= L_{SQCD} + \Delta L, \\ \Delta L &\sim \int d^4\theta M_Q (Q^\dagger e^V Q + \tilde{Q}^\dagger e^{-V} \tilde{Q}) + \int d^2\theta M_g S, \end{aligned} \tag{3.6.55}$$

where S is the superfield $S = Tr[W_\alpha W^\alpha]$, M_Q is a vector multiplet whose D-component equals the mass of the squarks $(-m_q^2)$ and M_g is a chiral multiplet whose F-component is the mass of the gluino. The authors of [73] argued that to leading order in the SUSY breaking parameters M_Q, M_g one can write an effective lagrangian in terms of mesons $\hat{M}$, baryons $(B, \tilde{B})$ and S,

$$\Delta L \sim \int d^4\theta B_M M_Q tr[\hat{M}^\dagger \hat{M}] + B_b M_Q (B^\dagger B + \tilde{B}^\dagger \tilde{B}) + \int d^2\theta M_g S + ... \tag{3.6.56}$$

The idea is then that one should supplement the usual actions and superpotentials discussed in the SUSY case with the SUSY breaking terms above. In particular, in the case $N_f = N_c$ we will need to minimize the potential term coming from eq.(3.6.56) together with the potential coming from the SUSY superpotential

$$W = W_{tree} + W_{quant} = \kappa Tr(\hat{M}^\dagger \hat{M}) + \xi(\det M - \tilde{B}B - \Lambda^{2N_c}). \tag{3.6.57}$$

Therefore, the vacua of the theory are those that minimize the potential coming from the tree level superpotential, together with that from the SUSY breaking term, all subject to the constraint in W_{quant}. The result is that in the non-SUSY case, one finds one vacuum state where the baryons get a VEV and the mesons are at the origin of the moduli space, $\hat{M} = 0$.

In this way, we have argued that our solution, which breaks SUSY due to masses for the gauginos has very similar behavior to the KS-cascade (actually to the baryonic branch in [13, 14]). We found that many non-perturbative aspects behave very similarly as the SUSY case: the expression of the domain wall tension is basically the same as in the SUSY case. Of course, numbers will differ as the functions in the IR pick the influence of the SUSY breaking terms. The tensions for k-strings gives an approximate sine-law, again with the SUSY breaking entering the value of the tension. In the UV, the beta function for the gauge couplings of the quiver and the leading order of the central charge behave at leading order in the UV like their SUSY counterpart, but in the case of the beta functions, the first correction is purely coming from SUSY breaking contributions. The Seiberg duality (identified here with the change of the Maxwell charge under large gauge transformations of the NS B-field) behaves very approximately as in the SUSY case. One can probably make an argument for self-similarity as presented in [75].

Obviously, what happens is that the SUSY breaking terms, for example the gaugino mass indicated by the quantity W_{20}, are not important at high energies. They enter some IR observables, correcting but not changing the qualitative behavior expected from the SUSY example. This suggests that we need to think that our SUSY

breaking scales are smaller than our strong coupling scale. Hence, the phenomena are the same as in the SUSY models, but numerically there will be differences. All this is in line with the analysis of [72]–[73].

3.6.4 Some words on (meta)-stability

We will briefly comment here on the stability of our solutions. The way in which perturbative stability can be directly checked is to consistently fluctuate our solutions and find the presence of tachyons. Of course, it may be the case that the precise fluctuations that we study are not those leading to instabilities, while on the other hand, finding a tachyonic mode will ensure the instability of the solution. We will not make a exhaustive analysis of fluctuations here, but postpone it for future work. We will content ourselves with presenting here some arguments in favour of the stability of the backgrounds of this chapter.

To begin with, we notice the close parallels between our backgrounds and the analogous SUSY (baryonic branch) solutions. Indeed, we are deforming the backgrounds by the presence of the coefficients v_2 or w_2 that break supersymmetry. These coefficients, as we have insisted throughout this chapter, are taken to be small. This was a technical requirement to ensure a good normalization of the energy functional — see Section 3.5. The parametric smallness of the SUSY breaking parameters implies a good mapping with the field theory results of the paper [73]. In that paper, it was shown, using field theory techniques, that the generated potential has a minimum which we believe — due to the analogous behavior — is the vacuum of the field theory that our background is dual to. This would imply that tachyons are perturbatively absent from the spectrum in analogy with the results of [73].

One may of course be worried about non-perturbative instabilities. In this case, one may appeal to an argument very similar to that presented in [32]. Indeed, in our case, the tension of domain walls is not modified by the SUSY breaking parameters — see Section 3.6.2 — we can then estimate the action of a vacuum bubble to be $S_{\text{bubble}} \sim N_c(\Lambda/m_\lambda)^3$, where m_λ is the mass of the gauginos and Λ the strong coupling scale. As in the rest of the chapter Λ is taken to be hierarchically bigger than the SUSY breaking scale. In this way, for these solutions quite close to the SUSY ones, the probability of decay is very small and the tunneling rate to the SUSY solutions is suppressed as $e^{-S_{\text{bubble}}}$.

Of course, the ideal would be to make an argument similar to the ones made in 'fake supergravity' [78], but in this case, to construct a fake superpotential seems a formidable task, if possible at all.

3.7 Summary and conclusions

In this chapter we study the full two-dimensional space of solutions which can be considered to be the non-SUSY generalisation of the baryonic branch . We include the solutions compatible with the PT ansatz which have both a regular IR, of the same form as that of the baryonic branch, and are related to the baryonic branch by a continuous change of parameters.

In addition to the SUSY baryonic branch and its limiting cases (Klebanov-Strassler and Chamseddine-Volkov/Maldacena-Núñez), this solution space also includes two previously studied one-dimensional families of non-SUSY solutions as

limits. In the limit which yields in the SUSY case the CVMN solution we obtain the solutions of Gubser, Tsyetlin and Volkov [24] (presented here in section 3.3.1), while in the limit corresponding to the KS solution itself we obtain those of Dymarsky and Kuperstein [32] (presented in section 3.4.4). The behaviour of generic non-SUSY solutions lying away from these boundaries can be understood as a combination of the effects which are present in the SUSY baryonic branch and the GTV solutions.

Alongside these cases we identify two additional one-dimensional families which are of interest. The first is the boundary of the solution space with $v_2 = w_2 = 0$ corresponding to the positive boundary of the GTV solutions. Here we can no longer argue that SUSY is softly broken (the gaugino mass appears to be infinite), and we find that $a = b = 1$ for all ρ. Notably, this changes the geometry to an explicity non-SUSY case (a cone over $S^2 \times S^3$). We also find an explicit UV expansion for the solutions on this boundary which is different from the generic UV. The second family lies on the line $w_2 = -2$, upon which the geometry possesses a $\mathbb{Z}_2$ symmetry just as in the Klebanov-Strassler solution. This family of solutions corresponds to the other boundary of the GTV solutions.

Moving away from the boundaries, we have also shown that solutions with $w_2 < -2$ are related to those with $w_2 > -2$ by a $\mathbb{Z}_2$ symmetry and describe the same physical system, although the solutions themselves appear different. In the two-dimensional solution space much of the SUSY structure survives. In addition to the various quantities calculated in [2], which are mostly unaffected by SUSY-breaking at leading order, we find that the presence of a $\mathbb{Z}_2$ symmetry of the geometry is still linked to the vanishing of a dimension-two operator. In the SUSY case this reflects the fact that in the dual field theory the $\mathbb{Z}_2$ transformation corresponds to the ability to interchange the baryons.

It would be interesting to know to what extent this description applies to the non-SUSY case. To address this, it would be necessary to gain a more detailed understanding of the field theory, including calculation of the mass spectrum. Another question which we did not address is the issue of stability. It would be useful to determine if, and how much, the parameter space is restricted by this requirement. Finally, we note that the transition between the generic UV (3.3.16) and the boundary case (3.4.2) is somewhat unclear. It appears that the solutions first approach the boundary case before switching to the generic behaviour in the UV, the scale at which this occurs presumably being associated with the gaugino mass. This is addressed further in chapter 4.

Chapter 4

The Non-SUSY Limit

In the course of chapter 3, we encountered hints of a one-dimensional family of solutions obtained when we increase the SUSY-breaking parameter as much as possible, presumably corresponding to a completely non-SUSY theory. In this chapter we discuss this in more detail.

4.1 Summary of some relevant aspects of the solution space

The solutions described in chapter 3 (and [2, 3]) correspond to a non-SUSY generalisation of the baryonic branch of Klebanov-Strassler. As discussed, they form a two-dimensional solution space. The most relevant details to the following discussion are summarised here.

The SUSY solutions on the baryonic branch can be parametrised by h_1, which corresponds to the leading coefficient in the warp factors in the IR,

$$e^{2g(\rho)} = \frac{h_1}{2} + O(\rho^2) \ , \quad e^{2h(\rho)} = \frac{h_1}{2}\rho^2 + O(\rho^4) \ , \quad e^{2k(\rho)} = \frac{h_1}{2} + O(\rho^2) \ . \tag{4.1.1}$$

In the SUSY case this has a natural interpretation as controlling the degree of breaking of the $\mathbb{Z}_2$ symmetry between the two 2-spheres of the conifold $(\theta, \varphi) \leftrightarrow (\tilde{\theta}, \tilde{\varphi})$ (see section 3.4.3). In the field theory context this corresponds to the VEV U of a dimension two operator

$$\mathrm{tr}\big(AA^\dagger - B^\dagger B\big). \tag{4.1.2}$$

It is then convenient to parametrise the additional degree of freedom which we obtain in the non-SUSY case by w_2, the coefficient of the next-to-leading term in the IR expansion for $a(\rho)$,

$$a(\rho) = 1 + w_2\rho^2 + O(\rho^4). \tag{4.1.3}$$

We expect this extra degree of freedom to correspond to the gaugino mass m_λ (or some combination of gaugino masses).

Of course, as the parameters h_1 and w_2 are defined with respect to the IR expansions, we would not expect them to be related to U and m_λ in a simple way. However, it is important to stress that there is essentially no meaningful sense

in which we can associate $h_1 \leftrightarrow \mathcal{U}$ and $w_2 \leftrightarrow m_\lambda$ at all. For example, we can recover the $\mathbb{Z}_2$ symmetry (i.e. $U = 0$) by setting $w_2 = -2$ independent of h_1, while it *seems* we can obtain the limit $U \to \infty$ either by taking $h_1 \to 2N_c$ independent of w_2, or $w_2 \to 0$ independent of h_1.[1] However, the limit $w_2 \to 0$ also corresponds to $m_\lambda \to \infty$.

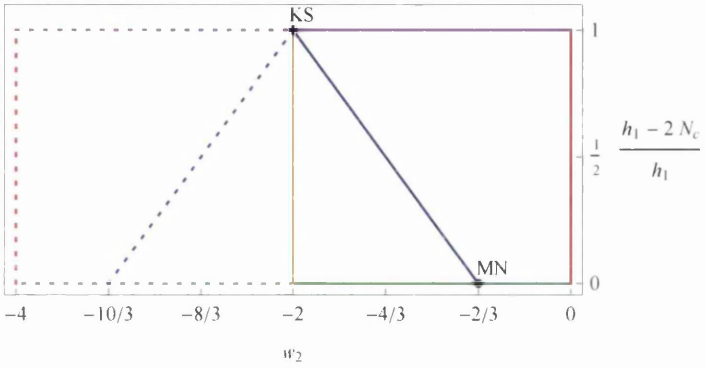

Figure 4.1: The solution space. The SUSY baryonic branch forms the blue line, while the $\mathbb{Z}_2$ symmetry is unbroken on the yellow line. The solutions of interest lie on the red line. The left-hand side of the diagram with dotted lines describes the same backgrounds after a relabeling of coordinates and background functions.

In the following we are concerned with this last limit: the special case solutions with $w_2 = 0$, and those generic solutions with large SUSY breaking, $w_2 \approx 0$. (For want of a better description, we will currently refer to the $w_2 = 0$ solutions as the right-hand boundary (RHB) based on their position in figure 4.1.) In this context, we can interpret an increase in w_2 as increasing both the baryonic VEV U and the gaugino mass m_λ. The interpretation of h_1 is less clear. In particular, the RHB solutions with $w_2 = 0$ are supposed to have infinite U (and the $\mathbb{Z}_2$ symmetry is broken all the way into the UV), but we still have the freedom in h_1. In fact its influence on the solutions appears to be qualitatively the same as in the SUSY baryonic branch.

4.2 The solutions in the limiting case

4.2.1 Solving for the UV expansions

As was discussed in section 3.4.2, inspection of numerical solutions suggests that solutions connecting our IR ansatz with a reasonable UV exist only for $w_2 \leq 0$, and that the limiting solutions (with $w_2 = 0$) have

$$g(\rho) = k(\rho), \qquad a(\rho) = b(\rho) = 1 \tag{4.2.1}$$

for all ρ. This is entirely based on the numerics; we have no analytic argument that these solutions form the boundary of the solution space or that they have sensible

[1] The interpretation of the point $(w_2, h_1) = (-2, 2N_c)$is unclear. Possibly it corresponds to more than one solution; this parametrisation may not cover the whole solution space.

UV behaviour. The solutions with $h_1 = 2N_c$ (green in figure 4.1) were found in [24] to be restricted to $w_2 \leq v_2$, with the limiting case satisfying (4.2.1).

We can easily impose (4.2.1) and obtain the equations of motion for the remaining functions. With $N_c = 1$ for simplicity we get

$$\begin{aligned} k'' &= 2 - 2e^{-4k} - 2h'k' - 2(k')^2 - 2k'\Phi', \\ h'' &= e^{2k-2h} - 2h'k' - 2(h')^2 - 2h'\Phi', \\ \Phi'' &= 2e^{-4k} - 2h'\Phi' - 2(\Phi')^2 - 2k'\Phi', \end{aligned} \tag{4.2.2}$$

with the additional first order constraint,

$$e^{-4k} - e^{2k-2h} - 3 + 6h'k' + 4h'\Phi' + 6k'\Phi' + (h')^2 + 3(k')^2 + 2(\Phi')^2 = 0. \tag{4.2.3}$$

Although this is much simpler than the full system of equations considered in [2, 3], we are still unable to find an analytic solution. As noted in section 3.4.2, it is possible to solve the equations of motion in the UV using an ansatz based on that used in [2],

$$\begin{aligned} e^{2h(\rho)} &= \sum_{m=0}^{\infty}\sum_{n=0}^{m} H_{mn}\rho^n e^{-2\alpha(m-1)\rho}, \qquad e^{2k(\rho)} = \sum_{m=0}^{\infty}\sum_{n=0}^{m} K_{mn}\rho^n e^{-2\alpha(m-1)\rho}, \\ e^{4\Phi(\rho)} &= \sum_{m=1}^{\infty}\sum_{n=0}^{m} \Phi_{mn}\rho^n e^{-2\alpha(m-1)\rho}. \end{aligned} \tag{4.2.4}$$

The difference here compared to [2] is that we allow a free parameter α, while [2] fixes $\alpha = 2/3$. This could equally well be described in terms of relaxing the relationship between the coefficients of the $\mathrm{d}\rho$ and $\tilde{\omega}_3$ terms in the metric. We find a solution for $\alpha = 1/\sqrt{2}$ which matches the numerical solutions at leading order.

However, we find that the numerical solutions show distinctive periodic behaviour at subleading order which is clearly not present in (4.2.4).

To include these effects, we write

$$\begin{aligned} e^{2h(\rho)} &= \sum_{m=0}^{\infty} F_m^{(h)}(\rho)e^{-2\alpha(m-1)\rho}, \qquad e^{2k(\rho)} = \sum_{m=0}^{\infty} F_m^{(k)}(\rho)e^{-2\alpha(m-1)\rho}, \\ e^{4\Phi(\rho)-4\Phi_\infty} &= 1 + \sum_{m=1}^{\infty} F_m^{(\Phi)}(\rho)e^{-2\alpha(m-1)\rho}, \end{aligned} \tag{4.2.5}$$

where we require that the the $F_m^{(f)}(\rho)$ grow slower than exponentially in the UV for consistency (or at least to avoid a large degree of redundancy in the parametrisation). Note that if we included all the functions, this would be general enough to include, for example, all the expansions seen in [2] and the normal baryonic branch solutions. In these $\alpha = 2/3$ and the various $F_m^{(f)}$ are polynomials in ρ.

Substituting (4.2.5) into the equations of motion, at each order in $e^{\alpha\rho}$ we obtain coupled second order *linear* equations, which can be solved for the $F_m^{(f)}$ in terms of various constants of integration. Many of the constants can be eliminated by requiring that exponential terms in the $F_m^{(f)}(\rho)$ vanish, and we obtain UV expansions

in terms of four non-trivial parameters,

$$\begin{aligned}
\frac{e^{2h}}{N_c} &= \frac{K_0}{2}e^{\sqrt{2}\rho} + K_1^- \sin(\sqrt{2}\rho) + K_1^+ \cos(\sqrt{2}\rho) + O(e^{-\sqrt{2}\rho}), \\
\frac{e^{2k}}{N_c} &= K_0 e^{\sqrt{2}\rho} + \frac{2}{5}(K_1^- - 2K_1^+)\cos(\sqrt{2}\rho) - \frac{2}{5}(2K_1^- + K_1^+)\sin(\sqrt{2}\rho) + O(e^{-\sqrt{2}\rho}), \\
e^{4(\Phi-\Phi_\infty)} &= 1 - \left(\frac{2\sqrt{2}\rho}{K_0^2} - K_2\right)e^{-2\sqrt{2}\rho} + O(e^{-3\sqrt{2}\rho}).
\end{aligned} \tag{4.2.6}$$

At higher orders we generically get terms like $\sin(l\sqrt{2}\rho)\rho^m e^{n\sqrt{2}\rho}$, with (l, m, n) integers. It appears that oscillating terms always come with factors of $K_1^\pm$, and there is complete mixing between the expansions (i.e. K_2 appears in the expansions for h and k, and the expansion for Φ has oscillating terms).

As usual, the four parameters $\{K_0, K_1^-, K_1^+, K_2\}$ appearing in 4.2.6 are not independent once we match to the IR. As a result, while it is possible to set $K_1^\pm = 0$ and recover the solution quoted in [3], that solution does not necessarily have the regular IR which we require.[2]

We would expect that similarly to the SUSY baryonic branch (in which there are several parameters in the UV which we must take to be functions of c_+) these solutions should be parametrised by K_0 alone.

4.2.2 Comments on the solutions

The three functions h, k, and Φ show behaviours which are qualitatively similar to in the generic case, and in the SUSY baryonic branch. This is essentially because the new oscillating terms are exponentially suppressed relative to the leading behaviour.

At leading order, these functions differ from the generic case in the asymptotic ratios between the warp factors and the fact that a and b are constant rather than decaying in the UV.

The effect of this is noticeable in the 5d field $M_1(\rho) = a^2 + 4e^{2h-2g} - 1$, which is associated with the baryonic VEV U. We first review the generic case with $w_2 < 0$, as discussed in [2, 3]. We had that in the UV

$$M_1 = \frac{1}{c_+}(8H_{11}\rho + 3c_+W_{20}^2 + 2Q_0)e^{-4\rho/3} + O(e^{-8\rho/3}). \tag{4.2.7}$$

Here W_{20} corresponds to the gaugino mass. In the SUSY case with $W_{20} = 0$, the parameters H_{11} and Q_0 are fixed, and so we can associate

$$U \leftrightarrow \frac{1}{c_+}. \tag{4.2.8}$$

Strictly, we can no longer make this association in the generic non-SUSY case, because the functions $H_{11}(c_+, W_{20})$ and $Q_o(c_+, W_{20})$ are not known. However, the numerical evidence is that increasing c_+ while keeping W_20 fixed would decrease U as in the SUSY case. On the other hand, taking $W_{20} \to \infty$ (corresponding to $w_2 \to 0$) results in $U \to \infty$ as both of the leading terms in M_1 diverge.

[2] With $K_1^\pm = 0$, setting $K_0 = K_{00}/N_c$ and $K_2 = -(4K_{00}K_{20} + N_c^2)/K_{00}^2$ gives the solution of [3].

We turn now to the RHB solutions. Using (4.2.1, 4.2.6), we get

$$M_1 = 2 + \frac{4}{5K_0}\left[(K_1^+ + 7K_1^-)\sin(\sqrt{2}\rho) + (7K_1^+ - K_1^-)\cos(\sqrt{2}\rho)\right] e^{-\sqrt{2}\rho} + O(e^{-2\sqrt{2}\rho}). \tag{4.2.9}$$

We now have $M_1 \to$ constant $\neq 0$ for $\rho \to \infty$, indicating that we do not recover the $\mathbb{Z}_2$ symmetry in the far UV. The next term is proportional to $e^{-2\alpha\rho}$, like the leading term in (4.2.7), and so corresponds to a dimension two operator. Possibly we should now associate this with U, so that we would write (schematically)

$$U \leftrightarrow \frac{K_1^\pm}{K_0}. \tag{4.2.10}$$

However, it is not clear how this is consistent with these solutions being in the limit $U \to \infty$ of the generic case.

It is perhaps interesting to note that in the RHB solutions the term in the expansion which we are associating with the dimension two operator contains an oscillating factor.

In the numerical solutions the oscillations are hard to detect due to the exponential suppression. We can overcome this by choosing combinations of the warp factors in which the leading terms cancel. In order for this to work in both the generic and RHB cases, we define

$$G(\rho) = \frac{1}{N_c}\left(3e^{2k} - e^{2g} - 4e^{2h}\right). \tag{4.2.11}$$

Using (4.2.1, 4.2.6) and the expansions in [2], we get

$$G(\rho) = \begin{cases} \dfrac{3c_+ W_{20}^2}{N_c} + O(e^{-4\rho/3}) & \text{for } w_2 < 0, \\ -\dfrac{4}{5}\Big[(K_1^+ + 7K_1^-)\sin(\sqrt{2}\rho) & \\ \qquad +(7K_1^+ - K_1^-)\cos(\sqrt{2}\rho)\Big] + O(e^{-2\sqrt{2}\rho}) & \text{for } w_2 = 0. \end{cases} \tag{4.2.12}$$

Note that the quantity appearing in the square brackets here is the same as in (4.2.9).

4.2.3 The geometry

After applying (4.2.1), we should (as discussed in section 4.2 of [3]) be able to make a coordinate transformation $(\tilde{\theta}, \tilde{\varphi}, \psi) \to (\bar{\theta}, \bar{\varphi}, \bar{\psi})$ which completely removes

the 'twist'. We are then left with

$$
\begin{aligned}
ds_E^2 &= e^{\Phi/2}\left[\hat{h}^{-1/2}dx_{1,3}^2 + \hat{h}^{1/2}\left(e^{2k}\mathrm{d}\rho^2 + e^{2h}d\Omega_2 + \frac{e^{2k}}{4}d\Omega_3\right)\right], \\
d\Omega_2 &= \mathrm{d}\theta^2 + \sin^2\theta\ \mathrm{d}\varphi, \qquad d\Omega_3 = \bar{\omega}_1^2 + \bar{\omega}_2^2 + \bar{\omega}_3^2, \\
F_{(3)} &= -\frac{N_c}{4}\bar{\omega}_1 \wedge \bar{\omega}_2 \wedge \bar{\omega}_3, \\
H_{(3)} &= -2\kappa N_c e^{2h-2k+2\Phi}\sin\theta\ \mathrm{d}\rho \wedge \mathrm{d}\theta \wedge \mathrm{d}\varphi, \\
C_{(4)} &= -\kappa\frac{e^{2\Phi}}{\hat{h}}\mathrm{d}t \wedge \mathrm{d}x_1 \wedge \mathrm{d}x_2 \wedge \mathrm{d}x_3, \\
\bar{\omega}_1 &= \cos\bar{\psi}\ \mathrm{d}\bar{\theta} + \sin\bar{\psi}\sin\bar{\theta}\ \mathrm{d}\bar{\varphi}, \qquad \bar{\omega}_2 = -\sin\bar{\psi}\ \mathrm{d}\bar{\theta} + \cos\bar{\psi}\sin\bar{\theta}\ \mathrm{d}\bar{\varphi}, \\
\bar{\omega}_3 &= \mathrm{d}\bar{\psi} + \cos\bar{\theta}\ \mathrm{d}\bar{\varphi}.
\end{aligned}
\tag{4.2.13}
$$

This is asymptotically the solution described in section 4.1 of [79] (see appendix B.4).

Geometric explanation of the expansion parameter

In section 4.2.1 we saw that in order to find the UV expansions for the RHB solutions we needed to expand in powers of $e^{\rho/\sqrt{2}}$ rather than $e^{2\rho/3}$ as in the generic case. This can be understood in terms of the geometry, given some reasonable assumptions about what the solutions should look like at leading order in the UV.

We expect a metric of the form

$$
ds^2 = H(r)^{-1/2}dx_{1,3}^2 + H(r)^{1/2}\left(\mathrm{d}r^2 + \cdots\right), \tag{4.2.14}
$$

where in order to get (almost) AdS, we need

$$
H(r) \sim \frac{\log r}{r^4}. \tag{4.2.15}
$$

If we consider the case where the background functions have essentially the same leading behaviour as the baryonic branch, that is

$$
e^{2g} = G_{00}e^{2\alpha\rho}, \quad e^{2h} = H_{00}e^{2\alpha\rho}, \quad e^{2k} = K_{00}e^{2\alpha\rho}, \quad \hat{h} = 1 - e^{2\Phi-2\Phi_\infty} \sim \rho e^{-4\alpha\rho}, \tag{4.2.16}
$$

we find that we need $r = e^{\alpha\rho}$ in order to satisfy (4.2.15).

Given these assumptions, we can fix α (as well as the ratios G_{00}/K_{00} and H_{00}/K_{00}) by looking at the internal space. In our solutions this has in general the form

$$
ds_6^2 = e^{2k}\mathrm{d}\rho^2 + e^{2h}\left(\mathrm{d}\theta^2 + \sin^2\theta\ \mathrm{d}\varphi^2\right) + \frac{1}{4}e^{2g}\left(\omega_1^2 + \omega_2^2\right) + \frac{1}{4}e^{2k}\left(\omega_3 + \beta\cos\theta\ \mathrm{d}\varphi\right)^2, \tag{4.2.17}
$$

where for the RHB solutions we have ($\omega = \bar{\omega},\ \beta = 0$), and for the generic case we have ($\omega = \tilde{\omega},\ \beta = 1$). In the generic case, the internal space asymptotes to the conifold, with metric

$$
ds_{R\times T^{1,1}}^2 = \mathrm{d}r^2 + r^2\left[\frac{1}{9}(\tilde{\omega}_3 + \cos\theta\ \mathrm{d}\varphi)^2 + \frac{1}{6}\left(\mathrm{d}\theta^2 + \sin^2\theta\ \mathrm{d}\varphi^2 + \tilde{\omega}_1^2 + \tilde{\omega}_2^2\right)\right], \tag{4.2.18}
$$

while the RHB solution asymptotes to the cone over $S^3 \times S^2$, with metric

$$ds^2_{R\times T^{1,0}} = \mathrm{d}r^2 + r^2\left[\frac{1}{4}\left(\mathrm{d}\theta^2 + \sin^2\theta\ \mathrm{d}\varphi^2\right) + \frac{1}{8}\left(\bar{\omega}_1^2 + \bar{\omega}_2^2 + \bar{\omega}_3^2\right)\right]. \tag{4.2.19}$$

As discussed in [9, 79], the (ratios of the) coefficients here are chosen by requiring that the space is Einstein; that is that $(R_{ab})_{6\mathrm{d}} \propto (g_{ab})_{6\mathrm{d}}$.

Inserting the asymptotic behaviour (4.2.16) into (4.2.17)

$$ds^2_6 = \frac{K_{00}}{\alpha^2}\Bigg[\mathrm{d}r^2 + \frac{\alpha^2 H_{00}}{K_{00}}r^2\left(\mathrm{d}\theta^2 + \sin^2\theta\ \mathrm{d}\varphi^2\right) + \frac{\alpha^2 G_{00}}{4K_{00}}r^2\left(\omega_1^2 + \omega_2^2\right) + \frac{\alpha^2}{4}r^2(\omega_3 + \beta\cos\theta\ \mathrm{d}\varphi)^2\Bigg]. \tag{4.2.20}$$

In the generic case we match to (4.2.18) and (after absorbing the overall constant into r), we get

$$\alpha = \frac{2}{3}, \qquad \frac{H_{00}}{K_{00}} = \frac{3}{8}, \qquad \frac{G_{00}}{K_{00}} = \frac{3}{2}, \tag{4.2.21}$$

which matches the generic solutions of [2, 3].

In the RHB case, we match to the cone metric (4.2.19), giving

$$\alpha = \frac{1}{\sqrt{2}}, \qquad \frac{H_{00}}{K_{00}} = \frac{1}{2}, \qquad \frac{G_{00}}{K_{00}} = 1, \tag{4.2.22}$$

which agrees with (4.2.6).

4.2.4 Solutions close to the RHB

In [3] the generic non-SUSY baryonic branch solutions were decribed in terms of two scales. These were ρ_{h_1}, at which the warp factors begin growing exponentially, and ρ_{SUSY}, at which the leading non-SUSY terms in a and b become significant. Counter-intuitively, it is not possible to associate ρ_{SUSY} with the gaugino mass m_λ. Firstly the non-SUSY behaviour is visible for $\rho > \rho_{\mathrm{SUSY}}$, and secondly the scale moves in the wrong direction — ρ_{SUSY} decreases as we move away from the SUSY solutions.

It appears ρ_{SUSY} only is only significant in the sense that it is the point at which the SUSY-breaking corrections to a and b become comparable in magnitude to the original functions. For example, if we write $a(\rho) = a_{\mathrm{SUSY}}(\rho) + \Delta a(\rho)$, then $a_{\mathrm{SUSY}}(\rho_{\mathrm{SUSY}}) \approx \Delta a(\rho_{\mathrm{SUSY}})$. This concept only makes sense in the context of a_{SUSY} and Δa being decaying functions, with a_{SUSY} decaying faster than Δa. For example, it is not clear what happens to this scale as it moves out of the region in which the UV expansions are valid, as it should for large SUSY-breaking.

In fact, it seems that the transition which occurs at ρ_{SUSY} is not particularly significant. The behaviour on both sides is essentially similar to that in the Klebanov-Strassler. However, as we increase w_2 further towards zero, after ρ_{SUSY} has disappeared into the IR another scale ρ_m becomes apparent. This moves in the opposite direction (from the IR to the UV as w_2 increases) and can be defined as the transition between the completely non-SUSY behaviour described in section 4.2.2 for

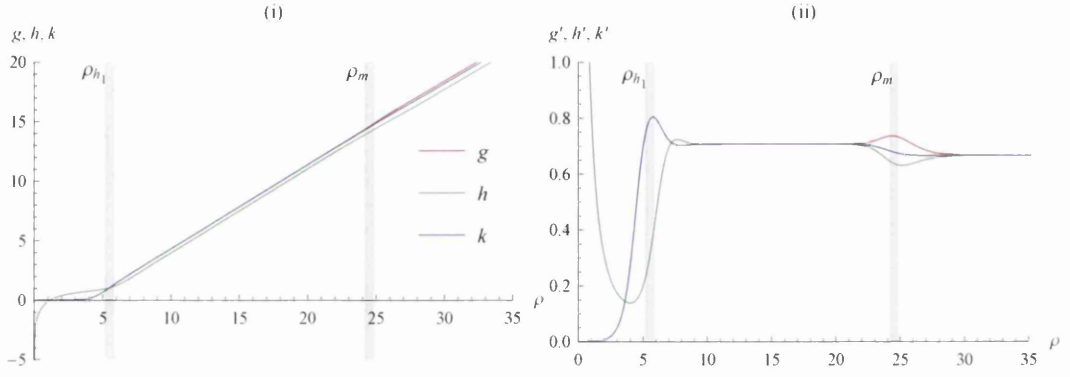

Figure 4.2: Plots of (i) the warp factors (g, h, k), and (ii) their derivatives in a solution close to the RHB, at $(w_2 \approx -10^{-9}, h_1 = 2.001)$ with $N_c = 1$. The vertical bars show the approximate locations of the scales ρ_{h_1} and ρ_m, with ρ_{SUSY} having beeen pushed into the IR. Starting from the IR, the solution transitions at ρ_{h_1} to the RHB type behaviour, with $g' \approx h' \approx k' \approx 1/\sqrt{2}$. Then at ρ_m there is a transition to the generic behavior, with $g' \approx h' \approx k' \approx 2/3$.

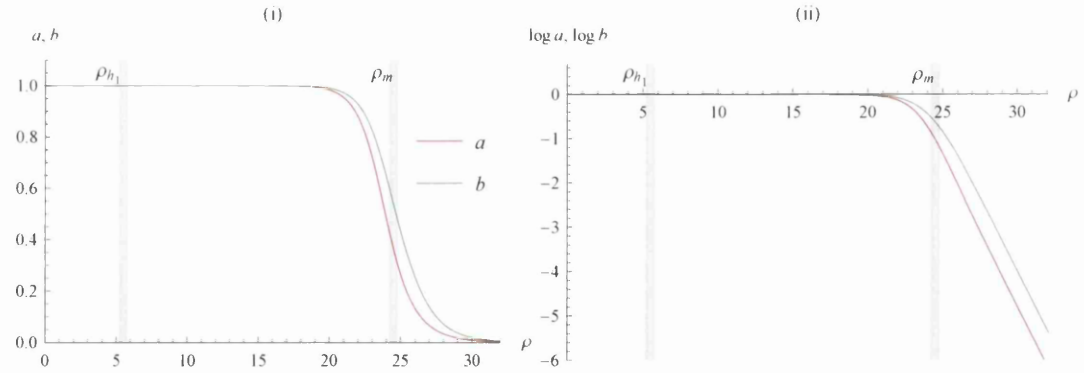

Figure 4.3: Plots showing the behaviour of a and b close to the RHB (the same solution as in figure 4.2). The transition to the generic $a, b \sim e^{-2\rho/3}$ behaviour at ρ_m is clearly visible.

$\rho_{h_1} < \rho < \rho_m$ and the generic (essentially SUSY) behaviour for $r > \rho_m$. This is clearly visible in figures (4.2–4.3).

As discussed in section 4.2.2, the RHB solutions themselves do not recover the $\mathbb{Z}_2$ symmetry $(\theta, \varphi) \leftrightarrow (\tilde{\theta}, \tilde{\varphi})$ in the UV. As a result, in the solutions close to the limit the symmetry is not restored until , rather than ρ_{h_1} as in the generic case. This is apparent in the behaviour of M_1, as can be seen in figure 4.4. There is the usual decay at ρ_{h_1}, but the function first approaches $M_1 = 2$, before decaying to zero at ρ_m.

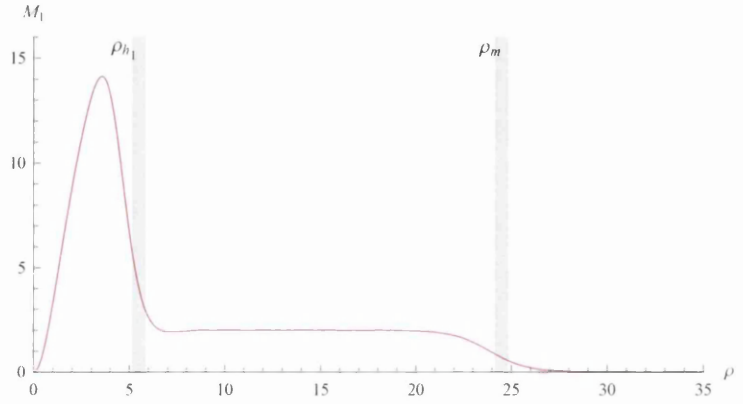

Figure 4.4: The behaviour of the 5d field M_1, which is non-zero when the $\mathbb{Z}_2$ symmetry $(\theta, \varphi) \leftrightarrow (\tilde{\theta}, \tilde{\varphi})$ is broken. There is a decay at ρ_{h_1}, as in the SUSY case, but the function then stabilises around $M_1 = 2$, with oscillations according to (4.2.9). Then at ρ_m there is a transition to the generic case, with $M_1 \sim e^{-4\rho/3}$ as given by (4.2.7).

In order to see that these solutions close to the limit really do include a region in which the behaviour is that of the limiting case, we can look at the function $G(\rho)$, as defined in (4.2.11). As shown in figure 4.5, this shows a series of oscillations for $\rho_{h_1} < \rho < \rho_m$. There is then a transition via exponential growth to a constant for $\rho > \rho_m$.

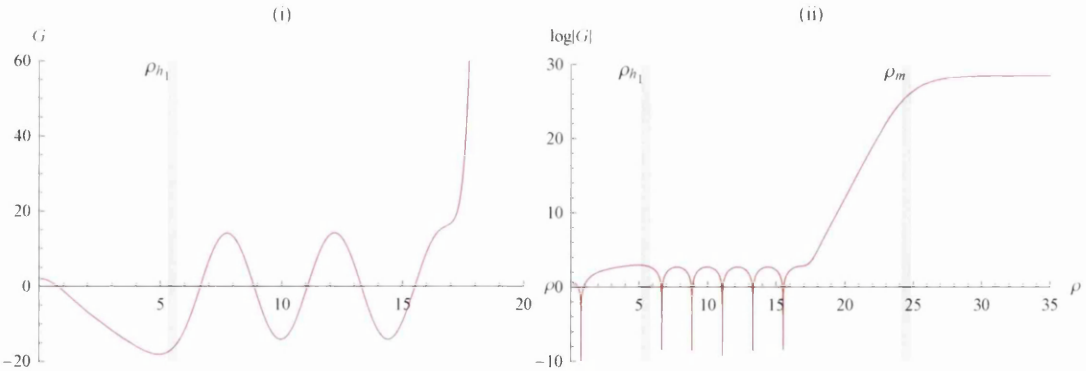

Figure 4.5: The function $G(\rho)$, defined in (4.2.11) such that the subleading behaviour of the warp factors is exposed. Oscillations are visible before rapid exponential growth to a constant for $r > \rho_m$.

4.2.5 Summary

There are two main points here. The first concerns the solutions we obtain when we actually take the limit $w_2 \to 0$. In this case, it seems that we obtain a completely non-SUSY solution with somewhat strange properties, namely the presence of oscillating terms in the UV expansions. This can perhaps be taken as evidence that these solutions are somewhat sick. However, when we examine the various observables discussed in section 3.6, we find that the oscillations all cancel at leading order, at least for generic values of the parameters. This is supported by numerical calculations, in which none of these quantities exhibited oscillations for any of the solutions tested.[3] This is perhaps an indication that at least in some cases (that is for some range of values of K_0) the solutions may have physical significance. We should be careful about reading too much into this, however, because most of the quantities in question were derived based on the assumption that we had deviated only slightly from the SUSY solutions, which is clearly untrue here.

Of course, with no supersymmetry there is little to suggest that these solutions are stable, and it is not clear how far we could get in the context of the gauge-gravity duality. It is perhaps also of interest to note that if we take the the large K_0 limit in the right way, we should presumably reach a non-SUSY analogue of KS. Then the corresponding limit of the solution discussed in appendix B.4 will be the analogue of Klebanov-Tseytlin. Note that as would be expected, the warp factor has the same $H \sim \log r/r^4$ form. Retracing the path taken in chapter 1, we then recover a non-SUSY version of the original $AdS_5 \times S^5$: we now have $AdS_5 \times T^{1,0} = AdS_5 \times S^3 \times S^2$.

The second significant outcome of this chapter is that it seems we have finally been able to see where the true SUSY-breaking scale is (ρ_m rather than ρ_{SUSY}). We are therefore able to see the effect of the SUSY-breaking on physically significant quantities such as M_1. It is also perhaps reassuring from the point of view of the extensive discussion of the field theory in chapter 3. In the light of these solutions it is clear that the the entire discussion there was indeed effectively taking place with 'small SUSY-breaking'. This would seem to support the idea that the effects seen there occur before we get so far from the baryonic branch that we must start to mistrust the results.

[3]Recall that we do not know the relationship between the various parameters analytically, so we cannot be sure that further cancellations occur, 'revealing' the oscillations at higher order. As a result, numerical calculations are required to check that the oscillations are actually absent.

Chapter 5

The Baryonic Branch in 5 Dimensions and Sum Rules

5.1 Introduction

In this chapter we use a 5d description of baryonic-branch type backgrounds (i.e. 4 'field theory' coordinates and one extra dimension) and consider probe fields which extend into the bulk. In 5d models (for example composite Higgs models) the 4d quantities are often expressed in terms of a sum over Kaluza-Klein states, e.g. a sum over masses

$$\sum_{n=1}^{\infty} \frac{1}{M_n^2}.$$

This can be written in terms of integrals of the warp factors in the 5d metric, as in [80].

For example, in [81] this method was used to calculate the S-parameter in a model for electroweak symmetry breaking. The fact that the sum over Kaluza-Klein states could be rewritten as a much simpler geometric quantity enabled a scan of the parameter space which would have been far too computationally intensive if the sums were calculated explicitly.

While it was unfortunately not possible to apply the methods described here in a practical calculation, the methods used yield some interesting insights. Firstly, we can demonstrate the perhaps surprising difficulties encountered when attempting to study these supergravity soultions numerically. These essentially result from the necessity of accessing regions of the parameter space in which the various scales are well-separated. Secondly, we can see examples of the effect of moving these scales and varying the length of the 'walking' region.

5.2 Field rescalings

The probe field $\varphi(z)$ in general satisfies a Sturm-Liouville equation of the form

$$-\partial(p\partial\varphi) + q\varphi = \lambda r\varphi, \tag{5.2.1}$$

where p, q and r are also functions of z. Here q results from the bulk mass, and the eigenvalues λ correspond to the M_n^2.

We briefly review the general effect of rescaling in a Sturm-Liouville problem. We reparametrise the system in terms of a rescaled field $\hat{\varphi}(z) = \varphi(z)/f(z)$. The first term of (5.2.1) then becomes

$$\begin{aligned}\partial\left[p\partial(f\hat{\varphi})\right] &= \partial(pf\partial\hat{\varphi} + p\hat{\varphi}\partial f) \\ &= \partial(f^{-1}pf^2\partial\hat{\varphi} + p\hat{\varphi}\partial f) \\ &= f^{-1}\partial(pf^2\partial\hat{\varphi}) + \partial(p\partial f)\hat{\varphi}. \end{aligned} \tag{5.2.2}$$

The factor of f^{-1} taken outside the derivative is the unique choice which leads to the cancellation of terms proportional to $\partial\hat{\varphi}$.

The rescaled field $\hat{\varphi}$ now satisfies a modified Sturm-Liouville equation

$$-\partial(pf^2\partial\hat{\varphi}) + \left[qf^2 - f\partial(p\partial f)\right]\hat{\varphi} = \lambda r f^2\hat{\varphi}. \tag{5.2.3}$$

As the eigenvalues are unchanged, we are free to rescale the field as convenient without affecting the sum rules, which depend on the M_n.

In particular, we can rescale the field to remove the q term which results from the bulk mass: Given a field $\varphi(z)$ satisfying (5.2.1) we can equivalently consider a field $\hat{\varphi}$ satisfying

$$-\partial(\hat{p}\partial\hat{\varphi}) = \lambda\hat{r}\hat{\varphi}, \tag{5.2.4}$$

where $\hat{p} = pf^2$, $\hat{r} = rf^2$, and f satisfies

$$-\partial(p\partial f) + qf = 0. \tag{5.2.5}$$

Notice that (5.2.5) is simply of the form of (5.2.1) with $r = 0$. Additionally, we must now use modified boundary conditions obtained from the recaling $\varphi = f\hat{\varphi}$. However, given that the condition (5.2.5) which determines f is second order, we may be able to choose the boundary behaviour of f so as to give convenient BCs for $\hat{\varphi}$ given the BCs for φ. This is presumably equivalent to the procedure with effective warp factors used to manage mixed BCs in section 4.2 of [82]. The equation of motion quoted there for the auxilliary function α is equivalent to (5.2.5) in the case with no bulk mass (so that $q = 0$).

Example — massive scalar

We consider the EOM for a scalar with a mass in the bulk [82],

$$-\partial(w^3\partial\varphi_n) + w^5 M_{\text{bulk}}^2\varphi_n = w^3\varphi_n M_n^2. \tag{5.2.6}$$

We want to remove the bulk mass term so that the procedure to find the sum rules works as in the massless case. We therefore rescale $\varphi = f\hat{\varphi}$ and obtain

$$-\partial(w^3f^2\partial\hat{\varphi}_n) = w^3f^2\hat{\varphi}_n M_n^2, \qquad -\partial(w^3\partial f) + w^5 M_{\text{bulk}}^2 f = 0. \tag{5.2.7}$$

Integrating the EOM for $\hat{\varphi}$ gives

$$\frac{\hat{\varphi}_n(z)}{M_n^2} = \int_{z_0}^{z} \mathrm{d}z'\, \frac{1}{w^3f^2}\int_{z'}^{z_1} \mathrm{d}z''\, w^3f^2\hat{\varphi}_n, \tag{5.2.8}$$

provided we can choose the BCs for f such that $\hat{\varphi}'(z_1) = \hat{\varphi}(z_0) = 0$.

Then, for example, we can write

$$\begin{aligned}\sum_n \frac{1}{M_n^2} &= \sum_n \int_{z_0}^{z_1} \mathrm{d}z\; w^3 f^2 \hat{\varphi}_n \frac{\hat{\varphi}_n}{M_n^2} \\ &= \sum_n \int_{z_0}^{z_1} \mathrm{d}z\; w^3 f^2 \hat{\varphi}_n \int_{z_0}^{z} \mathrm{d}z'\; \frac{1}{w^3 f^2} \int_{z'}^{z_1} \mathrm{d}z''\; w^3 f^2 \hat{\varphi}_n \\ &= \int_{z_0}^{z_1} \mathrm{d}z\; w^3 f^2 \int_{z_0}^{z} \mathrm{d}z'\; \frac{1}{w^3 f^2} \int_{z'}^{z_1} \mathrm{d}z''\; w(z'')^3 f(z'')^2 \sum_n \hat{\varphi}_n(z)\hat{\varphi}_n(z'') \\ &= \int_{z_0}^{z_1} \mathrm{d}z\; w^3 f^2 \int_{z_0}^{z} \mathrm{d}z'\; \frac{1}{w^3 f^2}. \end{aligned} \tag{5.2.9}$$

We have used the normalisation condition and completeness relation resulting from (5.2.7):

$$\int_{z_0}^{z_1} \mathrm{d}z\; w^3 f^2 \hat{\varphi}_m \hat{\varphi}_n = \delta_{mn}, \qquad w(z)^3 f(z)^2 \sum_n \hat{\varphi}_n(z)\hat{\varphi}_n(z') = \delta(z - z'). \tag{5.2.10}$$

A note on notation

In order to avoid unnecessary clutter, we will follow [80] and omit the limits on integrals which extend to the end of the space. Thus we write:

$$\begin{aligned}\int \mathrm{d}z\; f(z) &\equiv \int_{z_0}^{z_1} \mathrm{d}z\; f(z), \\ \int^{z} \mathrm{d}z'\; f(z') &\equiv \int_{z_0}^{z} \mathrm{d}z'\; f(z'), \\ \int_{z} \mathrm{d}z'\; f(z') &\equiv \int_{z}^{z_1} \mathrm{d}z'\; f(z'). \end{aligned} \tag{5.2.11}$$

5.3 A more general metric

In contrast to [80], it will be more convenient to work with a metric in the general form

$$ds^2 = w(y)^2 \eta_{\mu\nu} \mathrm{d}x^\mu \mathrm{d}x^\nu - v(y)^2 \mathrm{d}y^2, \tag{5.3.1}$$

rather than insisting $v = w$. Of course the two forms are related by a coordinate transformation $y \leftrightarrow z$, with $v\mathrm{d}y = \pm w\mathrm{d}z$, so we are not really doing anything here. It will simply be more convenient when we are dealing with our somewhat unwieldy solutions. Expressions of the form derived in e.g. [82] and [80] can be put in terms of y by inserting appropriate factors of $\pm w/z$ according to

$$\mathrm{d}z = \sigma \frac{v}{w} \mathrm{d}y\ , \qquad \partial_z = \sigma \frac{w}{v} \partial_y, \qquad \sigma \equiv \mathrm{sgn}\left(\frac{\mathrm{d}y}{\mathrm{d}z}\right). \tag{5.3.2}$$

We take both w and v to be positive.

Example and check — spin one case

We start from the action

$$S = -\frac{1}{4}\int \mathrm{d}^5x\ \sqrt{g}\ g^{MA}g^{NB}F^a_{MN}F^a_{AB}$$
$$= -\frac{1}{4}\int \mathrm{d}^5x\ \left(v\eta^{\mu\rho}\eta^{\nu\sigma}F^a_{\mu\nu}F^a_{\rho\sigma} - 2\frac{w^2}{v}\eta^{\mu\rho}F^a_{\mu 5}F^a_{\rho 5}\right), \tag{5.3.3}$$

with

$$F^a_{MN} = \partial_M A^a_N - \partial_N A^a_M + g_5 A^b_M A^c_N f^{bca}. \tag{5.3.4}$$

Then we decompose the field as

$$A^a_\mu(x^\nu, z) = \sum_n A^{a,n}_\mu(x^\nu)\varphi_n(z), \tag{5.3.5}$$

which results in

$$S = \sum_{m,n}\int \mathrm{d}^4x\Big[-\frac{1}{4}\eta^{\mu\rho}\eta^{\nu\sigma}H^{a,m}_{\mu\nu}H^{a,n}_{\rho\sigma}\int \mathrm{d}y\ v\varphi_m\varphi_n$$
$$+\frac{1}{2}\eta^{\mu\nu}A^{a,m}_{\mu\nu}A^{a,n}_{\rho\sigma}\int \mathrm{d}y\ \frac{w^2}{v}\partial_y\varphi_m\partial_y\varphi_n\Big], \tag{5.3.6}$$

where

$$H^a_{\mu\nu} = \partial_\mu A^a_\nu - \partial_\nu A^a_\mu = \sum_n H^{a,n}_{\mu\nu}(x^\rho)\varphi_n(z). \tag{5.3.7}$$

We require this to have the usual form

$$S = \int \mathrm{d}^4x\left(-\frac{1}{4}H^2 + \frac{M^2}{2}A^2\right) \tag{5.3.8}$$

The normalisation condition is therefore

$$\int \mathrm{d}y\ v\varphi_m\varphi_n = \delta_{mn}, \tag{5.3.9}$$

as given by (5.3.2). The mass term then results in

$$-\partial_y\left(\frac{w^2}{v}\partial_y\varphi_n\right) = M_n^2 v\varphi_n, \tag{5.3.10}$$

which is again consistent with (5.3.2), and with the normalisation (5.3.9)

Integrating with $(-,+)$ BCs we then get the expected

$$\frac{\varphi_n(y)}{M_n^2} = \int^y \mathrm{d}y'\ \frac{v}{w^2}\int_{y'}\mathrm{d}y''\ v\varphi_n. \tag{5.3.11}$$

The resulting sum rule for $\sum_n M_n^{-2}$ is again of the expected form. The calculation proceeds as before, except that for integrals with respect to y we must use the completeness relation resulting from (5.3.10), namely

$$v(y)\sum_n \varphi_n(y)\varphi_n(y') = \delta(y-y'). \tag{5.3.12}$$

The result is

$$\sum_n \frac{1}{M_n^2} = \int \mathrm{d}y\ v\int^y \mathrm{d}y'\ \frac{v}{w^2}. \tag{5.3.13}$$

Example — scalar

We can similarly adapt the sum rule (5.2.9) for a massive scalar. Using (5.3.2) in (5.2.7, 5.2.9) we obtain

$$\sum_n \frac{1}{M_n^2} = \int_{y_0}^{y_1} \mathrm{d}y\; v w^2 f^2 \int_{y_0}^{y} \mathrm{d}y'\; \frac{v}{w^4 f^2}, \qquad -\partial_y\left(\frac{w^4}{v}\partial_y f\right) + w^4 v M_{\text{bulk}}^2 f = 0. \tag{5.3.14}$$

5.4 Papadopoulos-Tseytlin ansatz

In [62] the (10d) metric is written as[1]

$$ds_{10}^2 = e^{2p-x}(e^{2A}dx_{1,3}^2 + du^2) + e^{x+\hat{g}}(e_1^2+e_2^2) + e^{x-\hat{g}}(\tilde{\epsilon}_1^2+\tilde{\epsilon}_2^2) + e^{-6p-x}\tilde{\epsilon}_3^2, \tag{5.4.1}$$

where

$$e_1 = -\mathrm{d}\theta, \quad e_2 = \sin\theta \mathrm{d}\varphi, \quad \tilde{\epsilon}_1 = \tilde{\omega}_1 + a\mathrm{d}\theta, \quad \tilde{\epsilon}_2 = \tilde{\omega}_2 - a\sin\theta\mathrm{d}\varphi, \quad \tilde{\epsilon}_3 = \tilde{\omega}_3 + \cos\theta\mathrm{d}\varphi. \tag{5.4.2}$$

We instead write

$$ds_{10}^2 = e^{\Phi/2}\hat{h}^{-1/2}dx_{1,3}^2 + e^{\Phi/2}\hat{h}^{1/2}\left[e^{2k}\mathrm{d}\rho^2 + e^{2h}(e_1^2+e_2^2) + \frac{e^{2g}}{4}(\tilde{\epsilon}_1^2+\tilde{\epsilon}_2^2) + \frac{e^{2k}}{4}\tilde{\epsilon}_3^2\right]. \tag{5.4.3}$$

Comparing the coefficients gives

$$e^{2x} = \frac{1}{4}e^{\Phi}\hat{h}e^{2h+2g}, \quad e^{2\hat{g}} = 4e^{2h-2g}, \quad e^{-6p} = \frac{1}{8}e^{\Phi}\hat{h}e^{g+h+2k}, \quad e^{6A} = \frac{1}{64}e^{4\Phi}\hat{h}e^{4g+4h+2k}. \tag{5.4.4}$$

5.5 5d description of the baryonic branch etc.

We write the 5d metric in the form

$$ds_5^2 = w(\rho)^2\eta_{\mu\nu}\mathrm{d}x^\mu\mathrm{d}x^\nu + v(\rho)^2\mathrm{d}\rho^2. \tag{5.5.1}$$

The signature is now $(-+++\cdots)$ to avoid changes of sign when we change dimensionality. The equations of motion for the wavefunctions are unchanged. The radial coordinate $0 \le \rho < \infty$ increases from the IR to the UV.

5.5.1 Metric functions

It is natural to describe the solutions in terms of the functions which appear as coefficients in the metric. The 10d metric can be written

$$ds_{10}^2 = e^{\Phi/2}\hat{h}^{-1/2}\eta_{\mu\nu}\mathrm{d}x^\mu\mathrm{d}x^\nu + e^{\Phi/2}\hat{h}^{1/2}e^{2k}\mathrm{d}\rho^2 + ds_{\text{int}}^2. \tag{5.5.2}$$

[1] We write the function g used in [62] as $\hat{g}$ to avoid confusion with the function g introduced in (5.4.3).

We have defined $\hat{h}(\rho) = 1 - \kappa^2 e^{2\Phi(\rho)}$, as in [47]. In the 'unrotated' case we set $\kappa = 0$, while in the 'rotated' case we set $\kappa = e^{-\Phi_\infty}$. The two cases have the same IR

According to [83], the 10d metric is related to the 5d one by

$$ds_{10}^2 = e^{2p-x} ds_5^2 + ds_{\rm int}^2, \tag{5.5.3}$$

where the functions $p(\rho)$ and $x(\rho)$ are in the standard PT notation [62] (section 5.4):

$$e^{-6p} = \frac{1}{8} e^{\Phi} \hat{h} e^{g+h+2k}, \qquad e^{2x} = \frac{1}{4} e^{\Phi} \hat{h} e^{2g+2h}. \tag{5.5.4}$$

The coefficients of the 5d metric are therefore given by

$$e^{2A} = w^2 = e^{\Phi/2} \hat{h}^{-1/2} e^{x-2p}, \qquad e^{-8p} = v^2 = e^{\Phi/2} \hat{h}^{1/2} e^{2k} e^{x-2p}, \tag{5.5.5}$$

giving

$$w^2 = \frac{1}{4} e^{4\Phi/3} \hat{h}^{1/3} e^{\frac{1}{3}(4g+4h+2k)}, \qquad v^2 = \frac{1}{4} e^{4\Phi/3} \hat{h}^{4/3} e^{\frac{1}{3}(4g+4h+8k)} = \hat{h} e^{2k} w^2 \tag{5.5.6}$$

5.5.2 Master equation functions

In [7] the solutions are described using functions $\{P, Q, \dots\}$ in which the BPS equations reduce to a single second-order 'master equation' for P. The solutions are specified once we know $P(\rho)$. According to [7], the 5d metric is

$$ds_5^2 = e^{2A(\rho)} \eta_{\mu\nu} \mathrm{d}x^\mu \mathrm{d}x^n + 4 e^{-8p(\rho)} \mathrm{d}\rho^2, \tag{5.5.7}$$

where

$$\begin{aligned} A &= \frac{1}{6} \log \left[\frac{1}{256} \hat{h} e^{4\Phi_o} (P^2 - Q^2) \sinh^2 2\rho \right], \\ e^{-24p} &= 2^{-17} \hat{h}^4 e^{4\Phi_o} (P^2 - Q^2) \sinh^2 2\rho \; (P')^3. \end{aligned} \tag{5.5.8}$$

This results in

$$\begin{aligned} w(\rho)^2 &= e^{2A} = 2^{-8/3} e^{4\Phi_o/3} \hat{h}^{1/3} (P^2 - Q^2)^{1/3} \sinh^{2/3} 2\rho, \\ v(\rho)^2 &= 4 e^{-8p} = 2^{-11/3} e^{4\Phi_o/3} \hat{h}^{4/3} (P^2 - Q^2)^{1/3} \sinh^{2/3} 2\rho \; P'(\rho). \end{aligned} \tag{5.5.9}$$

Note that

$$\frac{v}{w} = -\frac{\mathrm{d}z}{\mathrm{d}\rho} = \left(\frac{1}{2} \hat{h} P'(\rho) \right)^{1/2}. \tag{5.5.10}$$

To make use of these expressions we need the the dilaton $\Phi(\rho)$ and the remaining function $Q(\rho)$ and . These are given by

$$e^{4\Phi - 4\Phi_o} = \frac{8 \sinh^2 2\rho}{(P^2 - Q^2) P'}, \qquad Q = N_{\rm c} (2\rho \coth 2\rho - 1). \tag{5.5.11}$$

5.5.3 Expansions

The background is specified by the function $P(\rho)$, which we can describe by asymptotic expansions in the IR (small ρ) and UV (large ρ). Generically, in the UV we have

$$P(\rho) = c_+ e^{4\rho/3} + \frac{4N_c^2}{3c_+}\left(\rho^2 - \rho + \frac{13}{16}\right)e^{-4\rho/3} - \left(\frac{8c_+}{3}\rho - c_-\right)e^{-8\rho/3} + O\left(e^{-4\rho}\right). \tag{5.5.12}$$

By taking c_- to some specific value $c_- = c_-^{\text{BB}}$ we recover the baryonic branch. In this case the IR is of the form

$$P(\rho) = h_1\rho + \cdots. \tag{5.5.13}$$

The is then a family of solutions parameterised by h_1, or equivalently c_+. The relationship $c_+(h_1)$ must be determined numerically. Taking $c_- < c_-^{\text{BB}}$ results in an IR singularity where $P = Q$.

We will initially concentrate on the 'walking' solutions, obtained when $c_- > c_-^{\text{BB}}$. In this case we have a two-parameter family of solutions, and the IR is given by

$$P(\rho) = c_0 + k_3 c_0 \rho^3 + \frac{4}{5}k_3 c_0 \rho^5 - k_3^2 c_0 \rho^6 + \frac{16}{105 c_0}(2c_0^2 k_3 - 5k_3 N_c^2)\rho^7 + O(\rho^8). \tag{5.5.14}$$

Again, the relationship between the IR parameters (c_0, k_3) and the UV parameters (c_+, c_-) must be determined numerically. The length of the walking region is determined by c_-.

Expansions for the 5d warp factors — 'rotated'

We can easily determine the asymptotic behaviour of the warp factors (5.5.9) using the expansions (5.5.12–5.5.14). In the UV we have

$$\begin{aligned} w &= \frac{1}{4}e^{2\Phi_o/3}\left[\frac{3N_c^2}{2}(8\rho - 1)\right]^{1/6} e^{2\rho/3} + O\left(\rho^{13/6}e^{-2\rho}\right) && \sim \rho^{1/6}e^{2\rho/3}, \\ v &= \frac{1}{8}\frac{e^{2\Phi_o/3}}{\sqrt{c_+}}\left(\frac{3}{2}\right)^{1/6}\left[N_c^2(8\rho - 1)\right]^{2/3} + O\left(\rho^{8/3}e^{-8\rho/3}\right) && \sim \rho^{2/3}. \end{aligned} \tag{5.5.15}$$

In the IR the generic walking solutions ($c_- > c_-^{\text{BB}}$) have[2]

$$\begin{aligned} w &= e^{2\Phi_o/3}c_0^{1/3}\left(1 - \frac{8}{3}\sqrt{\frac{c_+^3}{c_0^3 k_3}}\right)^{1/6}\left[\frac{1}{2}\rho^{1/3} + \frac{1}{9}\rho^{7/3} + \frac{k_3}{6}\rho^{10/3} + O\left(\rho^{13/3}\right)\right] && \sim \rho^{1/3}, \\ v &= \sqrt{\frac{3k_3}{2}}e^{2\Phi_o/3}c_0^{5/6}\left(1 - \frac{8}{3}\sqrt{\frac{c_+^3}{c_0^3 k_3}}\right)^{2/3}\left[\frac{1}{2}\rho^{4/3} + \frac{4}{9}\rho^{10/3} + O\left(\rho^{13/3}\right)\right] && \sim \rho^{4/3}. \end{aligned} \tag{5.5.16}$$

[2]As in (5.5.14) this simple structure does not extend to the higher-order terms.

For the baryonic branch, with $c_- = c_-^{\rm BB}$ so that $P \sim \rho$ in the IR, we get

$$w = \frac{1}{2}e^{2\Phi_o/3}h_1^{1/3}\left[1-\frac{8}{\sqrt{3}}\left(\frac{c_+}{h_1}\right)^{3/2}\right]^{1/6}\rho^{2/3}+O\big(\rho^{8/3}\big) \qquad \sim \rho^{2/3},$$
$$v = \frac{1}{2\sqrt{2}}e^{2\Phi_o/3}h_1^{5/6}\left[1-\frac{8}{\sqrt{3}}\left(\frac{c_+}{h_1}\right)^{3/2}\right]^{2/3}\rho^{2/3}+O\big(\rho^{8/3}\big) \qquad \sim \rho^{2/3}. \tag{5.5.17}$$

Note that the c_+, one of the parameters defined with respect to the UV expansions, appears in these IR expansions. This mixing occurs because of the definition $\hat{h}(\rho) = 1 - e^{2\Phi(\rho)-2\Phi(\infty)}$, which depends on the UV behaviour of the dilaton.

Expansions for the 5d warp factors — 'unrotated'

Repeating the above analysis in the 'unrotated' case gives a completely different UV:

$$w = \frac{1}{2}\left(\frac{c_+}{4}\right)^{\frac{1}{3}}e^{\frac{2\Phi_o}{3}}\left[e^{10\rho/9}+\frac{N_c^2}{12c_+^2}(8\rho^2-8\rho+11)e^{-14\rho/9}+O\big(\rho e^{-26\rho/9}\big)\right] \qquad \sim e^{10\rho/9},$$
$$v = \frac{c_+^{5/6}}{2^{7/6}\sqrt{3}}e^{\frac{2\Phi_o}{3}}\left[e^{16\rho/9}-\frac{N_c^2}{24c_+^2}(32\rho^2-104\rho+53)e^{-8\rho/9}+O\big(\rho e^{-20\rho/9}\big)\right] \qquad \sim e^{16\rho/9}. \tag{5.5.18}$$

However, the IR is of the same form as in the 'rotated' case: For the walking solutions,

$$w = e^{2\Phi_o/3}c_0^{1/3}\left[\frac{1}{2}\rho^{1/3}+\frac{1}{9}\rho^{7/3}+\frac{k_3}{6}\rho^{10/3}+O\big(\rho^{13/3}\big)\right] \qquad \sim \rho^{1/3},$$
$$v = \sqrt{\frac{3k_3}{2}}e^{2\Phi_o/3}c_0^{5/6}\left[\frac{1}{2}\rho^{4/3}+\frac{4}{9}\rho^{10/3}-\frac{k_3}{3}\rho^{13/3}+O\big(\rho^{16/3}\big)\right] \qquad \sim \rho^{4/3}, \tag{5.5.19}$$

while for the baryonic branch

$$w = \frac{1}{2}e^{2\Phi_o/3}h_1^{1/3}\left[\rho^{2/3}+\frac{2}{135}\left(21-\frac{44N_c^2}{h_1^2}\right)\rho^{8/3}+O\big(\rho^{14/3}\big)\right] \qquad \sim \rho^{2/3},$$
$$v = \frac{1}{2\sqrt{2}}e^{2\Phi_o/3}h_1^{5/6}\left[\rho^{2/3}+\frac{16}{135}\left(6-\frac{19N_c^2}{h_1^2}\right)\rho^{8/3}+O\big(\rho^{14/3}\big)\right] \qquad \sim \rho^{2/3}. \tag{5.5.20}$$

Singularities

In 10 dimensions, the baryonic branch solution ($c_- = c_-^{\rm BB}$) is completely regular, while the walking solution ($c_- > c_-^{\rm BB}$) has a mild singularity in the IR where the Kretschmann scalar $R_{ABCD}R^{ABCD}$ diverges but both $R_{AB}R^{AB}$ and R remain finite. However, when reduced to 5 dimensions all three quantities diverge in the IR in both classes of solution: In the walking case we find

$$R \sim \rho^{-14/3}, \qquad R_{\mu\nu}R^{\mu\nu} \sim \rho^{-28/3}, \qquad R_{\mu\nu\rho\sigma}R^{\mu\nu\rho\sigma} \sim \rho^{-28/3}, \tag{5.5.21}$$

while for the baryonic branch

$$R \sim \rho^{-4/3}, \qquad R_{\mu\nu}R^{\mu\nu} \sim \rho^{-20/3}, \qquad R_{\mu\nu\rho\sigma}R^{\mu\nu\rho\sigma} \sim \rho^{-20/3}. \tag{5.5.22}$$

5.6 Example and numerics

We can demonstrate some of these ideas by looking at a simple example; the sum rule $\sum_n 1/M_n^2$ for a massless scalar with the simplest BCs (?). This is simply given by (5.3.14) with $f = 1$. We need to use the radial coordinate ρ of section 5.5, so we should rewrite (5.3.14) as

$$\Sigma \equiv \sum_n \frac{1}{M_n^2} = \int_0^\infty \mathrm{d}\rho \; vw^2 \int_\rho^\infty \mathrm{d}\rho' \; \frac{v}{w^4}. \tag{5.6.1}$$

It will be convenient to write this as

$$\Sigma = \int_0^\infty \mathrm{d}\rho \; \mathcal{G}(\rho)\mathcal{F}(\rho), \tag{5.6.2}$$

with $\mathcal{G} = vw^2$ and

$$\mathcal{F}(\rho) = \int_\rho^\infty \mathrm{d}\rho' \; \frac{v}{w^4}. \tag{5.6.3}$$

5.6.1 The numerical calculation

Solving for P and matching

We can solve the master equation for P quite easily, making use of `NDSolve` in *Mathematica*. We want to be able to vary the length of the walking region while keeping the leading UV behaviour fixed, corresponding to varying c_- at constant c_+. This means that it will be convenient to specify the boundary conditions by evaluating the expansion (5.5.12) with the chosen values of c_+ and c_- at some point $\rho = \rho_{\mathrm{UV}}$ in the UV. It is then simple to find the corresponding values of c_0 and k_3 by matching the IR expansion (5.5.14) to the numerical solution at some point in the IR $\rho = \rho_{\mathrm{IR}}$.

Finding solutions on the baryonic branch, corresponding to $c_- = c_-^{\mathrm{BB}}$, calls for a slightly different approach. If we were to specify boundary conditions in the UV we would have to solve for c_-^{BB} numerically. It is much more efficient to specify the boundary conditions in the IR where we have explicitly only one parameter h_1, and then match in the UV to determine both c_+ and c_-^{BB}.

Integrals for the sum rule

In order to calculate the value of Σ we can use the expansions (5.5.12, 5.5.14) for small and large ρ, and a numerical solution at intermediate ρ. We define ρ_{SIR} and ρ_{SUV} to be the points at which we switch between the expansions and the numerical solution, and denote functions evaluated using the expansions with the appropriate subscripts, like $w_{\mathrm{IR}}(\rho)$. Similarly, functions labeled like $w_{\mathrm{num}}(\rho)$ taken to be evaluated using a numerical solution for P.

We will also define a new radial coordinate $u = e^{-2\rho/3}$, corresponding to the expansion parameter in the UV. We will take all UV functions to be in terms of u rather than ρ.

We then split the integral for Σ into three, writing

$$\Sigma = \int_0^{\rho_{\rm SIR}} \mathrm{d}\rho\, \mathcal{G}_{\rm IR}(\rho)\mathcal{F}_{\rm IR}(\rho) + \int_{\rho_{\rm SIR}}^{\rho_{\rm SUV}} \mathrm{d}\rho\, \mathcal{G}_{\rm num}(\rho)\mathcal{F}_{\rm num}(\rho) + \int_0^{u_{\rm SUV}} \mathrm{d}u\, \frac{2u}{3}\mathcal{G}_{\rm UV}(u)\mathcal{F}_{\rm UV}(u). \tag{5.6.4}$$

Each of the functions representing $\mathcal{G}$ can be obtained simply by substituting the appropriate expansion of numerical solution for P into the expression resulting from (5.5.9). Similarly, we can simply define

$$\mathcal{F}_{\rm UV}(u) = \int_0^u \mathrm{d}u'\, \frac{2u'}{3}\frac{v_{\rm UV}(u')}{w_{\rm UV}(u')^4}. \tag{5.6.5}$$

For the purposes of the numerical calculation, we can obtain $\mathcal{F}_{\rm num}$ from the equation

$$\mathcal{F}'_{\rm num}(\rho) = -\frac{v_{\rm num}(\rho)}{w_{\rm num}(\rho)^4}, \tag{5.6.6}$$

subject to the boundary condition $\mathcal{F}_{\rm num}(\rho_{\rm SUV}) = \mathcal{F}_{\rm UV}(e^{-2\rho_{\rm UV}/3})$. The reason for rewriting the inner integral as a differential equation is that we will evaluate it using `NDSolve` in *Mathematica*. This is much more efficient than evaluating an `NIntegrate` separately for each value of ρ.

Finally, we define

$$\mathcal{F}_{\rm IR}(\rho) = \mathcal{F}_{\rm num}(\rho_{\rm SIR}) + \int_\rho^{\rho_{\rm SIR}} \mathrm{d}\rho'\, \frac{v_{\rm IR}(\rho')}{w_{\rm IR}(\rho')^4}. \tag{5.6.7}$$

Notice that the first and last integrals in (5.6.4) can be evaluated completely analytically, apart for the constant numerical contribution $\mathcal{F}_{\rm num}(\rho_{\rm SIR})$ to the first. This should enable us to keep control over any issues with convergence.

Expansions for $\mathcal{F}$ and $\mathcal{G}$

Using the expansions (5.5.15–5.5.17) for the warp factors we can write down the expansions for $\mathcal{F}$ and $\mathcal{G}$ in the IR and UV. We look first at the 'rotated' case. Then in the UV we find

$$\begin{aligned}
\mathcal{F} &= 4e^{-2\Phi_o}\sqrt{\frac{6}{c_+}}\left[e^{-8\rho/3} - \frac{N_c^2}{c_+^2}(128\rho^2 - 176\rho + 155)e^{-16\rho/3} + \left(\rho e^{-20\rho/3}\right)\right] && \sim e^{-8\rho/3},\\
\mathcal{G} &= \frac{e^{2\Phi_o}N_c^2}{128}\sqrt{\frac{3}{2c_+}}\,(8\rho - 1)e^{4\rho/3} + O\left(\rho^3 e^{-4\rho/3}\right) && \sim \rho e^{4\rho/3}.
\end{aligned} \tag{5.6.8}$$

In the case of the generic walking solutions, the IR is of the form

$$\begin{aligned}
\mathcal{F} &= \text{constant} + 12e^{-2\Phi_o}\sqrt{\frac{k_3}{c_0}}\left[\frac{1}{k_3}\rho - \frac{1}{2}\rho^4 - \frac{4}{15}\rho^6 + O\left(\rho^7\right)\right] && \sim \text{constant},\\
\mathcal{G} &= \frac{e^{2\Phi_o}}{\sqrt{6}}\left(3\sqrt{c_0^3 k_3} - 8c_+^{3/2}\right)\left[\frac{1}{8}\rho^2 + \frac{1}{6}\rho^4 + O\left(\rho^6\right)\right] && \sim \rho^2,
\end{aligned} \tag{5.6.9}$$

while for the baryonic branch we get

$$\begin{aligned}\mathcal{F} &= 4e^{-2\Phi_o}\sqrt{\frac{2}{h_1}}\left[\frac{1}{\rho}+\text{constant}+\frac{8}{15}\left(1-\frac{2N_c^2}{3h_1^2}\right)\rho+O\left(\rho^3\right)\right] && \sim\frac{1}{\rho},\\ \mathcal{G} &= \frac{e^{2\Phi_o}}{24\sqrt{2}}\left(3h_1^{3/2}-8\sqrt{3}c_+^{3/2}\right)\rho^2+O\left(\rho^4\right) && \sim\rho^2, \qquad (5.6.10)\end{aligned}$$

where the constant terms in $\mathcal{F}$ cannot be determined analytically.

Turning now to the 'unrotated' case we find that $\mathcal{F}$ is unchanged from the 'rotated' case above — referring to (5.5.9) we see that the factors of $\hat{h}$ cancel in v/w^4. However, for $\mathcal{G}$, we get a UV of the form

$$\mathcal{G} = \frac{4\sqrt{2}e^{2\Phi_o}c_+^{3/2}}{128\sqrt{3}}\left[e^{4\rho}+\frac{3N_c^2}{8c_+^2}(8\rho-1)e^{4\rho/3}-2+O\left(\rho^3e^{-4\rho/3}\right)\right] \quad \sim e^{4\rho}. \qquad (5.6.11)$$

This results in $\mathcal{GF}\sim e^{4\rho/3}$ in the UV, and the integral (5.6.2) for Σ does not converge.

Precision

We will be interested in the effect of varying the length of the walking region (controlled by c_-). If we allow the walking region to extend to large ρ we will be forced to take ρ_{SUV} very large — the UV expansion will only be valid for very large ρ. This will require the use of very high precision in solving for P. It appears that we will need between 70 and 100 decimal digits of `WorkingPrecision` (see figure 5.1).

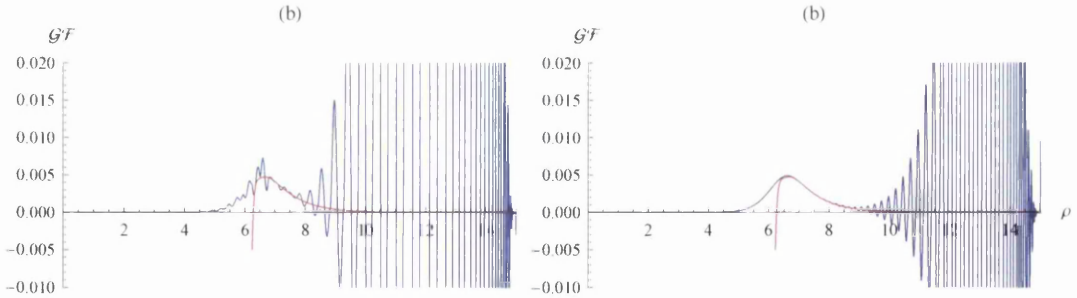

Figure 5.1: Here we plot the integrand $\mathcal{GF}$ as a function of ρ for a large value of c_-, with P calculated at two different precisions. The blue curves correspond to the result $\mathcal{G}_{\text{num}}\mathcal{F}_{\text{num}}$ obtained numerically, and the red to $\mathcal{G}_{\text{UV}}\mathcal{F}_{\text{UV}}$, resulting from the UV expansion. In (a) the precision used (70 digits `WorkingPrecision`) was insufficient; oscillations grow as we move towards the UV, and become large compared to the value of the function before the expansion is a good description. In (b) the precision was increased to 100 digits. Now the oscillations have been pushed further into the UV, and we could get good results by choosing $\rho_{\text{SUV}}\approx 7.5$.

5.6.2 Example 1 — walking solutions

The solutions

As an example calculation we investigate the dependence of Σ on the length of the walking region. This corresponds to keeping c_+ fixed while varying c_-. We

choose $c_+ = 1/10$ and increase c_- from c_-^{BB} up to $c_- = 10^{10}$. Note that because c_- enters into the expansion (5.5.12) at third order, its effect is very suppressed. As we will see, $c_- = 10^{10}$ is not in fact particularly large. Another important point is that we do not actually know the value of c_-^{BB}. In this case it was estimated as $-28\,008 < c_-^{\mathrm{BB}} < -28\,007$ by manually searching for the smallest value of c_- which gives $P \to$ constant in the IR. Ideally, we could determine the function $c_-^{\mathrm{BB}}(c_+)$ by generating multiple solutions on the baryonic branch. However, this seems to be difficult (section 5.6.3).

There are two additional parameters visible in the expansions which have little effect on the behaviour of the result; we choose $N_c = 1$ and $\Phi_o = 0$.

The effect of varying c_- on $P(\rho)$ is visible in figure 5.2. The upper end of the walking region corresponds to a transition from $P \sim c_0$ in the IR to $P \sim e^{4\rho/3}$ in the UV. We can therefore characterise the length of the walking region by a scale ρ_{W} satisying $P(\rho_{\mathrm{W}}) - c_0 = 1$. This may not be the best definition, because in the case of the baryonic branch we get $\rho_{\mathrm{W}} \approx 1/h_1$ rather than $\rho_{\mathrm{W}} = 0$.

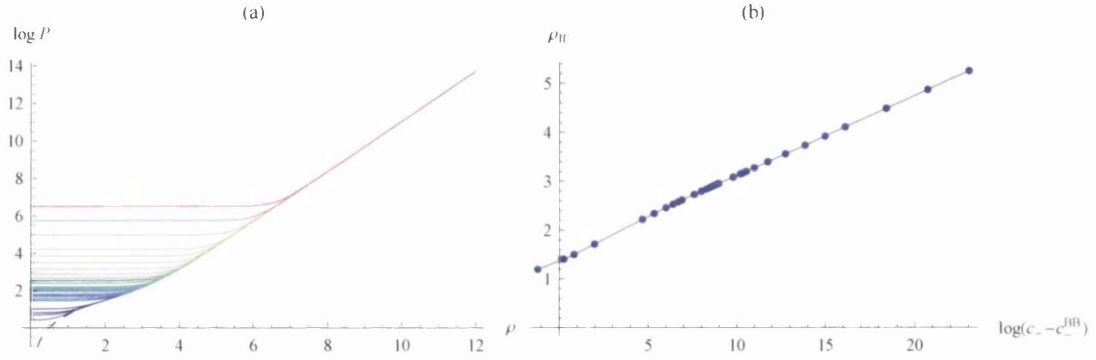

Figure 5.2: (a) Plot $\log P$ as a function of ρ for a range of c_-. The upper end of the walking region is visible as the transition to linear behaviour (exponential growth of P) in the UV. The dashed curve corresponds to the limiting case of the baryonic branch solution ($c_- = c_-^{\mathrm{BB}}$), as obtained from the results of section 5.6.3.
(b) The relationship between the length of the walking region, represented by ρ_{W}, and c_-. There is some uncertainty resulting from the unknown value of c_-^{BB}, which is only significant in the three left-most points. The value $c_-^{\mathrm{BB}} \approx -28\,007.3$ was obtained by assuming that the plots in figure 5.3 remain approximately linear for $c_- \to c_-^{\mathrm{BB}}$.

The values of the IR parameters are obtained by matching the IR expansion (5.5.14) to the numerical solution at $\rho = 1/10$. The results are shown in figure 5.3.

The integrals

Having obtained the solutions and determined the IR parameters we can proceed to the integrals (5.6.4). As discussed above, the first and last can be performed symbolically. The integrands of the inner and outer integrals are shown in figure 5.4.

The final result is shown in figure 5.5. It appears that $\Sigma \to 0$ for large c_- (corresponding to long walking). In the opposite limit, corresponding to the baryonic branch, it appears that Σ approaches some finite value. See section 5.6.3.

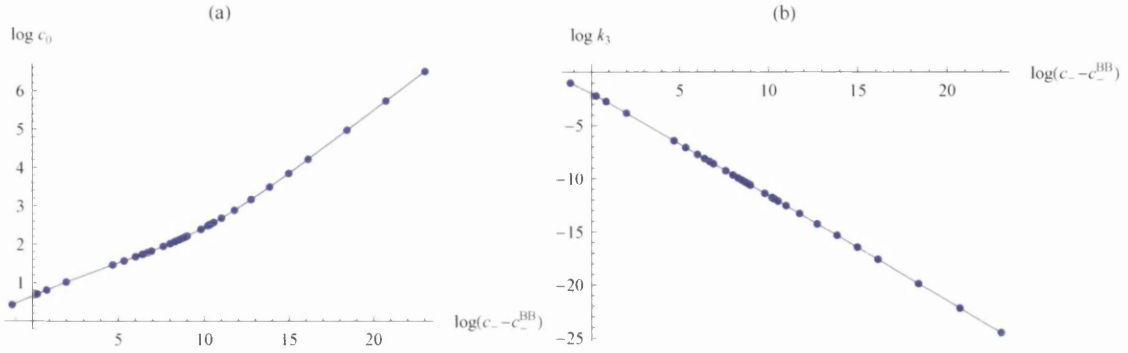

Figure 5.3: Plots showing the dependence of the IR parameters (a) c_0 and (b) k_3 on the UV parameter c_-. As above there is some uncertainty in the positions of the three left-most points in each plot resulting from the uncertainty in the value of c_-^{BB}.

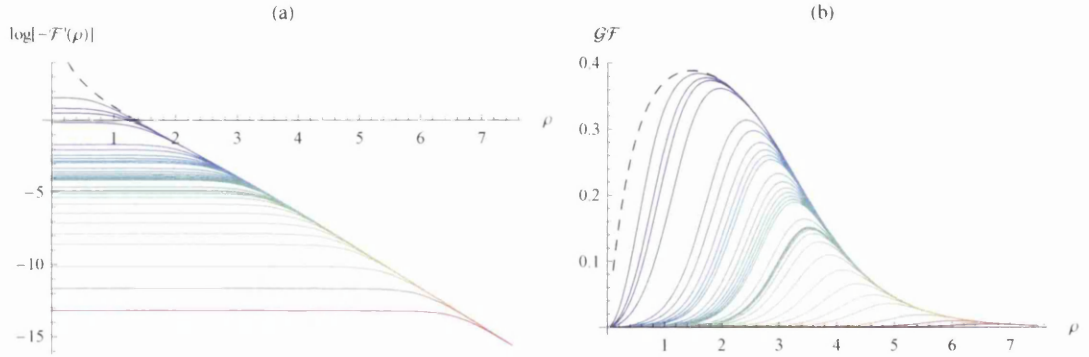

Figure 5.4: Plots showing the behaviour of the integrands of (a) the inner and (b) the outer integrals in (5.6.1) as we vary the length of the walking region. Again, the dashed curves show the corresponding baryonic branch solution from section 5.6.3.

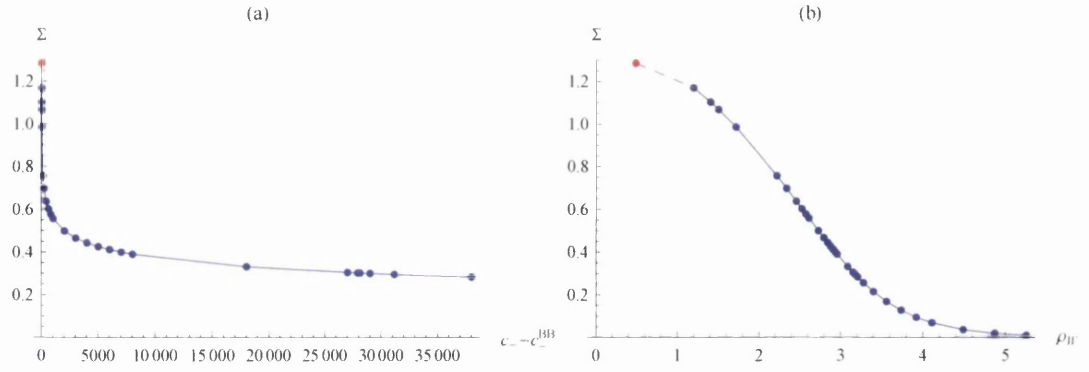

Figure 5.5: Plots showing the dependence of Σ on (a) c_- and (b) ρ_{W}. The red points show the values for the corresponding baryonic branch solution from section 5.6.3.

5.6.3 Example 2 — Baryonic branch solutions

The solutions

To get a feeling for the effect of c_+, we can look at the baryonic branch solutions with $c_- = c_-^{\mathrm{BB}}$. As discussed above, it is more practical to generate these solutions starting from the IR expansion, and so in order to change c_+ we vary h_1 (see figure 5.6). Again we fix $N_c = 1$ and $\Phi_o = 0$.

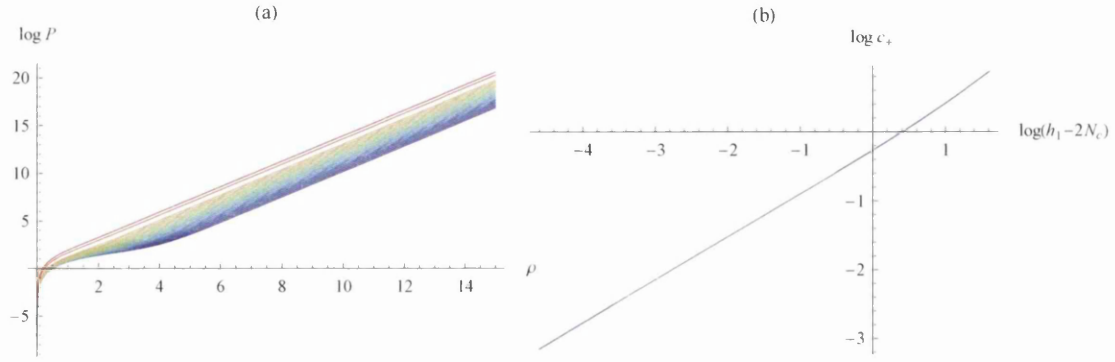

Figure 5.6: Plots showing the effect on varying h_1 on the baryonic branch. In (a) we show the effect on P. The purple curve corresponds to small h_1, and the red to large h_1. In (b) we show the corresponding change in c_+.

We are now in a position to see the behaviour of $c_-^{\mathrm{BB}}(c_+)$ (figure 5.7). However, it seems to be difficult to get precise values. For example, in section 5.6.2 we set $c_+ = 1/10$ and noted that $-28\,008 < c_-^{\mathrm{BB}} < -28\,007$. Interpolating between the solutions found here we obtain $c_-^{\mathrm{BB}}(1/10) \approx -27\,995$. There is some variation depending on the method of interpolation used, but the value obtained is consistently outside the possible range.

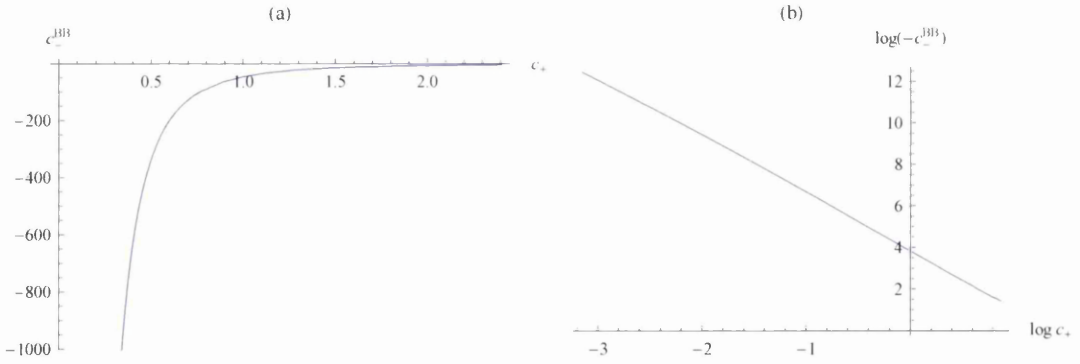

Figure 5.7: The behaviour of $c_-^{\mathrm{BB}}(c_+)$ as we move along the baryonic branch by varying c_+.

The integrals

We can now present the resulting behaviour of the integrands (figure 5.8) and Σ (figure 5.9) as we vary c_+. It appears that Σ may vanish in the limit of large c_+

(corresponding to Klebanov-Strassler) and diverge in the opposite limit $c_+ \to 0$ (or equivalently $h_1 \to 2N_c$).

Together with the results of section 5.6.2, we see that the integrand $\mathcal{GF}$ (figures 5.4,5.8) can be described in terms of two scales. One characterises the rate at which $\mathcal{GF}$ decays in the IR, and is controlled by c_-. This corresponds roughly to the scale at which P switches from being approximately constant in the IR to growing linearly or exponentially in the UV. The second scale characterises the rate at which $\mathcal{GF}$ decays in the UV. This is unaffected by c_-, but is controlled by c_+.

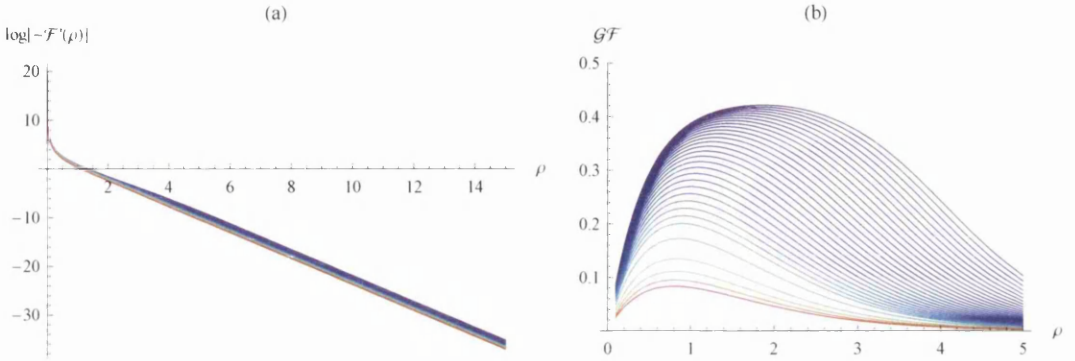

Figure 5.8: Plots showing the behaviour of the integrands of (a) the inner and (b) the outer integrals in (5.6.1) as we vary c_+. In (b) we include only the region $\rho_{\rm SIR} \leq \rho < \rho_{\rm SUV}$ in which we use the numerical solution.

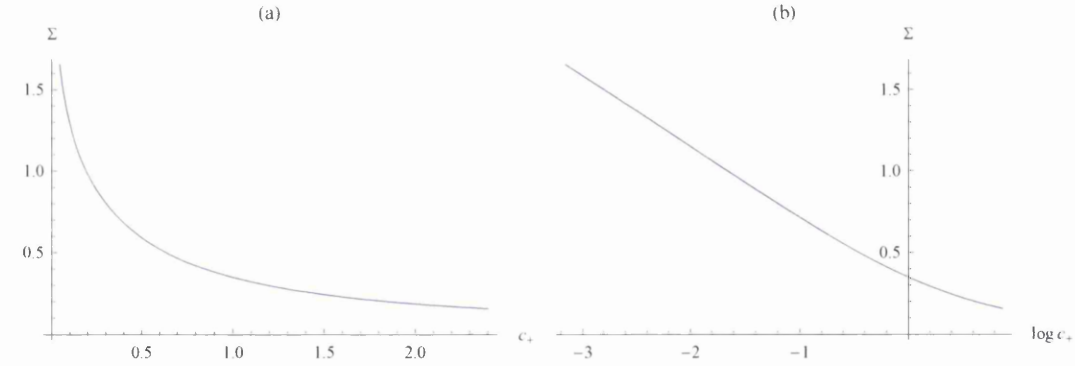

Figure 5.9: The dependence of Σ on c_+.

Appendices

Appendix A

Breaking SUSY

A.1 Appendix: Technical aspects of the SUSY background

We write in this appendix various technical aspects of the supersymmetric baryonic branch backgrounds. in order to decouple the non-linear system of BPS equations, one changes the basis of functions from Φ, h, g, k, a, b into $P, Q, Y, \tilde{\Phi}, \tau, \sigma$. As explained in [50], the change of basis functions is

$$
\begin{aligned}
& 4e^{2h} = \frac{P^2 - Q^2}{P\cosh\tau - Q}, \quad e^{2g} = P\cosh\tau - Q, \quad e^{2k} = 4Y, \\
& a = \frac{P\sinh\tau}{P\cosh\tau - Q}, \quad N_c b = \sigma.
\end{aligned} \tag{A.1.1}
$$

Using the relations above, one can solve for the decoupled BPS equations,

$$
\begin{aligned}
& Q(\rho) = (Q_0 + N_c)\cosh\tau + N_c(2\rho\cosh\tau - 1), \\
& \sinh\tau(\rho) = \frac{1}{\sinh(2\rho - 2\rho_0)}, \quad \cosh\tau(\rho) = \coth(2\rho - 2\rho_0), \\
& Y(\rho) = \frac{P'}{8}, \quad e^{4\Phi} = \frac{e^{4\Phi_o}\cosh(2\rho_0)^2}{(P^2 - Q^2)Y\sinh^2\tau}, \\
& \sigma = \tanh\tau(Q + N_c) = \frac{(2N_c\rho + Q_o + N_c)}{\sinh(2\rho - 2\rho_0)}.
\end{aligned} \tag{A.1.2}
$$

and the master equation (3.2.12). Solving the master equation in the UV and plugging back into eqs.(A.1.1)-(A.1.2) the background functions read at large ρ,

$$
\begin{aligned}
e^{2h} &\sim \left[\frac{c_+e^{4\rho/3}}{4}+\frac{N_c}{4}(2\rho-1)+\frac{N_c^2e^{-4\rho/3}}{16c_+}(16\rho^2-16\rho+13)+\frac{e^{-8\rho/3}}{4}(c_--c_+(2+\frac{8\rho}{3}))\right]\\
\frac{e^{2g}}{4} &\sim \left[\frac{c_+e^{4\rho/3}}{4}-\frac{N_c}{4}(2\rho-1)+\frac{N_c^2e^{-4\rho/3}}{16c_+}(16\rho^2-16\rho+13)+\frac{e^{-8\rho/3}}{4}(c_-+c_+(2-\frac{8\rho}{3}))\right]\\
\frac{e^{2k}}{4} &\sim \left[\frac{c_+e^{4\rho/3}}{6}-\frac{N_c^2e^{-4\rho/3}}{24c_+}(4\rho-5)^2+\frac{e^{-8\rho/3}}{3}(c_+(\frac{8\rho}{3}-1)-c_-)\right]\\
e^{4\Phi-4\Phi_0} &\sim \left[1+\frac{3N_c^2e^{-8\rho/3}}{4c_+^2}(1-8\rho)+\frac{3N_c^4e^{-16\rho/3}}{512c_+^4}(2048\rho^3+1152\rho^2+2352\rho-775)\right]\\
a &\sim 2e^{-2\rho}+\frac{2N_c}{c_+}(2\rho-1)e^{-10\rho/3}+\frac{2N_c^2}{c_+^2}(2\rho-1)^2e^{-14\rho/3}\\
b &= \frac{2\rho}{\sinh(2\rho)}\sim 4\rho e^{-\rho}+4\rho e^{-6\rho}
\end{aligned}
\tag{A.1.3}
$$

The geometry in eq. (3.2.6) asymptotes to the conifold after using the expansions above. In the IR we have

$$
\begin{aligned}
e^{2h} &\sim \frac{h_1\rho^2}{2}+\frac{4}{45}\left(-6h_1+15N_c-\frac{16N_c^2}{h_1}\right)\rho^4+\mathcal{O}(\rho^6),\\
\frac{e^{2g}}{4} &\sim \frac{h_1}{8}+\frac{1}{15}\left(3h_1-5N_c-\frac{2N_c^2}{h_1}\right)\rho^2+\frac{2\left(3h_1^4+70h_1^3N_c-144h_1^2N_c^2-32N_c^4\right)\rho^4}{1575h_1^3}\\
&\quad +\mathcal{O}(\rho^6),\\
\frac{e^{2k}}{4} &\sim \frac{h_1}{8}+\frac{\left(h_1^2-4N_c^2\right)\rho^2}{10h_1}+\frac{\left(6h_1^4-8h_1^2N_c^2-64N_c^4\right)\rho^4}{315h_1^3}+\mathcal{O}(\rho^6),\\
e^{4(\Phi-\Phi_0)} &\sim 1+\frac{64N_c^2\rho^2}{9h_1^2}+\frac{128N_c^2\left(-15h_1^2+124N_c^2\right)\rho^4}{405h_1^4}+\mathcal{O}(\rho^6),
\end{aligned}
\tag{A.1.4}
$$

$$
\begin{aligned}
a &\sim 1+\left(-2+\frac{8N_c}{3h_1}\right)\rho^2+\frac{2\left(75h_1^3-232h_1^2N_c+160h_1N_c^2+64N_c^3\right)\rho^4}{45h_1^3}+\mathcal{O}(\rho^6),\\
b &= \frac{2\rho}{\sinh(2\rho)}\sim 1-\frac{2}{3}\rho^2+\frac{14}{45}\rho^4+\mathcal{O}(\rho^6).
\end{aligned}
\tag{A.1.5}
$$

This space is free of singularities as can be checked by computing invariants.

A.2 Equations of motion

The equations of motion for the full non-SUSY system (section 3.3.2) can be obtained either from the Einstein, Maxwell, dilaton and Bianchi equations of the ten-dimensional system, or from a one-dimensional effective Lagrangian $L = T - U$, with

$$\begin{aligned}
T = &-\frac{1}{128}e^{2\Phi}\Big\{e^{4g}\left(a'\right)^2 + \left(b'\right)^2 N_c^2 - 8e^{2(g+h)}\Big[2g'\left(2h' + k' + 2\Phi'\right) + \left(g'\right)^2 \\
&+ 2h'\left(k' + 2\Phi'\right) + \left(h'\right)^2 + 2\Phi'\left(k' + \Phi'\right)\Big]\Big\}, \\
U = &\frac{1}{256}e^{-2(g+h-\Phi)}\Big[a^4e^{4g}\left(N_c^2 + e^{4k}\right) - 4a^3be^{4g}N_c^2 + 2a^2e^{2g}\Big(2b^2e^{2g}N_c^2 \\
&+ e^{2g}N_c^2 + 4e^{2h}N_c^2 - 8e^{2(g+h+k)} + 4e^{4g+2h} - e^{2g+4k} + 4e^{2h+4k}\Big) \\
&- 4abe^{2g}N_c^2\left(e^{2g} + 4e^{2h}\right) + 8b^2N_c^2e^{2(g+h)} + e^{4g}N_c^2 + 16e^{4h}N_c^2 \\
&- 16e^{2(2g+h+k)} - 64e^{2(g+2h+k)} + e^{4(g+k)} + 16e^{4(h+k)}\Big].
\end{aligned} \tag{A.2.1}$$

In addition to the equations of motion resulting from (A.2.1), there is a Hamiltonian constraint

$$T + U = 0 \tag{A.2.2}$$

resulting from invariance under reparametrisation of the radial coordinate.

The equations of motion themselves, setting $N_c = 1$ for simplicity, are

$$\begin{aligned}
g'' = &\frac{1}{8}e^{-4g-2h}\Big[e^{6g}\left(a'\right)^2 - 4a^2e^{2g+4k} - 4a^2e^{2g} + 4a^2e^{6g} + 8abe^{2g} \\
&- e^{2g}\left(b'\right)^2 - 4b^2e^{2g} - 16e^{4g+2h}g'h' - 16e^{4g+2h}g'\Phi' \\
&- 16e^{4g+2h}\left(g'\right)^2 + 32e^{2g+2h+2k} - 16e^{2h+4k} - 16e^{2h}\Big]
\end{aligned} \tag{A.2.3}$$

$$\begin{aligned}
h'' = &-\frac{1}{8}e^{-2g-4h}\Big[\left(a'\right)^2e^{4g+2h} + a^4e^{2g+4k} + a^4e^{2g} - 4a^3be^{2g} + 4a^2b^2e^{2g} \\
&- 8a^2e^{2g+2h+2k} + 4a^2e^{4g+2h} - 2a^2e^{2g+4k} + 2a^2e^{2g} \\
&+ 4a^2e^{2h+4k} + 4a^2e^{2h} - 4abe^{2g} - 8abe^{2h} + e^{2h}\left(b'\right)^2 \\
&+ 4b^2e^{2h} + 16e^{2g+4h}g'h' + 16e^{2g+4h}h'\Phi' + 16e^{2g+4h}\left(h'\right)^2 \\
&- 8e^{2g+2h+2k} + e^{2g+4k} + e^{2g}\Big]
\end{aligned} \tag{A.2.4}$$

$$\begin{aligned}
k'' = &\frac{1}{8}e^{-4g-4h}\Big(a^4e^{4g+4k} - a^4e^{4g} + 4a^3be^{4g} - 4a^2b^2e^{4g} + 8a^2e^{2g+2h+4k} \\
&- 8a^2e^{2g+2h} - 8a^2e^{6g+2h} - 2a^2e^{4g+4k} - 2a^2e^{4g} + 16abe^{2g+2h} \\
&+ 4abe^{4g} - 8b^2e^{2g+2h} - 16e^{4g+4h}g'k' - 16e^{4g+4h}h'k' \\
&- 16e^{4g+4h}k'\Phi' + e^{4g+4k} - e^{4g} + 16e^{4h+4k} - 16e^{4h}\Big)
\end{aligned} \tag{A.2.5}$$

$$\Phi'' = \frac{1}{8}e^{-4g-4h}\Big[a^4e^{4g} - 4a^3be^{4g} + 4a^2b^2e^{4g} + 8a^2e^{2g+2h} - 16abe^{2g+2h} + 2a^2e^{4g} - 4abe^{4g} + 2\left(b'\right)^2e^{2g+2h} + 8b^2e^{2g+2h} - 16e^{4g+4h}g'\Phi' - 16e^{4g+4h}h'\Phi' - 16e^{4g+4h}\left(\Phi'\right)^2 + e^{4g} + 16e^{4h}\Big] \tag{A.2.6}$$

$$a'' = e^{-4g-2h}\Big(-4a'e^{4g+2h}g' - 2a'e^{4g+2h}\Phi' + a^3e^{2g+4k} + a^3e^{2g} - 3a^2be^{2g} + 2ab^2e^{2g} - 8ae^{2g+2h+2k} + 4ae^{4g+2h} - ae^{2g+4k} + ae^{2g} + 4ae^{2h+4k} + 4ae^{2h} - be^{2g} - 4be^{2h}\Big) \tag{A.2.7}$$

$$b'' = -e^{-2h}\left(a^3e^{2g} - 2a^2be^{2g} + ae^{2g} + 4ae^{2h} + 2e^{2h}b'\Phi' - 4be^{2h}\right) \tag{A.2.8}$$

The case discussed in section 3.4.2, with $v_2 = 0$, is far simpler. After setting $a = b = 1$ and $g = k$ the equations of motion for the remaining three functions are

$$\begin{aligned} k'' &= 2 - 2e^{-4k} - 2h'k' - 2(k')^2 - 2k'\Phi', \\ h'' &= e^{2k-2h} - 2h'k' - 2(h')^2 - 2h'\Phi', \\ \Phi'' &= 2e^{-4k} - 2h'\Phi' - 2(\Phi')^2 - 2k'\Phi', \end{aligned} \tag{A.2.9}$$

and the constraint is

$$e^{-4k} - e^{2k-2h} - 3 + 6h'k' + 4h'\Phi' + 6k'\Phi' + (h')^2 + 3(k')^2 + 2(\Phi')^2 = 0. \tag{A.2.10}$$

A.3 Appendix: Explicit expansion of the functions

Here we include the explicit solutions for the expansions (3.3.12) and (3.3.8). In this section we again set $N_c = 1$.

A.3.1 UV

$$\begin{aligned} e^{2g} = {} & c_+e^{4\rho/3} - \left(2c_+W_{20}^2 + 4H_{11}\rho + Q_o\right) \\ & - \frac{1}{48c_+}\Big\{-12H_{11}\left[(32\rho - 6)Q_o - c_+W_{20}^2(8\rho + 93)\right] - 12c_+W_{20}^2Q_o \\ & + 72c_+^2W_{20}e^{2\rho_o} + 120c_+^2W_{20}^4\rho - 26c_+^2W_{20}^4 + 12c_+^2\Phi_{30}e^{-4\Phi_\infty} - 72\rho \\ & - 24H_{11}^2\left(32\rho^2 - 12\rho + 15\right) - 48Q_o^2 + 9\Big\}e^{-4\rho/3} + O\left(e^{-8\rho/3}\right) \end{aligned} \tag{A.3.1}$$

$$\begin{aligned} e^{2h} = {} & \frac{c_+}{4}e^{4\rho/3} + \left(H_{11}\rho + \frac{Q_o}{4}\right) \\ & - \frac{1}{192c_+}\Big\{-12H_{11}\left[c_+W_{20}^2(88\rho + 75) + (32\rho - 6)Q_o\right] - 396c_+W_{20}^2Q_o \\ & + 264c_+^2W_{20}e^{2\rho_o} + 440c_+^2W_{20}^4\rho - 626c_+^2W_{20}^4 + 12c_+^2\Phi_{30}e^{-4\Phi_\infty} - 72\rho \\ & - 24H_{11}^2\left(32\rho^2 - 12\rho + 15\right) - 48Q_o^2 + 9\Big\}e^{-4\rho/3} + O\left(e^{-8\rho/3}\right) \end{aligned} \tag{A.3.2}$$

$$e^{2k} = \frac{2c_+}{3}e^{4\rho/3} + \frac{c_+W_{20}^2}{3} - \frac{1}{24c_+}\Big[4H_{11}(16\rho-9)\left(3c_+W_{20}^2+2Q_o\right) + 16Q_o^2$$
$$+ 84c_+W_{20}^2Q_o - 72c_+^2W_{20}e^{2\rho_o} - 120c_+^2W_{20}^4\rho + 190c_+^2W_{20}^4 - 24\rho - 9$$
$$+ 4c_+^2\Phi_{30}e^{-4\Phi_\infty} + 8H_{11}^2\left(32\rho^2-36\rho+27\right)\Big]e^{-4\rho/3} + O\big(e^{-8\rho/3}\big) \qquad \text{(A.3.3)}$$

$$e^{4\Phi} = e^{4\Phi_\infty} + \left(\Phi_{30} - \frac{6\rho e^{4\Phi_\infty}}{c_+^2}\right)e^{-8\rho/3}$$
$$+ \frac{W_{20}^2\left(32c_+^2\Phi_{30} - 3(64\rho+25)e^{4\Phi_\infty}\right)}{24c_+^2}e^{-4\rho} + O\big(e^{-16\rho/3}\big) \qquad \text{(A.3.4)}$$

$$a = W_{20}e^{-2\rho/3} + \left(\frac{4H_{11}W_{20}\rho}{c_+} + 2e^{2\rho_o} + \frac{10W_{20}^3\rho}{3}\right)e^{-2\rho}$$
$$+ \frac{1}{48c_+^2}\Bigg(4c_+\Big\{H_{11}\left[96\rho e^{2\rho_o} + W_{20}^3\left(160\rho^2+552\rho+495\right)\right] + 2Q_o\Big[12e^{2\rho_o}$$
$$+ W_{20}^3(20\rho+87)\Big]\Big\} + c_+^2\left[W_{20}^5(391-480\rho) - 288W_{20}^2e^{2\rho_o}\right]$$
$$+ 12W_{20}\Big[2H_{11}(40\rho+27)Q_o$$
$$+ 6H_{11}^2\left(32\rho^2+36\rho+43\right) + 8Q_o^2 - 15\Big]\Bigg)e^{-10\rho/3} + O\big(e^{-4\rho}\big) \qquad \text{(A.3.5)}$$

$$b = \frac{9}{4}W_{20}e^{-2\rho/3} + \left\{\left[4e^{2\rho_o} + \frac{W_{20}^3}{6}(20\rho-23) - \frac{12W_{20}Q_o}{6c_+}\right]\rho + V_{40}\right\}e^{-2\rho}$$
$$+ \frac{3W_{20}e^{-4\Phi_\infty}}{512c_+^2}\Big\{e^{4\Phi_\infty}\Big[-3456H_{11}\left(3c_+W_{20}^2+2Q_o\right) - 3240c_+W_{20}^2Q_o$$
$$+ 192c_+^2V_{40}W_{20} + 2819c_+^2W_{20}^4 - 35712H_{11}^2 - 576Q_o^2 + 882\Big]$$
$$- 16\rho e^{4\Phi_\infty}\Big[144H_{11}\left(3c_+W_{20}^2+2Q_o\right) + 24c_+W_{20}^2Q_o$$
$$- c_+^2W_{20}\left(48e^{2\rho_o} + 269W_{20}^3\right) + 1728H_{11}^2 - 18\Big] + 3024c_+^2W_{20}e^{2\rho_o+4\Phi_\infty}$$
$$- 128\rho^2e^{4\Phi_\infty}\left(72H_{11}^2 - 5c_+^2W_{20}^4\right) - 48c_+^2\Phi_{30}\Big\}e^{-10\rho/3} + O\big(e^{-4\rho}\big) \qquad \text{(A.3.6)}$$

We can see the effect of the SUSY-breaking parameters by looking at functions of the form $\Delta(e^{2g}) = e^{2g} - e^{2g_{\rm SUSY}}$, where g corresponds to the full solution and $g_{\rm SUSY}$ corresponds to the SUSY case with $Q_o = -N_c$ and $\rho_o = 0$. Note that in general only one of the two solutions will go to the regular IR — if we start with a SUSY solution and turn on one of the SUSY-breaking parameters while keeping e.g. c_+ fixed, we will have to change c_- to recover the regular IR. Those SUSY-breaking parameters which have non-zero values in the SUSY case are expressed here in terms of e.g. $\Delta H_{11} = H_{11} - H_{11}^{\rm SUSY}$.

$$\begin{aligned}\Delta\left(e^{2g}\right) &= \left(-2c_+W_{20}^2 - \Delta Q_o - 4\Delta H_{11}\rho\right)\\ &+ \frac{e^{-4\Phi_\infty}}{24c_+}\Big\{-3c_+W_{20}^2e^{4\Phi_\infty}\left[-2\Delta Q_o + 2\Delta H_{11}(8\rho+93) + 8\rho + 95\right]\\ &- c_+^2\left[36W_{20}e^{2\rho_o+4\Phi_\infty} + W_{20}^4(60\rho-13)e^{4\Phi_\infty} + 6\Delta\Phi_{30}\right]\\ &+ 6e^{4\Phi_\infty}\Big[\Delta H_{11}\Big((32\rho-6)\Delta Q_o + 64\rho^2 - 56\rho + 36\Big) + \Delta Q_o\left(4\Delta Q_o + 16\rho - 11\right)\\ &+ \Delta H_{11}^2\left(64\rho^2 - 24\rho + 30\right)\Big]\Big\}e^{-4\rho/3} + O\left(e^{-8\rho/3}\right) \qquad \text{(A.3.7)}\end{aligned}$$

$$\begin{aligned}\Delta\left(e^{2h}\right) &= \left(\frac{\Delta Q_o}{4} + \Delta H_{11}\rho\right) + \frac{e^{-4\Phi_\infty}}{96c_+}\Bigg(3c_+W_{20}^2e^{4\Phi_\infty}\Big[66\Delta Q_o + 2\Delta H_{11}(88\rho+75) + 88\rho + 9\Big]\\ &- c_+^2\left[132W_{20}e^{2\rho_o+4\Phi_\infty} + W_{20}^4(220\rho-313)e^{4\Phi_\infty} + 6\Delta\Phi_{30}\right]\\ &+ 6e^{4\Phi_\infty}\Big\{\Delta H_{11}\left[(32\rho-6)\Delta Q_o + 64\rho^2 - 56\rho + 36\right] + \Delta Q_o\left(4\Delta Q_o + 16\rho - 11\right)\\ &+ \Delta H_{11}^2\left(64\rho^2 - 24\rho + 30\right)\Big\}\Bigg)e^{-4\rho/3} + O\left(e^{-8\rho/3}\right) \qquad \text{(A.3.8)}\end{aligned}$$

$$\begin{aligned}\Delta\left(e^{2k}\right) &= \frac{1}{3}c_+W_{20}^2 + \frac{e^{-4\Phi_\infty}}{12c_+}\Bigg(-3c_+W_{20}^2e^{4\Phi_\infty}\Big[14\Delta Q_o + 2\Delta H_{11}(16\rho-9) + 16\rho - 23\Big]\\ &+ c_+^2\left[36W_{20}e^{2\rho_o+4\Phi_\infty} + 5W_{20}^4(12\rho-19)e^{4\Phi_\infty} - 2\Delta\Phi_{30}\right]\\ &- 2e^{4\Phi_\infty}\Big\{2\Delta H_{11}\left[(16\rho-9)\Delta Q_o + 4\left(8\rho^2 - 13\rho + 9\right)\right]\\ &+ \Delta Q_o\left(4\Delta Q_o + 16\rho - 17\right)\\ &+ \Delta H_{11}^2\left(64\rho^2 - 72\rho + 54\right)\Big\}\Bigg)e^{-4\rho/3} + O\left(e^{-8\rho/3}\right) \qquad \text{(A.3.9)}\end{aligned}$$

$$\Delta\left(e^{4\Phi}\right) = \Delta\Phi_{30}e^{-8\rho/3} + \frac{W_{20}^2}{24c_+^2}\left[32c_+^2\Delta\Phi_{30} - 3(64\rho+17)e^{4\Phi_\infty}\right]e^{-4\rho} + O\left(e^{-16\rho/3}\right) \qquad \text{(A.3.10)}$$

$$\Delta a = W_{20}e^{-2\rho/3} + \frac{1}{c_+}\left[\frac{2}{3}c_+\left(3e^{2\rho_o} + 5W_{20}^3\rho - 3\right) + 2W_{20}\left(2\Delta H_{11} + 1\right)\rho\right]e^{-2\rho}$$
$$+ \frac{1}{48c_+^2}\Bigg(2c_+\Bigg\{W_{20}^3\Big[4(20\rho+87)\Delta Q_o + 2\Delta H_{11}\left(160\rho^2 + 552\rho + 495\right)$$
$$+ 160\rho^2 + 472\rho + 147\Big] + 48\left[4\Delta H_{11}\rho e^{2\rho_o} + \Delta Q_o e^{2\rho_o} + (2\rho-1)\left(e^{2\rho_o}-1\right)\right]\Bigg\}$$
$$+ c_+^2\left[W_{20}^5(391 - 480\rho) - 288W_{20}^2e^{2\rho_o}\right] + 6W_{20}\Bigg\{+(80\rho+22)\Delta Q_o$$
$$+ 4\Delta H_{11}\left[(40\rho+27)\Delta Q_o + 96\rho^2 + 68\rho + 102\right] + 16\Delta Q_o^2 + 12\Delta H_{11}^2\left(32\rho^2 + 36\rho + 43\right)$$
$$+ 96\rho^2 + 28\rho + 61\Bigg\}\Bigg)e^{-10\rho/3} + O\left(e^{-14\rho/3}\right) \qquad \text{(A.3.11)}$$

$$\Delta b = \frac{9}{4}W_{20}e^{-2\rho/3} + \Big[c_+\left\{\rho\left[24\left(e^{2\rho_o}-1\right) + W_{20}^3(20\rho - 23)\right] + 6V_{40}\right\}$$
$$- 12W_{20}\rho\left(\Delta Q_o - 1\right)\Big]\frac{e^{-2\rho}}{6c_+} + \frac{3W_{20}e^{-4\Phi_\infty}}{512c_+^2}\Bigg(c_+^2\Bigg\{48W_{20}e^{4\Phi_\infty}\left[(16\rho+63)e^{2\rho_o} + 4V_{40}\right]$$
$$+ W_{20}^4\left(640\rho^2 + 4304\rho + 2819\right)e^{4\Phi_\infty} - 48\Delta\Phi_{30}\Bigg\}$$
$$- 24c_+W_{20}^2e^{4\Phi_\infty}\left[(16\rho+135)\Delta Q_o + 144\Delta H_{11}(2\rho+3) + 128\rho + 81\right]$$
$$- 18e^{4\Phi_\infty}\Bigg\{64\Delta H_{11}\left[(4\rho+6)\Delta Q_o + 8\rho^2 + 20\rho + 25\right]$$
$$+ 128(\rho+1)\Delta Q_o + 32\Delta Q_o^2 + 64\Delta H_{11}^2\left(8\rho^2 + 24\rho + 31\right)$$
$$+ 128\rho^2 + 240\rho + 289\Bigg\}\Bigg)e^{-10\rho/3} + O\left(e^{-14\rho/3}\right) \qquad \text{(A.3.12)}$$

A.3.2 IR

$$e^{2g} = \frac{h_1}{2} - \frac{1}{8}\left[4k_2 - h_1\left(w_2^2+4\right) + \frac{4}{h_1}\left(v_2^2+4\right)\right]\rho^2 + \frac{1}{20160h_1^3}\Bigg\{1600h_1k_2\left(3v_2^2+8\right)$$
$$- 8h_1^2\Big[210k_2^2 + 144v_2\left(w_2-3\right)w_2 + 3v_2^2\left(105w_2^2 + 168w_2 + 580\right)$$
$$+ 4\left(55w_2^2 + 360w_2 + 652\right)\Big] - 480h_1^3k_2\left(w_2^2 + 18w_2 + 18\right)$$
$$+ 3h_1^4\left(75w_2^4 + 432w_2^3 + 488w_2^2 + 960w_2 + 1520\right)$$
$$+ 16\left(405v_2^4 + 1592v_2^2 + 656\right)\Bigg\}\rho^4 + O\left(\rho^6\right) \qquad \text{(A.3.13)}$$

$$e^{2h} = \frac{h_1}{2}\rho^2 + \frac{1}{72}\left[24k_2 - 3h_1\left(3w_2^2+4\right) - \frac{4}{h_1}(9v_2^2-4)\right]\rho^4$$
$$+ \frac{1}{907200h_1^3}\Big\{24h_1^2\Big[5250k_2^2 + 432v_2w_2\left(23w_2+57\right)$$
$$- 9v_2^2\left(189w_2^2+2016w_2+940\right) - 20940w_2^2 + 8640w_2 + 5680\Big]$$
$$+ 480h_1k_2\left(9v_2^2-172\right) - 360h_1^3k_2\left(627w_2^2-432w_2+44\right)$$
$$+ 9h_1^4\left(2007w_2^4 - 6624w_2^3 + 11352w_2^2 - 5760w_2 + 1520\right)$$
$$+ 16\left(19359v_2^4 + 27288v_2^2 - 22672\right)\Big\}\rho^6 + O\left(\rho^8\right) \tag{A.3.14}$$

$$e^{2k} = \frac{h_1}{2} + k_2\rho^2 + \frac{2}{315h_1^3}\Big\{5h_1k_2\left(27v_2^2+2\right) + \frac{15}{4}h_1^3k_2\left(9w_2^2+36w_2+22\right)$$
$$+ \frac{3}{2}h_1^2\Big[175k_2^2 + 12v_2w_2\left(w_2+4\right) - 30v_2^2 + 30w_2^2 + 120w_2 + 208\Big]$$
$$- \frac{9}{16}h_1^4\left(w_2^4 + 8w_2^3 + 36w_2^2 + 80w_2 + 80\right)$$
$$+ 9v_2^4 + 36v_2^2 - 528\Big\}\rho^4 + O\left(\rho^6\right) \tag{A.3.15}$$

$$e^{4\Phi} = e^{4\phi_0} + \frac{4e^{4\phi_0}}{3h_1^2}\left(3v_2^2+4\right)\rho^2 + \frac{e^{4\phi_0}}{135h_1^4}\Big\{-60h_1k_2\left(3v_2^2-8\right)$$
$$+ 3h_1^2\Big[3v_2^2\left(9w_2^2+36w_2+40\right) - 36v_2w_2\left(w_2+4\right) - 176\Big]$$
$$+ 4\left(243v_2^4 + 672v_2^2 + 944\right)\Big\}\rho^4 + O\left(\rho^6\right) \tag{A.3.16}$$

$$a = 1 + w_2\rho^2 + \frac{1}{90h_1^2}\Big\{w_2\Big[150h_1k_2 - 3h_1^2\left(6w_2^2 - 9w_2 + 28\right) + 400\Big]$$
$$+ 36v_2^2\left(w_2+2\right) - 72v_2\left(w_2+2\right)\Big\}\rho^4 + O\left(\rho^6\right) \tag{A.3.17}$$

$$b = 1 + v_2\rho^2 - \frac{1}{90h_1^2}\Big\{v_2\Big[30h_1k_2 - h_1^2\left(9w_2^2+36w_2+60\right) + 176\Big]$$
$$+ 9h_1^2w_2\left(w_2+4\right) + 72v_2^3\Big\}\rho^4 + O\left(\rho^6\right) \tag{A.3.18}$$

The effect of the SUSY-breaking parameters can be seen from the differences:

$$\Delta\left(e^{2g}\right) = \frac{1}{24h_1}\Big[-4h_1\left(3\Delta k_2 - 4\Delta w_2\right) + 3h_1^2\left(\Delta w_2 - 4\right)\Delta w_2 + 4\left(4 - 3\Delta v_2\right)\Delta v_2\Big]\rho^2$$
$$+ \frac{1}{60480h_1^3}\Big\{-24h_1^2\Big[320\Delta k_2\left(\Delta w_2 + 7\right) + 210\Delta k_2^2 - 4\Delta v_2\left(69\Delta w_2^2 + 224\right)$$
$$+ 3\Delta v_2^2\left(105\Delta w_2^2 - 252\Delta w_2 + 584\right) + 8\left(112 - 129\Delta w_2\right)\Delta w_2\Big]$$
$$+ 16\Delta v_2\left(1215\Delta v_2^3 - 3240\Delta v_2^2 + 3216\Delta v_2 - 2944\right)$$
$$+ 9h_1^4\Delta w_2\left(75\Delta w_2^3 - 168\Delta w_2^2 - 368\Delta w_2 + 896\right)$$
$$- 96h_1^3\Big[3\Delta k_2\left(5\Delta w_2^2 + 70\Delta w_2 - 56\right) + \Delta w_2\left(-75\Delta w_2^2 + 126\Delta w_2 + 184\right)\Big]$$
$$+ 64h_1\Big[3\Delta k_2\left(75\Delta v_2^2 - 100\Delta v_2 + 264\right) - 126\Delta v_2^2\left(5\Delta w_2 - 6\right)$$
$$+ 552\Delta v_2\Delta w_2 + 464\Delta w_2\Big]\Big\}\rho^4 + O\left(\rho^6\right) \qquad \text{(A.3.19)}$$

$$\Delta\left(e^{2h}\right) = \frac{1}{24h_1}\Big[8h_1\left(\Delta k_2 - 2\Delta w_2\right) - 3h_1^2\left(\Delta w_2 - 4\right)\Delta w_2 + 4\left(4 - 3\Delta v_2\right)\Delta v_2\Big]\rho^4$$
$$+ \frac{1}{302400h_1^3}\Big\{24h_1^2\Big[-80\Delta k_2\left(209\Delta w_2 - 490\right) + 1750\Delta k_2^2$$
$$+ \Delta v_2^2\left(-567\Delta w_2^2 - 3780\Delta w_2 + 7032\right) + 4\Delta v_2\left(1017\Delta w_2^2 - 3136\right)$$
$$+ 40\Delta w_2\left(157\Delta w_2 - 1288\right)\Big] + 32h_1\Big[5\Delta k_2\left(9\Delta v_2^2 - 12\Delta v_2 - 4352\right)$$
$$- 4\left(189\Delta v_2^2\left(3\Delta w_2 + 10\right) - 4068\Delta v_2\Delta w_2 + 856\Delta w_2\right)\Big]$$
$$- 24h_1^3\Big[5\Delta k_2\left(627\Delta w_2^2 - 2940\Delta w_2 + 3136\right)$$
$$- 4\Delta w_2\left(669\Delta w_2^2 - 5670\Delta w_2 + 14872\right)\Big]$$
$$+ 9h_1^4\Delta w_2\left(669\Delta w_2^3 - 7560\Delta w_2^2 + 29744\Delta w_2 - 49280\right)$$
$$+ 48\Delta v_2\left(2151\Delta v_2^3 - 5736\Delta v_2^2 + 6704\Delta v_2 + 7936\right)\Big\}\rho^6 + O\left(\rho^8\right) \qquad \text{(A.3.20)}$$

$$\Delta\left(e^{2k}\right) = \Delta k_2\rho^2 + \frac{1}{7560h_1^3}\Big\{36h_1^3\Big[15\Delta k_2\left(3\Delta w_2^2 + 14\right) - 8\Delta w_2\left(\Delta w_2^2 - 6\right)\Big]$$
$$+ 72h_1^2\left(120\Delta k_2\Delta w_2 + 175\Delta k_2^2 + 12\Delta v_2\Delta w_2^2 + 6\Delta v_2^2 - 56\Delta v_2 - 30\Delta w_2^2\right)$$
$$+ 16h_1\Big[15\Delta k_2\left(27\Delta v_2^2 - 36\Delta v_2 - 106\right) + 16\left(18\Delta v_2 - 29\right)\Delta w_2\Big]$$
$$+ 16\Delta v_2\left(27\Delta v_2^3 - 72\Delta v_2^2 - 468\Delta v_2 + 1072\right)$$
$$- 27h_1^4\Delta w_2^2\left(\Delta w_2^2 - 12\right)\Big\}\rho^4 + O\left(\rho^6\right) \qquad \text{(A.3.21)}$$

$$\Delta\left(e^{4\Phi}\right) = \frac{4e^{4\phi_0}\Delta v_2}{3h_1^2}\left(3\Delta v_2 - 4\right)\rho^2 + \frac{e^{4\phi_0}}{135h_1^4}\Big\{4h_1\Big[\Delta k_2\left(-45\Delta v_2^2 + 60\Delta v_2 + 100\right) + 36\left(3\Delta v_2^2 - 8\Delta v_2 + 4\right)\Delta w_2\Big] + 3h_1^2\Big[3\Delta v_2^2\left(9\Delta w_2^2 - 4\right) - 8\Delta v_2\left(9\Delta w_2^2 - 20\right) + 36\Delta w_2^2\Big] + 4\Delta v_2\big(243\Delta v_2^3 - 648\Delta v_2^2 + 1536\Delta v_2 - 1664\big)\Big\}\rho^4 + O\left(\rho^6\right) \tag{A.3.22}$$

$$\Delta a = \Delta w_2\rho^2 + \frac{1}{90h_1^3}\Big\{4h_1\Big[100\Delta k_2 + \left(9\Delta v_2^2 - 30\Delta v_2 - 40\right)\Delta w_2\Big] + 6h_1^2\Big[25\Delta k_2\left(\Delta w_2 - 2\right) - 24\left(\Delta w_2 - 5\right)\Delta w_2\Big] + 32\Delta v_2\left(3\Delta v_2 - 10\right) - 3h_1^3\Delta w_2\left(6\Delta w_2^2 - 45\Delta w_2 + 116\right)\Big\}\rho^4 + O\left(\rho^6\right) \tag{A.3.23}$$

$$\Delta b = \Delta v_2\rho^2 + \frac{1}{90h_1^2}\Big\{h_1\Big[\Delta k_2\left(20 - 30\Delta v_2\right) + 16\left(3\Delta v_2 - 5\right)\Delta w_2\Big] + 3h_1^2\Big[\Delta v_2\left(3\Delta w_2^2 + 4\right) - 5\Delta w_2^2\Big] - 8\Delta v_2\left(9\Delta v_2^2 - 18\Delta v_2 + 20\right)\Big\}\rho^4 + O\left(\rho^6\right) \tag{A.3.24}$$

A.4 Appendix: Details of the numerical analysis

Here we shall discuss in detail our approach to connecting the given IR and UV expansions numerically. We start by noting that we have chosen to solve the equations of motion (A.2.3–A.2.8) starting from the IR boundary conditions. As the IR parameter space is much smaller than that of the UV, this makes a search for solutions with the correct behaviour much less computationally expensive than if we started from the UV.

We use as our boundary conditions the IR expansions (A.3.13–A.3.24), extended up to order ρ^8. Using `NDSolve` in Mathematica 7 we then are able to generate numerical solutions which extend into the UV. We start at $\rho_{IR} = 10^{-4}$ as we found that in the SUSY case this gives approximately optimal accuracy. We use 40-digit `WorkingPrecision` in `NDSolve`.

Comparing the numerical solutions obtained by this method, with the known behaviour in the SUSY case, suggests that the results are trustable up to $\rho \sim 11$. This is supported by the observation that the constraint (A.2.2) is almost completely satisfied over this range. More explicitly, we find $T + U \lesssim 10^{-8}$ throughout this range. In fact it appears that the numerical solutions only fail when b decreases past $\sim 10^{-9}$. In the SUSY case (in which $b \sim e^{-2\rho}$) this does correspond to $\rho \sim 11$, but in the non-SUSY case (with $b \sim e^{2\rho/3}$) it occurs further into the UV.

In the IR we have five parameters $\{h_1, \phi_0, w_2, k_2, v_2\}$ which we can manipulate although we set $\phi_0 = 0$ (along with $N_c = 1$) without loss of generality. Given a value of h_1 we want to study the effects of the SUSY-breaking deformations for the remaining three $\{w_2, k_2, v_2\}$. We find that for a general deformation of these IR parameters the resulting solution does not exhibit the expected UV behaviour. Initially we find that the general behaviour of solutions in this parameter space has

$$b \sim \pm e^{2\rho} \quad \text{and} \quad e^{2g} \sim e^{2h} \sim e^{2k} \sim e^{8\rho/3} \tag{A.4.1}$$

going into the UV. The $e^{8\rho/3}$ behaviour appears to be suppressed by a very small numerical factor relative to the expected $e^{4\rho/3}$ term, and in fact is not visible in plots of g, h and k themselves. It is apparent, however, if we examine quantities of the form

$$e^{2k} - e^{2k_{\text{SUSY}}} \sim e^{8\rho/3}, \tag{A.4.2}$$

in which the $e^{4\rho/3}$ behaviour (almost) cancels.

Given a value for one of the three non-SUSY deformations, we believe it is possible to obtain the desired UV behaviour (A.3.1–A.3.6), i.e.

$$e^{-2\rho/3} \quad \text{and} \quad e^{2g} \sim e^{2h} \sim e^{2k} \sim e^{4\rho/3}, \tag{A.4.3}$$

with the correct choice of the remaining two. In practice it seems easier to vary three but keep one very close to its starting value.

Having obtained a numerical solution with the correct UV behaviour, we look to determine the corresponding values of the expansion coefficients in the UV, i.e.

$$\{c_+, c_-, \Phi_\infty, Q_o, \rho_o, H_{11}, W_{20}, \Phi_{30}, V_{40}\}. \tag{A.4.4}$$

We define the mismatch function

$$m = \sum_i \left[f_i^{\text{Numerical}}(\rho_{\text{match}}) - f_i^{\text{Expansion}}(\rho_{\text{match}}) \right]^2, \tag{A.4.5}$$

with $f_i \in \{g, h, k, \Phi, a, b, g', h', k', \Phi', a', b'\}$. We then minimise m to match our numerical solution and a UV expansion using `NMinimize` (with 60-digit `WorkingPrecision`) at a large ρ value, ρ_{match}.

With this setup and given the SUSY IR, `NMinimize` recovers the SUSY values for the UV parameters with an acceptable accuracy, even allowing all nine parameters to vary. The only restrictions we apply to the parameter space are $c_+ \geq 0$ and $\Phi_\infty \geq \phi_0 = 0$.

We now present a non-SUSY solution found using the above methods for one set of values of the IR parameters. It has the expected behaviour for all functions at least up to $\rho \sim 11$ (where the corresponding SUSY solution fails) and possibly as far as $\rho \sim 17$. We first choose $h_1 = 5$ (and have set $\phi_0 = 0$ as mentioned above). The corresponding SUSY solution has

$$w_2 = \frac{8}{3h_1} - 2 = -\frac{22}{15}, \qquad k_2 = \frac{2}{5h_1}(h_1^2 - 4) = \frac{42}{25}, \qquad v_2 = -\frac{2}{3}.$$

This results in an `NMinimize` output (with $\rho_{match} = 6$) of

$$\begin{array}{lll} c_+ \approx 1.6, & c_- \approx 2.0 \times 10^3, & \Phi_\infty \approx 0.076, \\ Q_o \approx -1.0, & \rho_o \approx -6.8 \times 10^{-11}, & W_{20} \approx 6.9 \times 10^{-14}, \\ V_{40} \approx 2.7 \times 10^{-9}, & H_{11} \approx 0.50, & \Phi_{30} \approx 0.38. \end{array}$$

The associated mismatch value is $m \lesssim 10^{-29}$. We take this as a good value for the mismatch as we know that the SUSY solution does indeed exist, and these values are in good agreement with (3.3.17).

To obtain a non-SUSY deformation, we follow the procedure described and modify the three IR parameters $\{k_2, v_2, w_2\}$ away from their SUSY values so as to manually scan the parameter space, until we gain a solution with the correct UV behaviour. We find that a suitable choice of deformations is[1]

$$\Delta k_2 \approx -2.471 \times 10^{-5}, \quad \Delta v_2 \approx 2.574 \times 10^{-5}, \quad \Delta w_2 \approx 1.029 \times 10^{-4}.$$

[1] The exact values used were $\Delta k_2 = -24\,705\,875 \times 10^{-12}$, $\Delta v_2 = 25\,744\,091\,286\,331\,971\,640\,358 \times 10^{-27}$ and $\Delta w_2 = 1\,029\,383\,373\,181\,636\,875 \times 10^{-22}$.

The minimization routine (again at $\rho_{match} = 6$) then finds that the UV parameters are modified from their SUSY values according to

$$\begin{array}{lll} \Delta c_+ \approx -6.6 \times 10^{-6}, & \Delta c_- \approx 1.6, & \Delta\Phi_\infty \approx -4.0 \times 10^{-7}, \\ \Delta Q_o \approx -1.5 \times 10^{-4}, & \Delta\rho_o \approx -7.1 \times 10^{-5}, & \Delta W_{20} \approx 5.2 \times 10^{-5}, \\ \Delta V_{40} \approx 5.6 \times 10^{-4}, & \Delta H_{11} \approx 9.1 \times 10^{-5}, & \Delta\Phi_{30} \approx -5.0 \times 10^{-5}, \end{array}$$

again with a mismatch value of $m \lesssim 10^{-29}$. However, we are unsure of the precision of these values — they appear to be slightly sensitive to the value of ρ_{match}, and so should be interpreted with caution.

A.5 Finding the UV parameters (improved method)

To look for the UV behaviour of the solutions in [2], a matching procedure was proposed to provide a fit of the UV parameters. However, we find this process is unreliable when we match at large ρ. Here we are interested in looking at solutions where the the two scales ρ_{h_1} and ρ_{SUSY} are varied over a large range. In particular, we need to include cases in which one or both have large values. The correct UV behaviour for solutions of this type is only manifest at large ρ, meaning that the matching procedure used in [2] is unsuitable.

Instead of performing this full matching procedure, it is possible to estimate some parameters from the leading behaviour of appropriate combinations of the background functions. For example, we can use the combination

$$-\frac{3}{2}e^{2\rho/3}a'(\rho) \to W_{20} \tag{A.5.1}$$

to give an approximation of the SUSY breaking parameter in cases where the matching procedure fails. Using this method, we find that it appears that $W_{20} \to \infty$ for $v_2 \to 0$ (see figure A.1). The case $w_2 = -2$ has $W'_{20}(w_2) = 0$, as would be expected from the invariance of W_{20} under the transformation (3.4.11).

Using the same method, the leading coefficients in M_1 (see (3.6.8, 3.6.9)), can be seen to have similar behaviour. However, both these quantities vanish for $w_2 = 0$, with probably non-zero derivatives. This reflects the fact that their signs change under the transformation (3.4.11).

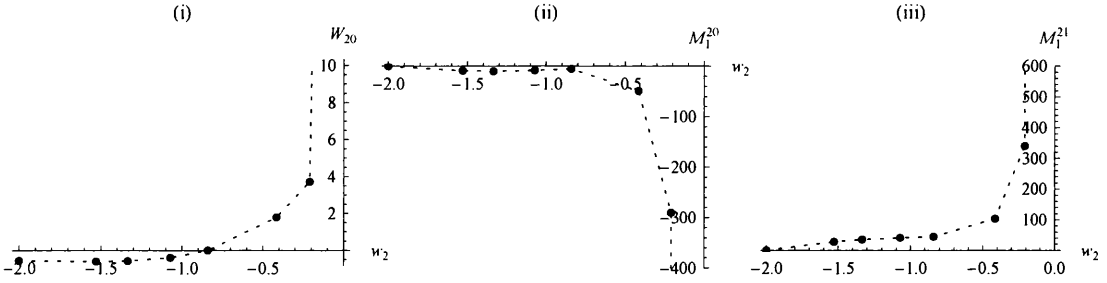

Figure A.1: Plots of the some of the UV parameters, estimated using the method described above for $h_1 = 2.3$ with $N_c = 1$ and $\phi_0 = 0$ (this includes the solutions plotted in figure 3.8). In (i) we plot W_{20}, corresponding to the gaugino mass which breaks SUSY. We also include (ii) $M_1^{20} \equiv 3W_{20}^2 + 2Q_o/c_+$ and (iii) $M_1^{21} \equiv 8H_{11}/c_+$, which contribute to the leading term in M_1 discussed in section 3.6.1. The dotted lines diverging for $w_2 \to 0$ indicate the position of the next point, at $w_2 \approx 1.3 \times 10^{-3}$. This has $W_{20} \approx 10^2$, $M_1^{20} \approx -6 \times 10^5$ and $M_1^{21} \approx 3 \times 10^5$.

Appendix B

The non-SUSY solutions

B.1 Appendix: Free Energy

Consider the Euclidean action $\mathcal{I}$ for the wrapped D5 background of section 3.3.2. The free energy is $F = \mathcal{I}/\beta$, where β is the period of the compactified time direction.

$$\begin{aligned}\mathcal{I} &= \mathcal{I}_{\text{grav}} + \mathcal{I}_{\text{surf}} \\ &= -\frac{1}{16\pi}\int_{\mathcal{M}} d^{10}x\sqrt{\mathbf{g}}R + \frac{1}{32\pi}\int_{\mathcal{M}}\left(d\Phi\wedge\star d\Phi + e^{\Phi}F_3\wedge\star F_3\right) \\ &\qquad - \frac{1}{8\pi}\oint_{\Sigma_r} {}^9K d\Sigma_r. \end{aligned} \tag{B.1.1}$$

$\mathcal{M}$ is a ten dimensional volume enclosed by a nine dimensional boundary Σ_r. The boundary Σ_r is taken to be surface at constant radial direction r. ${}^9K$ is the extrinsic curvature of the boundary,

$${}^9K = \nabla_\mu n^\mu = \frac{1}{\sqrt{\mathbf{g}}}\partial_\mu\left(\sqrt{\mathbf{g}}\, n^\mu\right) = \frac{1}{4}e^{-\Phi/4}e^{-k}\left[9\Phi' + 8(g'+h') + 4k'\right] \tag{B.1.2}$$

where n^μ is the boundary outward normal vector, $n^\mu = \sqrt{g^{rr}}\delta^\mu_r$. Using the equations of motion $\mathcal{I}_{\text{grav}}$ reduces to a volume integral of a total derivative,

$$\begin{aligned}\mathcal{I}_{\text{grav}} &= \frac{1}{32\pi}\int_{\mathcal{M}} d^{10}x\sqrt{\mathbf{g}}\nabla_\mu\nabla^\mu\Phi = \frac{1}{32\pi}\int_{\mathcal{M}} d^{10}x\partial_\mu(\sqrt{\mathbf{g}}\mathbf{g}^{\mu\nu}\partial_\nu\mathbf{\Phi}) \\ &= vol_8\beta\frac{1}{32\pi}\lim_{r\to\infty}\left(\frac{1}{8}e^{2(\Phi+g+h)}\Phi'\right). \end{aligned} \tag{B.1.3}$$

Explicitly, the surface term is

$$\mathcal{I}_{\text{surf}} = -vol_8\beta\frac{1}{8\pi}\lim_{r\to\infty}\left\{\frac{1}{32}e^{2(\Phi+g+h)}\left[9\Phi' + 8(g'+h') + 4k'\right]\right\}. \tag{B.1.4}$$

Thus,

$$\begin{aligned}\mathcal{I} =& \mathcal{I}_{\text{grav}} + \mathcal{I}_{\text{surf}} \\ =& -\frac{vol_8\beta}{256\pi}\lim_{r\to\infty}\left\{e^{2(\Phi+g+h)}\left[8(\Phi'+g'+h') + 4k'\right]\right\}. \end{aligned} \tag{B.1.5}$$

Equation (B.1.5) gives the value of the on-shell action in terms of the asymptotic fields at infinity. It typically contains divergences and has to be regularized. One way of doing this is to subtract the action of a reference background. In our case the natural choice is to subtract a supersymmetric background. We also require that both backgrounds induce the same metric at the boundary, Σ_r,

$$\begin{aligned} e^{\frac{\Phi_{ns}}{2}}e^{2g_{ns}} &= e^{\frac{\Phi_{su}}{2}}e^{2g_{su}}, \quad e^{\frac{\Phi_{ns}}{2}}e^{2h_{ns}} = e^{\frac{\Phi_{su}}{2}}e^{2h_{su}}, \\ e^{\frac{\Phi_{ns}}{2}}e^{2k_{ns}} &= e^{\frac{\Phi_{su}}{2}}e^{2k_{su}}, \quad e^{\frac{\Phi_{ns}}{2}} = e^{\frac{\Phi_{su}}{2}} \end{aligned} \tag{B.1.6}$$

and that the matter fields coincide at the boundary. In order to achieve the matching of the induced metrics and matter fields at the boundary we have to choose particular values for the integration constants of the supersymmetric background that we use as a regulator. We can then evaluate the free energy,

$$\begin{aligned} F &= \frac{1}{\beta}(\mathcal{I}^{ns} - \mathcal{I}^{su}) \\ &= -\frac{vol_8}{256\pi}\lim_{r_c\to\infty}\left\{e^{2\Phi_{ns}+2g_{ns}+2h_{ns}}(8\Phi'_{ns}+8g'_{ns}+8h'_{ns}+4k'_{ns})\right. \\ &\qquad \left. -e^{2\Phi_s+2g_s+2h_s}(8\Phi'_s+8g'_s+8h'_s+4k'_s)\right\}. \end{aligned} \tag{B.1.7}$$

Using the UV expansion (3.3.12), to first order in W_{20},

$$F = E = \frac{vol_8}{24\pi}c_+^2 e^{2\rho_0+2\Phi_\infty}W_{20}. \tag{B.1.8}$$

which agrees with the ADM calculation. A similar evaluation of the free energy can be carried out for the backgrounds after the rotation. Due to the presence of F_5 and the Chern-Simons term the calculation is more involved and the equality of the energy before and after rotation cannot be expressed as simply as (3.5.12). Nevertheless, after plugging in the appropiate UV expansions we get, to first order in W_{20}, $F_{before} \sim F_{after} \sim c_+^2 e^{2\rho_0+2\Phi_\infty}W_{20}$ as expected.

B.2 Appendix: Calculation of B_2

In the SUSY case, we have

$$B_2 = \kappa\frac{e^{\frac{3}{2}\Phi}}{\hat{h}^{1/2}}\Big[e^{\rho 3} - \cos\alpha(e^{\theta\varphi}+e^{12}) - \sin\alpha(e^{\theta 2}+e^{\varphi 1})\Big], \tag{B.2.1}$$

with

$$\cos\alpha = \frac{\cosh(2\rho)-a}{\sinh(2\rho)}, \qquad \sin\alpha = -\frac{2e^{h-g}}{\sinh(2\rho)}. \tag{B.2.2}$$

This is not valid in the general non-SUSY case. We obtain the same H_3 as in the SUSY case (3.2.9), but the relationship to (B.2.1) requires the BPS equations, as does the consistency of the definitions (B.2.2).

Instead, we must determine B_2 by requiring that $dB_2 = H_3$. We assume that B_2 has the same general structure as (B.2.1),

$$B_2 = b_1(\rho)e^{\rho 3} + b_2(\rho)e^{\theta\varphi} + b_3(\rho)e^{12} + b_4(\rho)e^{\theta 2} + b_5(\rho)e^{\varphi 1}, \tag{B.2.3}$$

which results in

$$
\begin{aligned}
dB_2 = & \frac{e^{-h-k-\frac{\Phi}{4}}\left(ab_3e^g+2b_4e^h\right)}{\hat{h}^{1/4}}e^{1\theta 3}+\frac{e^{-h-k-\frac{\Phi}{4}}\left(ab_3e^g+2b_5e^h\right)}{\hat{h}^{1/4}}e^{\varphi 23} \\
& -\frac{\left(b_4-b_5\right)e^{-h-\frac{\Phi}{4}}\cot\theta}{\hat{h}^{1/4}}e^{\theta\varphi 1} \\
& +\frac{e^{-2g-k-\frac{\Phi}{4}}}{2\hat{h}^{5/4}}\left(e^{2g}\left\{\hat{h}\left[b_3\left(4g'+\Phi'\right)+2b_3'\right]+b_3\hat{h}'\right\}+4b_1\hat{h}e^{2k}\right)e^{\rho 12} \\
& +\frac{e^{-h-k-\frac{\Phi}{4}}}{2\hat{h}^{5/4}}\Bigg(b_3e^g\hat{h}a'-2ab_1e^{-g}\hat{h}e^{2k} \\
& \qquad +e^h\left\{\hat{h}\left[b_4\left(2g'+2h'+\Phi'\right)+2b_4'\right]+b_4\hat{h}'\right\}\Bigg)e^{\rho\theta 2} \\
& +\frac{e^{-h-k-\frac{\Phi}{4}}}{2\hat{h}^{5/4}}\Bigg(b_3e^g\hat{h}a'-2ab_1e^{-g}\hat{h}e^{2k} \\
& \qquad +e^h\left\{\hat{h}\left[b_5\left(2g'+2h'+\Phi'\right)+2b_5'\right]+b_5\hat{h}'\right\}\Bigg)e^{\rho\varphi 1} \\
& +\frac{e^{-h-k-\frac{\Phi}{4}}}{2\hat{h}^{5/4}}\Bigg(-(b_4+b_5)e^g\hat{h}a'-\left(a^2-1\right)b_1\hat{h}e^{2k-h} \\
& \qquad +e^h\left\{\hat{h}\left[b_2\left(4h'+\Phi'\right)+2b_2'\right]+b_2\hat{h}'\right\}\Bigg)e^{\rho\theta\varphi}. \qquad \text{(B.2.4)}
\end{aligned}
$$

Comparing with (3.2.9), we see that the $e^{\theta\varphi 1}$ component of H_3 is zero, from which we immediately obtain that $b_4 = b_5$. The $e^{\rho\theta 2}$ and $e^{\rho\varphi 1}$ components of (B.2.4) are then identical, as are the $e^{1\theta 3}$ and $e^{\varphi 23}$ components. This is also the case in H_3, so we are left with four independent equations.

Equating the $(e^{1\theta 3}+e^{\varphi 23})$ components results in

$$
b_4 = -\frac{1}{2}e^{g-h}ab_3-\frac{\kappa N_c e^{\frac{3\Phi}{2}-g-h}b'}{4\hat{h}^{1/2}}, \qquad \text{(B.2.5)}
$$

and the $e^{\rho 12}$ component gives

$$
\begin{aligned}
b_1 = \frac{e^{2g-2k}}{4\hat{h}}\Big[& 2b_3\Phi'-3\hat{h}b_3\Phi'-4\hat{h}b_3g'-2\hat{h}b_3' \\
& +\kappa N_c e^{\frac{3\Phi}{2}-2h}\hat{h}^{\frac{1}{2}}\left(a^2-2ab+1\right)\Big]. \qquad \text{(B.2.6)}
\end{aligned}
$$

This leaves b_2 and b_3 to be determined. Substituting these results into (B.2.4), we find that the $(e^{\rho\theta 2}+e^{\rho\varphi 1})$ component of $H_3 = dB_2$ reduces to the equation of motion (A.2.8) for b. The only remaining equation is then the $e^{\rho\theta\varphi}$ component. This is a first order differential equation in b_2 and b_3,

$$
\begin{aligned}
0 = & 8\hat{h}e^{2g+4h}b_2'+2\left(a^2-1\right)\hat{h}e^{4g+2h}b_3'+e^{2(g+h)}\hat{h}'\left[\left(a^2-1\right)e^{2g}b_3+4e^{2h}b_2\right] \\
& +\hat{h}e^{2(g+h)}\left[4ae^{2g}a'b_3+(a^2-1)e^{2g}\left(4g'+\Phi'\right)b_3+4b_2e^{2h}\left(4h'+\Phi'\right)\right] \\
& -\kappa N_c\sqrt{\hat{h}}e^{3\Phi/2}\Big[-2a'b'e^{2(g+h)}+(a^4-1)e^{4g} \\
& \qquad -2(a^2-1)abe^{4g}+2abe^{4g}-16e^{4h}\Big]. \qquad \text{(B.2.7)}
\end{aligned}
$$

Solving for b_2 we obtain

$$b_2 = \frac{e^{-2h-\Phi/2}}{\sqrt{\hat{h}}}\int^{\rho} d\rho' \Bigg(\frac{e^{-2g-2h+\frac{\Phi}{2}}}{8\sqrt{\hat{h}}} \Big\{ -\left(a^2-1\right) e^{4g+2h}\hat{h}' b_3 \\ - \hat{h}e^{4g+2h}\Big[4aa' + a^2\left(4g'+\Phi'\right) - 4g' - \Phi'\Big] b_3 \\ + \kappa N_c \sqrt{\hat{h}} e^{3\Phi/2}\left[(a^4-1)e^{4g} - 2(a^2-1)abe^{4g} - 2a'b'e^{2(g+h)} - 16e^{4h}\right]\Big\} \\ - \frac{1}{4}\left(a^2-1\right)\sqrt{\hat{h}}e^{2g+\frac{\Phi}{2}} b_3' \Bigg), \tag{B.2.8}$$

which does not appear to be very useful. Instead, we can use the fact that we want $Q_{\text{Page, D3}} = 0$ (see eq. 3.6.15). We therefore impose that the $e^{\theta\varphi 123}$ component of $F_5 - B_2 \wedge F_3$ vanishes. The resulting equation is algebraic in b_2 and b_3, and results in

$$b_2 = \frac{e^{-2h}}{4\hat{h}^{1/2}}\left\{ e^{2g}\hat{h}^{\frac{1}{2}}\left(1-a^2\right) b_3 - \frac{\kappa}{N_c} e^{\frac{3\Phi}{2}}\left[N_c^2(a-b)b' + 4e^{2(g+h)}\Phi'\right]\right\}. \tag{B.2.9}$$

Together with the above results for $b_{1,4,5}$ this completes (3.6.2).

It remains to check that this b_2 is also compatible with the requirement that $dB_2 = H_3$. Substituting into (B.2.7) we find that b_3 cancels, giving

$$0 = 4e^{4(g+h)}\left\{2\hat{h}\left[2g'\Phi' + 2h'\Phi' + \Phi'' + 2\left(\Phi'\right)^2\right] - 2g'\hat{h}' - 2h'\hat{h}' - \hat{h}''\right\} \\ + N_c^2\Big[a^4e^{4g} - 2a^3be^{4g} + 2(a-b)b''e^{2(g+h)} + 4(a-b)b'e^{2(g+h)}\Phi' \\ + 2abe^{4g} - 2\left(b'\right)^2 e^{2(g+h)} - e^{4g} - 16e^{4h}\Big]. \tag{B.2.10}$$

This is solved by the equations of motion (A.2.6, A.2.8) for Φ and b.

To determine the effect of the undetermined function b_3, we can look at the difference $\Delta B_2 = B_2 - (B_2)_{b_3=0}$, which we find to be of the form

$$\Delta B_2 = F_1(\rho)\sin\theta\; d\theta\wedge d\varphi + F_2(\rho)\sin\tilde{\theta}\; d\tilde{\theta}\wedge d\tilde{\varphi} + F_3(\rho)\cos\theta\; d\rho\wedge d\varphi \\ + F_4(\rho)\cos\tilde{\theta}\; d\rho\wedge d\tilde{\varphi} + F_5(\rho)\; d\rho\wedge d\psi, \tag{B.2.11}$$

where the F_i depend on g, Φ, $\hat{h}$, b_3 and their derivatives. If we set this equal to

$$d\Big[\beta_1(\rho)\cos\theta\; d\varphi + \beta_2(\rho)\cos\tilde{\theta}\; d\tilde{\varphi} + \beta_3(\rho)\; d\psi\Big] \tag{B.2.12}$$

we can solve for the β_i, giving

$$\Delta B_2 = -\frac{1}{4}d\left[e^{2g+\Phi/2}\sqrt{\hat{h}}b_3(\cos\theta\; d\varphi + \cos\tilde{\theta}\; d\tilde{\varphi} + d\psi)\right] \\ = -\frac{1}{2}d\Big(e^{2g-k+\Phi/4}\hat{h}^{1/4}b_3\; e^3\Big). \tag{B.2.13}$$

B.3 Appendix: Seiberg-like duality

In section 3.6.2 we discuss how the operation known as Seiberg duality in the KS cascade acts for our non-SUSY solution. In order to do so, we find it instructive to compare to two different cases: the KS case and the baryonic branch case. These are summarized here.

B.3.1 The KS case

We follow here the treatment in [68], specified in the case of no flavors ($N_f = 0$). The NS potential B_2 is given by,

$$B_2 = \frac{N_c}{2}[f g_1 \wedge g_2 + \tilde{k} g_3 \wedge g_4] \tag{B.3.1}$$

where the definition of $g_1, ..., g_4$ can be found in [68]. When specialized to the cycle

$$\Sigma_2 = [\theta = \tilde{\theta}, \varphi = 2\pi - \tilde{\varphi}, \psi = \psi_0] \tag{B.3.2}$$

we obtain that

$$B_2|_{\Sigma_2} = \frac{N_c}{2}[(f + \tilde{k}) + (\tilde{k} - f)\cos\psi_0]\sin\theta d\theta \wedge d\varphi \tag{B.3.3}$$

from which one finds

$$b_0 = \frac{1}{4\pi^2}\int_{\Sigma_2} B_2 = \frac{N_c}{\pi}[f\sin^2(\frac{\psi_0}{2}) + k\cos^2(\frac{\psi_0}{2})] \tag{B.3.4}$$

On the other hand, as computed in [68], we can see that the Maxwell charge of D3 branes is

$$Q_{Max,D3} = \frac{N_c^2}{\pi}[f - (f - \tilde{k})F] \tag{B.3.5}$$

We see that under the change

$$f \to f - \frac{\pi}{N_c}, \quad \tilde{k} \to \tilde{k} - \frac{\pi}{N_c} \tag{B.3.6}$$

the D3-Maxwell charge changes by

$$Q_{Max,D3} \to Q_{Max,D3} - N_c, \quad b_0 \to b_0 - 1. \tag{B.3.7}$$

these transformations, are equivalent to changing the NS potential with a large gauge transformation

$$B_2 \to B_2 + \frac{\pi}{2}[g_1 \wedge g_2 + g_3 \wedge g_4] \tag{B.3.8}$$

which when evaluated on the cycle Σ_2, produces the changes in eq.(B.3.7). We move now to analyze the baryonic branch (SUSY) case.

B.3.2 Baryonic branch case

In this case the NS potential is

$$B_2 = \frac{\kappa e^{3\Phi/2}}{\hat{h}^{1/2}}[e^{\rho 3} - \cos\alpha(e^{12} + e^{\theta\varphi}) - \sin\alpha(e^{\theta 2} + e^{\varphi 1})] \tag{B.3.9}$$

Evaluating this on the Σ_2 we get

$$\begin{aligned}
b_0 &= \frac{\kappa e^{2\Phi}}{\pi}\Big[(\tilde{k} + f) + (\tilde{k} - f)\cos\psi_0\Big], \\
\tilde{k} + f &= \frac{\kappa e^{2\Phi}}{N_c}\Big[\cos\alpha(\frac{e^{2g}}{4}(a^2 + 1) - e^{2h}) + \sin\alpha a e^{h+g}\Big], \\
\tilde{k} - f &= \frac{\kappa e^{2\Phi}}{N_c}\Big[\cos\alpha\frac{e^{2g}}{2}a + \sin\alpha e^{h+g}\Big],
\end{aligned} \tag{B.3.10}$$

Using the explicit expressions, we have

$$\tilde{k} = -\frac{\kappa e^{2\Phi}}{4N_c} Q \coth(\rho), \quad f = -\frac{\kappa e^{2\Phi}}{4N_c} Q \tanh(\rho) \tag{B.3.11}$$

The Maxwell charge for D3 branes can be written as,

$$Q_{Max,D3} = \frac{\kappa}{\pi} e^{2g+2h+2\Phi} \Phi' \tag{B.3.12}$$

and using the BPS equation for Φ' we have

$$Q_{Max,D3} = \frac{N_c^2}{\pi} \Big[2f + (\tilde{k} - f) F \Big], \tag{B.3.13}$$

where $F = (1 - b)$. So, once again, we obtain that under a large gauge transformation,

$$b_0 \to b_0 - 1, \quad Q_{Max,D3} \to Q_{Max,D3} - N_c. \tag{B.3.14}$$

B.4 UV asymptotics of the RHB

The RHB solution asymptotes in the UV to (a special case of) the solution described in section 4.1 of [79]. This solution is parametrised in terms of $\{P, Q, h_0, r_0, g_s\}$,[1] and has the form

$$\begin{aligned}
ds^2 &= H(r)^{-1/2} d\hat{x}_{1,3}^2 + H(r)^{1/2} \left(\mathrm{d}r^2 + \frac{1}{4} r^2 d\Omega_2 + \frac{1}{8} r^2 d\Omega_3 \right), \\
F_{(3)} &= P\, \bar{\omega}_1 \wedge \bar{\omega}_2 \wedge \bar{\omega}_3, \\
H_{(3)} &= f'(r) \sin\theta \, \mathrm{d}\rho \wedge \mathrm{d}\theta \wedge \mathrm{d}\varphi, \\
F_{(5)} &= \mathcal{F} + *\mathcal{F}, \qquad \mathcal{F} = K(r) \sin\theta \, \mathrm{d}\theta \wedge \mathrm{d}\varphi \wedge \bar{\omega}_1 \wedge \bar{\omega}_2 \wedge \bar{\omega}_3.
\end{aligned} \tag{B.4.1}$$

By comparing with (4.2.13), we immediately obtain

$$P = -\frac{N_c}{4}. \tag{B.4.2}$$

If we then identify $r = e^{\rho/\sqrt{2}}$, and use the UV expansions (4.2.6), we find that the metric in (4.2.13) can be matched to that in (B.4.1) with

$$H = 4 N_c^2 K_0^2 e^{\Phi_\infty} \frac{1}{r^4} \left(\frac{2}{K_0^2} \log r - \frac{K_2}{2} \right). \tag{B.4.3}$$

Comparing with the expression in [79], we get $g_s = e^{\Phi_\infty}$, as expected, and

$$Q = 2^{-7/2} N_c^2 e^{\Phi_\infty} \left(4 \log r_0 - K_0^2 K_2 - 1 \right). \tag{B.4.4}$$

[1] To avoid confusion, we adapt the notation of [79]: $r_{\text{here}} = \rho_{[79]}$, $(r_0)_{\text{here}} = (\rho_0)_{[79]}$ and $H_{\text{here}} = h_{[79]}$.

Bibliography

[1] S. Bennett, Annals Phys. **326**, 2934 (2011), arXiv:1102.5731.

[2] S. Bennett, E. Caceres, C. Nunez, D. Schofield, and S. Young, JHEP **2012**, 1 (2011), arXiv:1111.1727.

[3] S. Bennett and D. Schofield, JHEP **1206**, 176 (2012), arXiv:1204.2799.

[4] J. M. Maldacena, Adv. Theor. Math. Phys. **2**, 231 (1998), arXiv:hep-th/9711200.

[5] S. Gubser, I. R. Klebanov, and A. M. Polyakov, Phys.Lett. **B428**, 105 (1998), arXiv:hep-th/9802109.

[6] E. Witten, Adv.Theor.Math.Phys. **2**, 253 (1998), arXiv:hep-th/9802150.

[7] D. Elander, J. Gaillard, C. Nunez, and M. Piai, JHEP **07**, 056 (2011), arXiv:1104.3963.

[8] I. R. Klebanov and E. Witten, Nucl.Phys. **B536**, 199 (1998), arXiv:hep-th/9807080.

[9] L. Romans, Phys.Lett. **B153**, 392 (1985).

[10] I. R. Klebanov and N. A. Nekrasov, Nucl.Phys. **B574**, 263 (2000), arXiv:hep-th/9911096.

[11] I. R. Klebanov and A. A. Tseytlin, Nucl.Phys. **B578**, 123 (2000), arXiv:hep-th/0002159.

[12] I. R. Klebanov and M. J. Strassler, JHEP **08**, 052 (2000), arXiv:hep-th/0007191.

[13] A. Butti, M. Grana, R. Minasian, M. Petrini, and A. Zaffaroni, JHEP **03**, 069 (2005), arXiv:hep-th/0412187.

[14] S. S. Gubser, C. P. Herzog, and I. R. Klebanov, Comptes Rendus Physique **5**, 1031 (2004), arXiv:hep-th/0409186.

[15] J. M. Maldacena and C. Nunez, Phys. Rev. Lett. **86**, 588 (2001), arXiv:hep-th/0008001.

[16] A. H. Chamseddine and M. S. Volkov, Phys. Rev. Lett. **79**, 3343 (1997), arXiv:hep-th/9707176.

[17] J. Gaillard, D. Martelli, C. Nunez, and I. Papadimitriou, Nucl. Phys. **B843**, 1 (2011), arXiv:1004.4638.

[18] E. Conde, J. Gaillard, C. Nunez, M. Piai, and A. V. Ramallo, JHEP **1202**, 145 (2012), arXiv:1112.3350.

[19] E. Conde, J. Gaillard, and A. V. Ramallo, JHEP **1110**, 023 (2011), arXiv:1107.3803.

[20] E. Witten, Adv. Theor. Math. Phys. **2**, 505 (1998), arXiv:hep-th/9803131.

[21] A. Buchel, Nucl. Phys. **B600**, 219 (2001), arXiv:hep-th/0011146.

[22] A. Buchel, C. P. Herzog, I. R. Klebanov, L. A. Pando Zayas, and A. A. Tseytlin, JHEP **04**, 033 (2001), arXiv:hep-th/0102105.

[23] S. S. Gubser, C. P. Herzog, I. R. Klebanov, and A. A. Tseytlin, JHEP **05**, 028 (2001), arXiv:hep-th/0102172.

[24] S. S. Gubser, A. A. Tseytlin, and M. S. Volkov, JHEP **09**, 017 (2001), arXiv:hep-th/0108205.

[25] N. J. Evans, M. Petrini, and A. Zaffaroni, JHEP **06**, 004 (2002), arXiv:hep-th/0203203.

[26] O. Aharony, E. Schreiber, and J. Sonnenschein, JHEP **04**, 011 (2002), arXiv:hep-th/0201224.

[27] R. Apreda (2003), arXiv:hep-th/0301118.

[28] V. Borokhov and S. S. Gubser, JHEP **05**, 034 (2003), arXiv:hep-th/0206098.

[29] J. Babington, D. E. Crooks, and N. J. Evans, JHEP **02**, 024 (2003), arXiv:hep-th/0207076.

[30] J. Babington, D. E. Crooks, and N. J. Evans, Phys. Rev. **D67**, 066007 (2003), arXiv:hep-th/0210068.

[31] R. Apreda, F. Bigazzi, and A. L. Cotrone, JHEP **12**, 042 (2003), arXiv:hep-th/0307055.

[32] A. Dymarsky and S. Kuperstein (2011), arXiv:1111.1731.

[33] K. G. Wilson, Phys. Rev. D **10**, 2445 (1974).

[34] J. Sonnenschein (1999), arXiv:hep-th/0003032.

[35] S.-J. Rey and J.-T. Yee, Eur. Phys. J. **C22**, 379 (2001), arXiv:hep-th/9803001.

[36] J. M. Maldacena, Phys. Rev. Lett. **80**, 4859 (1998), arXiv:hep-th/9803002.

[37] C. Nunez, M. Piai, and A. Rago, Phys. Rev. **D81**, 086001 (2010), arXiv:0909.0748.

[38] N. Drukker, D. J. Gross, and H. Ooguri, Phys. Rev. **D60**, 125006 (1999), arXiv:hep-th/9904191.

[39] A. Brandhuber and K. Sfetsos, Adv. Theor. Math. Phys. **3**, 851 (1999), arXiv:hep-th/9906201.

[40] S. D. Avramis, K. Sfetsos, and K. Siampos, Nucl. Phys. **B769**, 44 (2007), arXiv:hep-th/0612139.

[41] C. Bachas, Phys. Rev. D **33**, 2723 (1986).

[42] Y. Kinar, E. Schreiber, and J. Sonnenschein, Nucl. Phys. **B566**, 103 (2000), arXiv:hep-th/9811192.

[43] S. D. Avramis, K. Sfetsos, and K. Siampos, Nucl. Phys. **B793**, 1 (2008), arXiv:0706.2655.

[44] S.-J. Rey, S. Theisen, and J.-T. Yee, Nucl. Phys. **B527**, 171 (1998), arXiv:hep-th/9803135.

[45] A. Brandhuber, N. Itzhaki, J. Sonnenschein, and S. Yankielowicz, Phys. Lett. **B434**, 36 (1998), arXiv:hep-th/9803137.

[46] R. E. Arias and G. A. Silva, JHEP **01**, 023 (2010), arXiv:0911.0662.

[47] J. Maldacena and D. Martelli, JHEP **01**, 104 (2010), arXiv:0906.0591.

[48] R. Casero, C. Nunez, and A. Paredes, Phys. Rev. **D73**, 086005 (2006), arXiv:hep-th/0602027.

[49] R. Casero, C. Nunez, and A. Paredes, Phys. Rev. **D77**, 046003 (2008), arXiv:0709.3421.

[50] C. Hoyos-Badajoz, C. Nunez, and I. Papadimitriou, Phys. Rev. **D78**, 086005 (2008), arXiv:0807.3039.

[51] M. Warschawski (2012), arXiv:1212.3472.

[52] R. P. Andrews and N. Dorey, Phys. Lett. **B631**, 74 (2005), arXiv:hep-th/0505107.

[53] R. P. Andrews and N. Dorey, Nucl. Phys. **B751**, 304 (2006), arXiv:hep-th/0601098.

[54] R. Minasian, M. Petrini, and A. Zaffaroni, JHEP **04**, 080 (2010), arXiv:0907.5147.

[55] N. Halmagyi (2010), arXiv:1003.2121.

[56] E. Caceres, C. Nunez, and L. A. Pando-Zayas, JHEP **03**, 054 (2011), arXiv:1101.4123.

[57] C. Nunez, A. Paredes, and A. V. Ramallo, Adv. High Energy Phys. **2010**, 196714 (2010), arXiv:1002.1088.

[58] F. Bigazzi, A. L. Cotrone, and A. Zaffaroni, Phys. Lett. **B519**, 269 (2001), arXiv:hep-th/0106160.

[59] J. P. Gauntlett, N. Kim, D. Martelli, and D. Waldram, JHEP **11**, 018 (2001), arXiv:hep-th/0110034.

[60] E. G. Gimon, L. A. Pando Zayas, J. Sonnenschein, and M. J. Strassler, JHEP **05**, 039 (2003), arXiv:hep-th/0212061.

[61] U. Gursoy and C. Nunez, Nucl. Phys. **B725**, 45 (2005), arXiv:hep-th/0505100.

[62] G. Papadopoulos and A. A. Tseytlin, Class. Quant. Grav. **18**, 1333 (2001), arXiv:hep-th/0012034.

[63] S. S. Gubser, C. P. Herzog, and I. R. Klebanov, JHEP **09**, 036 (2004), arXiv:hep-th/0405282.

[64] S. Hawking and G. T. Horowitz, Class.Quant.Grav. **13**, 1487 (1996), arXiv:gr-qc/9501014.

[65] S. S. Gubser, A. A. Tseytlin, and M. S. Volkov, JHEP **0109**, 017 (2001), arXiv:hep-th/0108205.

[66] A. Dymarsky, I. R. Klebanov, and N. Seiberg, JHEP **01**, 155 (2006), arXiv:hep-th/0511254.

[67] S. Kuperstein and J. Sonnenschein, JHEP **0402**, 015 (2004), arXiv:hep-th/0309011.

[68] F. Benini, F. Canoura, S. Cremonesi, C. Nunez, and A. V. Ramallo, JHEP **09**, 109 (2007), arXiv:0706.1238.

[69] L. Girardello, M. Petrini, M. Porrati, and A. Zaffaroni, JHEP **9812**, 022 (1998), arXiv:hep-th/9810126.

[70] I. R. Klebanov, D. Kutasov, and A. Murugan, Nucl. Phys. **B796**, 274 (2008), arXiv:0709.2140.

[71] A. Dymarsky, JHEP **05**, 053 (2011), arXiv:1102.1734.

[72] A. Masiero and G. Veneziano, Nucl.Phys. **B249**, 593 (1985).

[73] O. Aharony, J. Sonnenschein, M. E. Peskin, and S. Yankielowicz, Phys. Rev. **D52**, 6157 (1995), arXiv:hep-th/9507013.

[74] N. J. Evans, S. D. Hsu, and M. Schwetz, Phys.Lett. **B355**, 475 (1995), arXiv:hep-th/9503186.

[75] M. J. Strassler, pp. 419–510 (2005), arXiv:hep-th/0505153.

[76] N. Arkani-Hamed and R. Rattazzi, Phys.Lett. **B454**, 290 (1999), arXiv:hep-th/9804068.

[77] N. Seiberg, Nucl.Phys. **B435**, 129 (1995), arXiv:hep-th/9411149.

[78] D. Freedman, C. Nunez, M. Schnabl, and K. Skenderis, Phys.Rev. **D69**, 104027 (2004), arXiv:hep-th/0312055.

[79] L. A. Pando Zayas and A. A. Tseytlin, Phys.Rev. **D63**, 086006 (2001), arXiv:hep-th/0101043.

[80] J. Hirn and V. Sanz, Phys.Rev. **D76**, 044022 (2007), arXiv:hep-ph/0702005.

[81] J. Hirn and V. Sanz, JHEP **0703**, 100 (2007), arXiv:hep-ph/0612239.

[82] R. Diener, *Kaluza-Klein Spectroscopy* (2010).

[83] M. Berg, M. Haack, and W. Mueck, Nucl. Phys. **B736**, 82 (2006), arXiv:hep-th/0507285.